UNIVERSITY OF ALBERTA

SYNTHESIS AND REACTIONS OF HYDROTRIS(PYRAZOLYL)BORATE COMPLEXES OF DIVALENT LANTHANIDES

by

XINGWANG ZHANG ©

A thesis submitted to the Faculty of Graduate Studies and Research in partial fulfillment of the requirements for the Degree of Doctor of Philosophy.

DEPARTMENT OF CHEMISTRY

EDMONTON, ALBERTA

Fall 1995

ISBN 0-612-06314-3

UNIVERSITY OF ALBERTA

RELEASE FORM

NAME OF AUTHOR:	XINGWANG ZHANG
TITLE OF THESIS:	SYNTHESIS AND REACTIONS OF HYDROTRIS(PYRAZOLYL)BORATE COMPLEXES OF DIVALENT LANTHANIDES
DEGREE:	DOCTOR OF PHILOSOPHY
YEAR THIS DEGREE GRANTED:	1995

#305, 10625-81 Ave.

Edmonton, Alberta

T6E 1Y1

September 28, 1995

THE UNIVERSITY OF ALBERTA

FACULTY OF GRADUATE STUDIES AND RESEARCH

The undersigned certify that they have read, and recommend to the Faculty of Graduate Studies and Research for acceptance, a thesis entitled SYNTHESIS AND REACTIONS OF HYDROTRIS(PYRAZOLYL)BORATE COMPLEXES OF DIVALENT LANTHANIDES submitted by XINGWANG ZHANG in partial fulfillment of the requirements for the degree of DOCTOR OF PHILOSOPHY.

J. Takats (Supervisor)

R.G. Cavell

W.J. Evans(External Examiner)

R.B. Jordan

D.D. Tanner

M.C. Williams

Date: September 15, 1995

To my wife Susan, my daughter Catherine and my son Anthony

ABSTRACT

The reactions of LnI_2 with two equiv of the sterically moderately demanding $KTp^{R,R'}$ (R=R'=Me; R=H, R'=Ph, 2-thienyl) readily gave solvent-free bis-ligand complexes, $(Tp^{R,R'})_2Ln$ (Ln=Sm, Yb). The Tp^{Me2} and Tp^{Ph} complexes have been structurally characterized. They are six-coordinate with the $Tp^{R,R'}$ ligands η^3-bonded to the metal centers. In contrast to the bent-metallocene structures of $(C_5Me_5)_2Ln$ (Ln=Sm, Yb, Eu), the planes defined by pyrazolyl nitrogen donors from each ligand are parallel. Except for the Tp^{Me2} complexes, the compounds are soluble in THF. The insolubility of $(Tp^{Me2})_2Ln$ (Ln=Sm, **1**; Yb, **2**) is attributed to the hexagonal close-packed solid state structure which leads to high lattice energy. Interestingly, despite the insolubility, $(Tp^{Me2})_2Sm$ reacts readily with reducible substrates to afford mononuclear species. Thus, addition of azobenzene to $(Tp^{Me2})_2Sm$ in 1:1 or 1:2 molar ratio leads to formation of the same product, dark green $(Tp^{Me2})_2Sm(PhN{=}NPh)$ (**8**), and reaction with 2,6-di-tert-butyl-1,4-benzoquinone gives $(Tp^{Me2})_2Sm[OC_6H_2(^tBu)_2O]$, **9**. Importantly, reaction of $(Tp^{Me2})_2Sm$ with dioxygen at low temperature generated the first superoxo lanthanide complex, $(Tp^{Me2})_2Sm(O_2)$, **10**. The X-ray structures of **8**, **9** and **10** have been determined. In all three complexes, the Tp^{Me2} ligands retain their η^3-coordination mode. The azobenzene ligand in **8** is symmetrically bonded to Sm via two nitrogen atoms, while in **9** the quinone is coordinated via the less hindered oxygen atom. Complex **10** contains a symmetrical, side-on bonded superoxo ligand; the Sm-O distances are 2.329(3) and 2.321(3)Å with an O-O length of 1.319(5)Å. The Raman spectrum of the molecule shows the O-O stretch at 1124 cm^{-1} which shifts to 1059 cm^{-1} upon $^{18}O_2$ substitution. Both **8** and **10** have distorted pentagonal bipyramidal geometry in the solid state. However, in solution **10** is fluxional while **9** is rigid. The fluxionality is apparently due to the lack of substituents on the O_2 moiety.

Reaction of YbI_2 with one equiv of Tp^{Me2} ligand gave the half-sandwich complex $(Tp^{Me2})YbI(THF)_2$, **11**. The same reaction with Sm led to ligand-redistribution and gave the bis-ligand complex $(Tp^{Me2})_2Sm$. Although isolable, the ytterbium complex (**11**) slowly converts to the bis-ligand compound **2**. Reaction of $KTp^{tBu,Me}$ with one equiv of LnI_2 afforded the half-sandwich compounds $(Tp^{tBu,Me})LnI(THF)_n$ (Ln=Sm, n=2, **12**; Yb, n=1, **13**) in high yields. The solvent-free molecule $(Tp^{tBu,Me})SmI$ (**14**) can be prepared by repeated cycles of dissolution in toluene and removal of the solvent. The compounds **12-14** are stable towards ligand-redistribution even at 80°C. Addition of one equiv of bulky KER ligands (ER = $N(SiMe_3)_2$, $CH(SiMe_3)_2$) to $(Tp^{tBu,Me})LnI(THF)_n$ at -40°C in diethyl ether resulted in the formation of $(Tp^{tBu,Me})LnER$ (Ln=Sm, Yb). The monomeric and solvent-free nature has been verified by X-ray structure analyses of $(Tp^{tBu,Me})YbER$ (ER = $N(SiMe_3)_2$, **17**; $CH(SiMe_3)_2$, **19**). $(Tp^{tBu,Me})YbI(THF)$ reacted with moderate sized ligands to give mono-solvated $(Tp^{tBu,Me})YbER(THF)$ (ER= CH_2SiMe_3, **20**; $O(2,4,6\text{-}Me_3C_6H_2)$, **22**) while the same reaction with Sm gave $(Tp^{tBu,Me})_2Sm$, **21**, a ligand redistribution product. The hydrocarbyl complexes **19** and **20** undergo slow hydrogenolysis under 1 atm of H_2.

Complex **21** and the ytterbium analogue, $(Tp^{tBu,Me})_2Yb$, **27**, can be obtained by the more conventional reaction of LnI_2 with two equivalents of $KTp^{tBu,Me}$, although the reactions are slow. The X-ray structure of the samarium complex has been determined. Unlike the symmetrical bis-(η^3-Tp) bonding observed in the other $(Tp^{R,R'})_2Ln$ complexes, the large size of $Tp^{tBu,Me}$ prevents coordination of both ligands in an η^3-bonding mode. One $Tp^{tBu,Me}$ ligand is bonded *via* classical η^3-bonding mode, the other is coordinated *via* two pyrazolyl nitrogens and an agostic B-H $\rightarrow$ Sm interaction. $(Tp^{tBu,Me})_2Ln$ represent the first examples of bis-ligand formation by this sterically very demanding ligand. The spectroscopic data are consistent with a solution structure that is identical to the solid state form. In particular, the observation of ^{171}Yb-HB coupling of 85 Hz confirms the persistence of the agostic interaction in solution. Variable temperature NMR studies show

that the molecules are fluxional in solution and execute two distinct and specific rearrangement processes. The low temperature process involves exchange of the pyrazolyl rings within individual $Tp^{tBu,Me}$ ligands *without* exchanging the bonding modes of the ligands, it is also suggested that the process preserves the B-H $\rightharpoonup$ Ln interaction. Above room temperature, the two different $Tp^{tBu,Me}$ ligands also begin to slowly exchange their bonding modes. Estimates of the free energy for the exchange processes are 8.5 and 16.5 kcal/mol, respectively.

ACKNOWLEDGEMENTS

I would like to thank Professor Josef Takats for his guidance and encouragement, for his sincere friendship and understanding, and for his assistance in the writing of this thesis.

I thank my friends and colleagues especially Yimin Sun, Wenyi Fu, Tianfu Mao, John Washington, Jason Cooke and Ken Hoffmann for support and providing a pleasant atmosphere for research. I would also like to thank Jackie for her assistance with the typing of this thesis.

I would like to thank Glen Bigam, Tom Nakashima, Tom Brisbane, Gerdy Aarts and Lai Kong for performing numerous experiments for me: their enthusiasm and professionalism is appreciated. The X-ray determinations provided by Bob McDonald, Victor W. Day, Andrew Bond and Robin Rogers are gratefully acknowledged.

I would like to thank other technical support staff of the Department of Chemistry for all their assistance, and practical help.

Finally, I would also like to thank my family for their support and patience during my studies.

TABLE OF CONTENTS

PAGE

Chapter 1

Introduction 1

1.1. The Lanthanides 1

1.2. Organometallic Chemistry of the Trivalent Lanthanides 2

1.2.1. $(C_5R_5)_3Ln$ Complexes (R=H, Me) 2

1.2.2. $(C_5R_5)_{3-m}LnX_m$ Complexes (R=H, Me; X=halides; m=1, 2) 4

1.2.3. $(C_5R_5)_2LnR$ and $[(C_5R_5)_2LnH]_2$ (R=H, Me) Complexes 4

1.3. Organometallic Chemistry of the Divalent Lanthanides 7

1.3.1. The Lanthanide(II) Ions 7

1.3.2. $(C_5R_5)_2Ln$ Complexes (R=H, Me; Ln=Sm, Yb) 7

1.4. Complexes of the Lanthanides with Hydrotris(pyrazolyl)borate Ligands 12

1.4 1. The $Tp^{R,R'}$ Ligand System 12

1.4.2. $(Tp)_3Ln$ Complexes 15

1.4.3. $(Tp)_mLnCl_{3-m}$ and $(Tp)_2Ln$ Complexes (m=1, 2) 15

1.5. Scope of the Thesis 17

1.6. References 18

Chapter 2

Synthesis and Characterization of Divalent Lanthanides Hydrotris(pyrazolyl)borates: $(Tp^{R,R'})_2Ln$ ($Tp^{R,R'}$=Tp^{Me2}, Tp^{Ph}, Tp^{Tn}; Ln=Sm, Yb), a Structural Comparison 23

2.1. Introduction 23

2.2. Synthetic Aspects 25

2.2.1. Synthesis of$(Tp^{Me2})_2Ln$ 25

2.2.2. Synthesis of $(Tp^{Ph})_2Ln$ and $(Tp^{Tn})_2Ln$ Complexes 26

2.3. Solid State Structures of 1-4 30

2.4. Structural Comparison 36

2.5. Conclusions 37

2.6. Experimental Section 38

2.6.1. General Techniques and Solvents 38

2.6.2. Physical Measurements 38

2.6.3. Starting Materials and Reagents 39

2.6.4. Synthetic Procedures 39

2.6.5. X-ray Structure Determinations 41

2.7. **References** 44

Chapter 3

Reactivity Survey of $(Tp^{Me2})_2Sm$ 46

3.1. Introduction 46

3.2. Reactivity Survey of $(Tp^{Me2})_2Sm$, **1** 47

3.2.1. Reaction with $TlBPh_4$ 47

3.2.2. Reaction with PhN=NPh 47

3.2.3. Reaction with 2,6-di-tert-butyl-1,4-benzoquinone 51

3.2.4. Reaction with Dioxygen 52

3.2.5. Reactions with TCNQ, TCNE and DMAD 56

3.2.6. Reactions with HC≡CPh, HC≡CH, PhC≡CPh, CO, $H_2C=CH_2$, $CH_3CH=CH_2$ 56

3.3. Solid-State Structures of **7**, **8**, **9** and **10** 56

3.4. Conclusions 61

3.5. Experimental Section 62

3.5.1. Starting Materials and Methods 62

3.5.2. Synthesis of the Compounds 63

3.5.3. X-ray Structure Determinations 66

3.6. References 68

Chapter 4

Consequence of Steric Control Provided by Highly Hindered Hydrotris(3-tert-butyl-5-methylpyrazolyl)borate ($Tp^{tBu,Me}$) Ligand: Stabilization and Isolation of a Series of Monomeric, Half-sandwich Ln(II) Complexes 71

4.1. Introduction 71

4.2. The Precursor Complexes $(Tp^{Me2})YbI(THF)_2$ and $(Tp^{tBu,Me})LnI(THF)_n$ 72

4.2.1. Synthetic Aspects 72

4.2.2. Oxidation of $(Tp^{tBu,Me})SmI(THF)_2$ 75

4.2.3. Molecular structures of complexes **11, 13, 15** 76

4.3. Derivatization of $(Tp^{tBu,Me})LnI(THF)_n$ 80

4.3.1. Synthetic Aspects 80

4.3.2. Crystallographic Studies 89

4.4. ^{171}Yb NMR Studies 98

4.5. Conclusions 99

4.6. Experimental Section 101

4.6.1. Starting Materials and Reagents 101

4.6.2. Synthetic Procedures 101

4.6.3. ^{171}Yb NMR Study 110

4.6.4. X-ray Structure Determinations 110

4.7. References 113

Chapter 5

Synthesis and Structure of the First Bis-hydrotris(3-^{t}Bu-5-Me pyrazolyl)borate Complexes, $(Tp^{tBu,Me})_2Ln$ (Ln = Sm, Yb): Fluxionality, Bonding Mode Exchange and B-H-Ln Bridge Bonding 116

5.1. Introduction 116

5.2. Synthesis of $(Tp^{tBu,Me})_2Ln$ (Sm, **21**; Yb, **27**) 117

5.3. Molecular Structure of $(Tp^{tBu,Me})_2Sm$ 121

5.4. Variable Temperature NMR Studies: Solution Structure of $(Tp^{tBu,Me})_2Ln$ Complexes; Fluxionality and Bonding Mode Changes of the $Tp^{tBu,Me}$ Ligands 127

5.5. Conclusions 137

5.6. Experimental Section 138

5.6.1. Synthetic Procedures 138

5.6.2. Variable Temperature NMR Studies 141

5.6.3. X-ray Structure Determination 142

5.7. References 146

Chapter 6

Conclusions 148

6.1. References 150

LIST OF FIGURES

Chapter 1

Figure 1.1 Molecular structure of $[(\eta^5\text{-}C_5H_5)_2La(\mu\text{-}\eta^5{:}\eta^2\text{-}C_5H_5)]_n$ 3

Figure 1.2 Molecular structure of $[(\eta^5\text{-}C_5H_5)_2Lu(\mu\text{-}\eta^1{:}\eta^1\text{-}C_5H_5)]_n$ 3

Figure 1.3 Molecular structure of $[(C_5Me_5)_2LuCH_3]_2$ 6

Figure 1.4 Molecular structure of $[(C_5Me_5)_2Sm]_2(\mu\text{-}O)$ 11

Figure 1.5 Molecular structure of $[(C_5Me_5)_2Sm]_2(\mu\text{-}Te_2)$ 12

Figure 1.6 A perspective view of $Tp^{R,R'}$ 12

Chapter 2

Figure 2.1 400MHz ^1H NMR spectrum of $(Tp^{Ph})_2Sm$ (3) in benzene-d_6 27

Figure 2.2 400MHz ^1H NMR spectrum of $(Tp^{Ph})_2Yb$ (4) in toluene-d_8 28

Figure 2.3 Diagram and numbering scheme of $(Tp^{Tn})_2Sm$ 30

Figure 2.4 ORTEP view of $(Tp^{Me2})_2Sm$ (1) 31

Figure 2.5 ORTEP view of $(Tp^{Me2})_2Yb$ (2) 31

Figure 2.6 ORTEP view of $(Tp^{Ph})_2Sm$ (3) 32

Figure 2.7 ORTEP view of $(Tp^{Ph})_2Yb$ (4) 32

Chapter 3

Figure 3.1 400 MHz ^1H NMR spectrum of $(Tp^{Me2})_2Sm(PhN{=}NPh)$ (8) in toluene-d_8 49

Figure 3.2 400 MHz ^1H NMR spectrum of $(Tp^{Me2})_2Sm[OC_6H_2(^tBu)_2O]$ (9) in toluene-d_8 52

Figure 3.3 Raman spectra of $(Tp^{Me2})_2Sm(\eta^{2\text{-}16}O_2)$ (top) and $(Tp^{Me2})_2Sm(\eta^{2\text{-}18}O_2)$ (bottom) 55

Figure 3.4 ORTEP view of $(Tp^{Me2})_2SmBPh_4$ (7) 57

Figure 3.5 ORTEP view of $(Tp^{Me2})_2Sm(PhN{=}NPh)$ (**8**) 57

Figure 3.6 ORTEP view of $(Tp^{Me2})_2Sm[OC_6H_2(^tBu)_2O]$ (**9**) 58

Figure 3.7 ORTEP view of $(Tp^{Me2})_2Sm(O_2)$ (**10**) 58

Chapter 4

Figure 4.1 ORTEP view of $(Tp^{Me2})YbI(THF)_2$ (**11**) 77

Figure 4.2 ORTEP view of $(Tp^{tBu,Me})YbI(THF)$ (**13**) 77

Figure 4.3 ORTEP view of $(Tp^{tBu,Me})SmI(THF)_2[BPh_4]$ (**15**) 78

Figure 4.4 400 MHz ^1H NMR spectrum of $(Tp^{tBu,Me})Yb[HB(CH_2CH_3)_3](THF)$ (**24**) in benzene-d_6 86

Figure 4.5 400 MHz ^1H NMR spectrum of $(Tp^{tBu,Me})Sm[HB(CH_2CH_3)_3]$ (**23**) in benzene-d_6 87

Figure 4.6 ORTEP view of $(Tp^{tBu,Me})Yb[N(SiMe_3)_2]$ (**17**) 90

Figure 4.7 ORTEP view of $(Tp^{tBu,Me})Yb[CH(SiMe_3)_2]$ (**19**) 90

Figure 4.8 ORTEP view of $(Tp^{tBu,Me})YbCH_2SiMe_3(THF)$ (**20**) 91

Figure 4.9 ORTEP view of $(Tp^{tBu,Me})Yb[O(2,4,6\text{-}Me_3C_6H_2)](THF)$ (**22**) 92

Figure 4.10 ORTEP view of $(Tp^{tBu,Me})Yb[HB(CH_2CH_3)_3](THF)$ (**24**) 93

Chapter 5

Figure 5.1 Room temperature ^1H NMR spectra (400 MHz) of $Sm(Tp^{tBu,Me})_2$ (**21**) and $Yb(Tp^{tBu,Me})_2$ (**27**) in toluene-d_8 119

Figure 5.2 ORTEP view of $Sm(Tp^{tBu,Me})_2$ (**21**) showing the atom labeling scheme. 122

Figure 5.3 Alternative view of **21** emphasizing the coordination geometry of Sm and the twisted-boat conformation of the "η^2-$Tp^{tBu,Me}$" ligand 124

Figure 5.4 Low temperature ^1H NMR spectra (400 MHz) of $Sm(Tp^{tBu,Me})_2$ (**21**) in diethyl ether-d_{10} 128

Figure 5.5 Variable temperature ^1H NMR spectra (400 MHz) of $Yb(Tp^{tBu,Me})_2$ (**27**) in toluene-d_8, only the pyrazolyl 4-H region is shown 130

Figure 5.6 Variable temperature ^1H NMR spectra (400 MHz) of a 1:1 mixture of compounds **21** and **27** in toluene-d_8 135

LIST OF TABLES

Chapter 2

Table 2.1 Selected Bond Lengths and Non-bonded Contacts (Å) for $(Tp^{Me2})_2Sm$ (**1**), $(Tp^{Me2})_2Yb$ (**2**), $(Tp^{Ph})_2Sm$ (**3**) and $(Tp^{Ph})_2Yb$ (**4**) 33

Table 2.2 Selected Bond Angles (deg) for $(Tp^{Me2})_2Sm$ (**1**), $(Tp^{Me2})_2Yb$ (**2**), $(Tp^{Ph})_2Sm$ (**3**) and $(Tp^{Ph})_2Yb$ (**4**) 34

Table 2.3 Summary of Crystallographic Data for $(Tp^{Me2})_2Sm$ (**1**), $(Tp^{Me2})_2Yb$ (**2**), $(Tp^{Ph})_2Sm$ (**3**), $(Tp^{Ph})_2Yb$ (**4**) 43

Chapter 3

Table 3.1 Selected Interatomic Distances and Angles (deg) for $(Tp^{Me2})_2SmBPh_4$ (**7**), $(Tp^{Me2})_2Sm(PhN{=}NPh)$ (**8**), $(Tp^{Me2})_2Sm(OC_6H_2(^tBu)_2O)$ (**9**) and $(Tp^{Me2})_2Sm(O_2)$ (**10**) 59

Table 3.2 Summary of Crystallographic Data for $(Tp^{Me2})_2SmBPh_4$ (**7**), $(Tp^{Me2})_2Sm(PhN{=}NPh)$ (**8**), $(Tp^{Me2})_2Sm(C_{14}H_{20}O_2)$ (**9**), $(Tp^{Me2})_2Sm(O_2)\cdot C_4H_{10}O_2$ (**10**) 67

Chapter 4

Table 4.1 Selected Bond Lengths (Å) and Bond Angles (deg) for $(Tp^{Me2})YbI(THF)_2$ (**11**), $(Tp^{tBu,Me})YbI(THF)$ (**13**) 79

Table 4.2 Selected Bond Lengths (Å) and Angles (deg) for $(Tp^{tBu,Me})Yb[N(SiMe_3)_2]$ (**17**), $(Tp^{tBu,Me})Yb[CH(SiMe_3)_2]$ (**19**) 89

Table 4.3 Selected Bond Lengths (Å) and Angles (deg) for $(Tp^{tBu,Me})Yb(CH_2SiMe_3)(THF)$ (**20**), $(Tp^{tBu,Me})Yb[O\text{-}(2,4,6\text{-}Me_3C_6H_2)](THF)$ (**22**) and $(Tp^{tBu,Me})Yb(HBEt_3)(THF)$ (**24**) 94

Table 4.4 The ^{171}Yb NMR Chemical Shifts of Ytterbium Complexes 99

Table 4.5 Summary of Crystallographic Data for $(Tp^{Me2})YbI(THF)_2$ (**11**), $(Tp^{tBu,Me})YbI(THF)$ (**13**), $(Tp^{tBu,Me})Yb(CH_2SiMe_3)(THF)$ (**20**) 111

Table 4.6 Summary of Crystallographic Data for $(Tp^{tBu,Me})Yb[N(SiMe_3)_2]$ (**17**), $(Tp^{tBu,Me})Yb[CH(SiMe_3)_2]$ (**19**), $(Tp^{tBu,Me})Yb[O\text{-}(2,4,6\text{-}Me_3C_6H_2)](THF)$ (**22**) and $(Tp^{tBu,Me})Yb(HBEt_3)(THF)$ (**24**) 112

Chapter 5

Table 5.1 Selected Interatomic Distances (Å) and Angles (deg) for $Sm(Tp^{tBu,Me})_2 \cdot 1/2\ C_6H_{14}$ 121

Table 5.2 Crystallographic Data for $Sm(Tp^{tBu,Me})_2 \cdot 1/2\ C_6H_{14}$ 144

LIST OF SCHEMES

Chapter 4

Scheme 4.1 Derivatization of $(Tp^{tBu,Me})LnI(THF)_n$ 81

Chapter 5

Scheme 5.1 Exchange of pyrazolyl groups within individual $Tp^{tBu,Me}$ ligand in **21** and **27**; low temperature process 133

Scheme 5.2 Exchange of bonding mode between η^3- and η^2-$Tp^{tBu,Me}$ ligands in **21** and **27**; high temperature process 137

LIST OF ABBREVIATIONS AND SYMBOLS

Å	Angstrom(s)
Anal.	analytical
atm	atmosphere(s)
av	average
acac	acetylacetonate
^{t}Bu	tertiary-butyl, $C(CH_3)_3$-
B	Lewis base
br.	broad
bzac	benzoylacetonate
ca.	circa (approximately)
calcd	calculated
DME	dimethoxyethane
DMF	dimethylformamide
dmpe	bis(dimethylphosphino)ethane
dpmH	2,2,6,6-tetramethyl-3,5-heptane-dione
dbm	dibenzoylmethane
deg	degree(s)
dd	doublet of doublets
EI	electron ionization
ESR	electron spin resonance
eV	electron volts
FT-IR	Fourier Transform Infrared
Hz	Hertz
h	hour(s)
J	coupling constant
K	Kelvin

Me	methyl, CH_3-
MHz	megahertz
MS	mass spectrometry
mg	milligram(s)
mL	milliliters
mmol	millimoles
ms	millisecond
m/z	mass to charge ratio
m	meta-
N-MeIm	N-methylimidazole
NMR	nuclear magnetic resonance
nm	nanometer(s)
OTf	triflate
o	ortho-
^{i}Pr	isopropyl, $HC(CH_3)_2$-
Ph	phenyl, C_6H_5-
pmdeta	N,N,N',N",N"-pentamethyldiethylenetriamine
p	para-
ppm	parts per million
pz	pyrazolyl
s	singlet
s	second
THF	tetrahydrofuran
Tn	2-thienyl, C_4H_3S
$Tp^{Mementh}$	Tris[7(S)-tert-butyl-4(R)-methyl-4,5,6,7-tetrahydro-2-indazolyl]hydroborate
tfacH	3-trifluoroacetyl-D-camphor

t	triplet
tt	triplet of triplets
td	triplet and doublet
ν	stretching frequency
δ	chemical shift in ppm
Δ	chemical shift difference
$\Delta\nu_{1/2}$	linewidth at half-height
ε	molar extinction coefficient

Chapter 1

Introduction

1.1. The lanthanides

Lanthanum and the following 14 elements are normally referred to as the lanthanides; Ln has been used as a generic symbol for these elements. They are naturally occurring elements which closely resemble one another chemically and physically. The discovery of the lanthanides proved to be challenging and was a hallmark in the history of inorganic chemistry. As a result of their similar properties, separation is difficult and it took nearly two centuries to identify all the lanthanides. The history of lanthanides has been well described.[1] Of special interest to this work are ytterbium, which was discovered by J.C.G. de Marignac in 1878 and named after the city of Ytterby in Stockholm where a mineral containing the lanthanides was first found, and samarium which was found by Boisbandran in 1879, and named after the mineral samarskite, in honor of a Russian mining official, C. Samarski.

The ground-state electronic configuration of lanthanides is $[Xe]4f^n$, where electrons are successively added to f orbitals on going from lanthanum (Z=57) to lutetium (Z=71).[2] Because of their poor radial extension, the 4f valence orbitals are largely uninvolved in bonding and this leads to similarity in the chemical properties of the lanthanides. This feature distinguishes the lanthanides from the d-type transition elements in which the valence d-electrons are involved in chemical interactions. It is generally agreed that the bonding in lanthanide complexes is predominantly ionic and the coordination number and geometry are controlled more by steric factors than by orbital interactions. Thus, magnetic and spectroscopic properties of the lanthanides show little dependence on the nature and number of the ligands. As a result of more

ionic bonding, ligand redistribution reactions have been a pervasive problem in lanthanide chemistry.[3]

The most stable oxidation state for the lanthanides is +3. The six-coordinate ionic radius decreases steadily from 1.032Å (La^{+3}) to 0.861Å (Lu^{+3}) due to the lanthanide contraction.[2] Other accessible oxidation states include Ce^{+4} ($4f^0$), Sm^{+2} ($4f^6$), Eu^{+2} ($4f^7$), and Yb^{+2} ($4f^{14}$), but no single metal appears to have both +2 and +4 oxidation states. Thus some important processes such as two electron oxidative addition and reductive elimination reactions, common with transition metals, are not accessible at a single lanthanide center.[4] However, single electron processes are possible.

Because of the large size, the coordination number of the lanthanides is generally higher than that of the transition metals. A common coordination number is 8 although it can be as low as 3 and as high as 12. Due to their electropositive nature the lanthanides prefer hard Lewis bases, especially oxygen donor ligands; they are highly oxophilic. Finally, most of the lanthanide ions, with the exception of La^{+3}, Ce^{+4} and Yb^{+2}, are paramagnetic.

1.2. Organometallic Chemistry of the Trivalent Lanthanides

1.2.1. $(C_5R_5)_3Ln$ Complexes (R=H, Me)

The tris(cyclopentadienyl) complexes, $(C_5H_5)_3Ln$, reported by Birmingham and Wilkinson,[5] were the first well-characterized organometallic compounds of the lanthanides. X-ray structure analyses revealed that the structures of the $(C_5H_5)_3Ln$ complexes exhibit substantial variations with the size of the Ln ion. The lanthanum and praseodymium compounds have a polymeric structure,[6] $[(\eta^5\text{-}C_5H_5)_2Ln(\mu\text{-}\eta^5{:}\eta^2\text{-}C_5H_5)]_n$ (Figure 1.1 for Ln=La), while the erbium complex is monomeric,[7] $(\eta^5\text{-}C_5H_5)_3Er$. The smallest lanthanide, lutetium, exhibits a polymeric chain structure[8],

$[(\eta^5\text{-}C_5H_5)_2Lu(\mu\text{-}\eta^1\text{:}\eta^1\text{-}C_5H_5)]_n$ shown in Figure 1.2. The coordination number of the central lanthanide decreases from 11 to 9 and to 7 across the series, which is consistent with the decreasing size of the metal. The origin of the polymeric nature of the structures can be traced to either steric unsaturation or oversaturation around the metal center. The $(C_5H_5)_3Ln$ complexes form interesting acid-base adducts, $(\eta^5\text{-}C_5H_5)_3LnB$, with a wide variety of neutral donors.[3] In contrast to their parent base-free complexes, these adducts are much more soluble and display similar structural patterns.[9-12] It is noteworthy that there is only one reported tris-cyclopentadienyl metal complex with the bulky C_5Me_5 ligand, $(C_5Me_5)_3Sm$. The X-ray structure indicates that the molecule is monomeric and Sm is surrounded in a trigonal planar array by three $\eta^5\text{-}C_5Me_5$ ligands.[13]

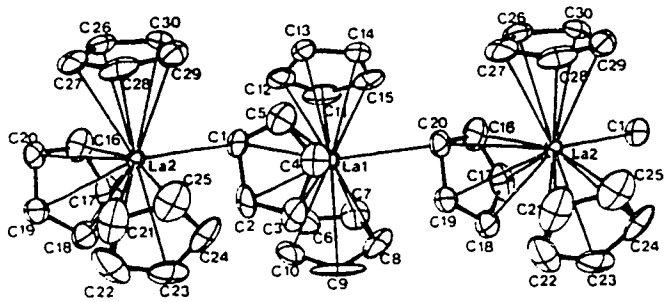

Figure 1.1 Molecular structure of $[(\eta^5\text{-}C_5H_5)_2La(\mu\text{-}\eta^5\text{:}\eta^2\text{-}C_5H_5)]_n$

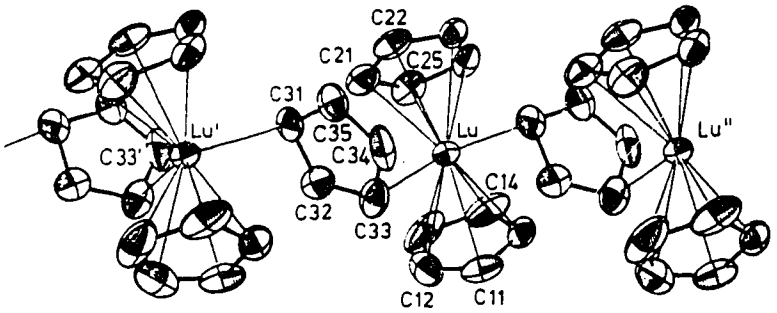

Figure 1.2 Molecular structure of $[(\eta^5\text{-}C_5H_5)_2Lu(\mu\text{-}\eta^1\text{:}\eta^1\text{-}C_5H_5)]_n$

1.2.2. $(\eta^5\text{-}C_5R_5)_{3-m}LnX_m$ Complexes (R=H, Me; X=halides; m=1, 2)

Compounds $[(\eta^5\text{-}C_5H_5)_2LnCl]_2$ and $(\eta^5\text{-}C_5H_5)LnCl_2(THF)_n$ can be readily prepared by reaction of anhydrous $LnCl_3$ with NaC_5H_5 in 1:2 or 1:1 molar ratio.[3] However, for the early lanthanides, these complexes are usually unstable and tend to undergo ligand-redistribution to form tris-C_5H_5 complexes due to the larger size and hence less sterically saturated metal centers. Obviously the steric size of the ligand set has to be increased in order to inhibit ligand-redistribution reactions. Thus, Bruno et al.[14] discovered that the mono(pentamethylcyclopentadienyl) complexes, $(C_5Me_5)LnI_2(THF)_3$ (Ln=La, Ce), can be synthesized from $LnI_3(THF)_3$ and KC_5Me_5. The stability of $C_5Me_5LnI_2(THF)_3$ was attributed to the larger size of the C_5Me_5 and iodide ligands. Reaction of $(C_5Me_5)LaI_2(THF)_3$ with $KCH(SiMe_3)_2$ afforded the hydrocarbyl compound, $(C_5Me_5)La[CH(SiMe_3)_2]_2(THF)$.[15] The mono-$C_5Me_5$ compounds, $(C_5Me_5)Ce[N(SiMe_3)_2]_2$ and $(C_5Me_5)Ce[CH(SiMe_3)_2]_2$ have also appeared in the literature.[16,17] Utilizing the bulky C_5Me_5 ligand, the first bis-C_5R_5 halide complex of an early lanthanide was stabilized and isolated, eq 1.1.[18]

$$NdCl_3 \quad + \quad 2LiC_5Me_5 \xrightarrow{THF} (C_5Me_5)_2NdCl_2Li(THF)_2 \quad + \quad LiCl \qquad 1.1$$

One year later, Andersen et al. reported the salt-free complexes, $(C_5Me_5)_2NdCl(THF)$ and $(C_5Me_5)_2NdN(SiMe_3)_2$.[19] The synthetic route shown in eq 1.1 for the Nd compound proved to be general for the preparation of $(C_5Me_5)_2LnCl_2Li(ether)_2$ complexes ranging from the heaviest lanthanide, Lu, to the lightest La.[20]

1.2.3. $(C_5R_5)_2LnR$ and $[(C_5R_5)_2LnH]_2$ (R=H, Me) complexes

Many of the advances in lanthanide hydrocarbyl and hydride chemistry have been achieved with the bis(cyclopentadienyl) and especially with the bis(pentamethylcyclopentadienyl) ligand systems. The $[(C_5H_5)_2LnCl]_2$ and

$(C_5Me_5)_2LnCl_2Li(ether)_2$ complexes are good precursors to hydrocarbyl derivatives. The hydride complexes are prepared by hydrogenolysis of the corresponding hydrocarbyl compounds. As an example, the important lanthanide hydrocarbyl compound, $(C_5H_5)_2Lu(^tBu)(THF)$, which has played a significant role in understanding the principles governing Ln-C chemistry was readily prepared by metathesis of $[(C_5H_5)_2LuCl]_2$ with Li^tBu at -78°C.[21] Hydrogenolysis of $(C_5H_5)_2Lu(^tBu)(THF)$ afforded the dimeric hydride, $[(C_5H_5)_2Lu(\mu\text{-}H)(THF)]_2$,[22] eq 1.2.

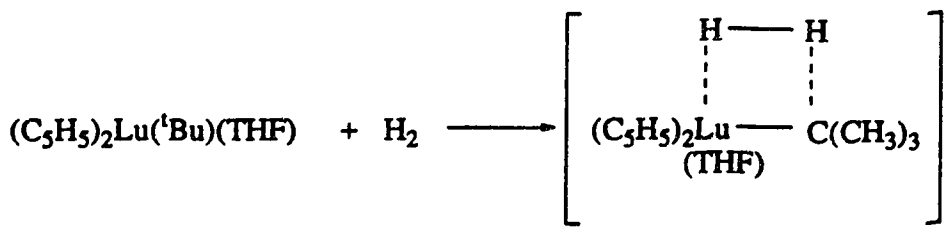

$$\longrightarrow [(C_5H_5)_2Lu(THF)(\mu\text{-}H)]_2 + HC(CH_3)_3 \qquad 1.2$$

The first bis(pentamethylcyclopentadienyl) hydrocarbyl, $(C_5Me_5)_2LuCH_3(Et_2O)$ was obtained in several steps.[23,24] The reactions are reported to be solvent- and alkali metal-dependent, and only the best and most reliable sequence is shown in eq 1.3. The ether-free complex, $(C_5Me_5)_2LuCH_3$, was obtained by conversion to the NEt_3 adduct followed by desolvation of $(C_5Me_5)_2LuCH_3(NEt_3)$.

$$(C_5Me_5)_2Lu(\mu\text{-}Cl)_2Li(Et_2O)_2 \xrightarrow[-\,2LiCl]{2CH_3Li/THF} (C_5Me_5)_2Lu(CH_3)_2Li(THF)_3 \xrightarrow[\text{vacuum}]{75°C}$$

$$(C_5Me_5)_2Lu(CH_3)_2Li \xrightarrow[-\,LiAl(CH_3)_4]{2Al(CH_3)_3} (C_5Me_5)_2Lu(CH_3)_2Al(CH_3)_2 \xrightarrow[-40°C]{ether}$$

$$(C_5Me_5)_2LuCH_3(Et_2O) \xrightarrow[2.\ Vacuum]{1.\ NEt_3} (C_5Me_5)_2LuCH_3 \qquad 1.3$$

Hydrogenolysis of $(C_5Me_5)_2LuCH_3$ generated the hydride, $(C_5Me_5)_2LuH$. The combination of sterically demanding C_5Me_5 ligands with the small Lu and CH_3 (or H) imparts unique structural and reactivity patterns to the latter two complexes. The X-ray structure of $(C_5Me_5)_2LuCH_3$, Figure 1.3, revealed an asymmetrical dimeric structure in which a methyl moiety from one Lu binds, via agostic C-H → Lu interactions, to the Lu center of a second molecule.[25] In solution, $(C_5Me_5)_2LuX$ (X=H, CH_3) exhibited an equilibrium between monomeric and asymmetric dimeric

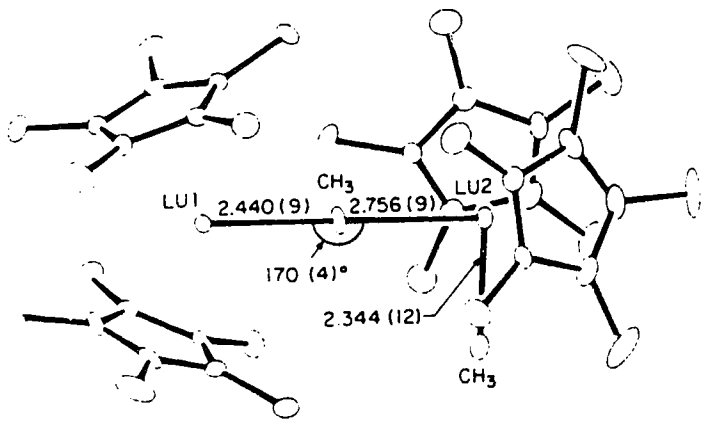

Figure 1.3 Molecular structure of $[(C_5Me_5)_2LuCH_3]_2$

species.[26,27] It was discovered that $(C_5Me_5)_2LuX$ polymerizes ethylene and oligomerizes propylene, providing an excellent model for homogeneous Ziegler-Natta catalysis.[23] The $(C_5Me_5)_2LuX$ compounds metallate a broad class of substrates. Remarkably they can even activate methane as shown in eq 1.4.[25] This represents a rare example of the activation of methane with a homogeneous organometallic compound. It is interesting to note that the sterically saturated $[(C_5H_5)_2Lu(\mu\text{-}CH_3)]_2$ complex is much less reactive than $(C_5Me_5)_2LuCH_3$.

$$(C_5Me_5)_2LuX \quad + \quad {}^{13}CH_4 \rightleftharpoons (C_5Me_5)_2Lu^{13}CH_3 \quad + \quad XH \qquad 1.4$$

A wide range of lanthanide hydrocarbyls, $(C_5Me_5)_2LnCH(SiMe_3)_2$ (Ln=La, Nd, Sm and Lu) can be prepared simply by the reaction of $(C_5Me_5)_2LnCl_2Li(ether)_2$ with bulky $LiCH(SiMe_3)_2$, this is in contrast to the complex synthesis of $(C_5Me_5)_2LuCH_3$ mentioned above. Hydrogenolysis of $(C_5Me_5)_2LnCH(SiMe_3)_2$ under mild conditions gives the corresponding hydrides $[(C_5Me_5)_2LnH]_2$. The hydrides are active catalysts for ethylene polymerization. The order of activity, La>Nd>>Lu, follows the decrease in ionic radius.[20]

1.3. Organometallic Chemistry of the Divalent Lanthanides

1.3.1. The Lanthanide (II) Ions

As mentioned earlier, the divalent lanthanides, accessible under mild condition, are Sm^{+2}, Eu^{+2} and Yb^{+2}. The standard electrode potentials (E^0) in aqueous solution for the Ln^{+3}/Ln^{+2} couple are -1.5V (Sm), -0.35V (Eu) and -1.1V (Yb).[28,29] Clearly, Eu^{+2} is a poor reductant and hence it is not very reactive. Indeed, the divalent lanthanide chemistry has mainly focused on Sm^{+2} and Yb^{+2} ions. The following discussions will be confined to these two metal ions. The complexes of Yb^{+2} ($4f^{14}$) are diamagnetic, hence NMR spectroscopy provides a useful tool for the characterization of compounds. This is further enhanced by the availability of NMR active ^{171}Yb NMR probe. Although Sm^{+2} is paramagnetic, the paramagnetism is small and consequently the ^1H NMR signals are normally located within the ±20 ppm range and are relatively sharp due to the short electron spin relaxation time.

1.3.2. $(C_5R_5)_2Ln$ Complexes (R=H, Me; Ln=Sm, Yb)

The biscyclopentadienyl ytterbium complex was first prepared by the reaction of ytterbium metal with cyclopentadiene in liquid ammonia.[30] The ammonia-free compound, $(C_5H_5)_2Yb$, was obtained via sublimation. The complex is insoluble in

hydrocarbon and ether solvents, but soluble in dimethylformamide and ammonia. A more recent and economic synthesis involves the reaction of YbI_2 with NaC_5H_5 (eq 1.5).[31] The analogous samarium derivative was originally isolated from the reaction

$$YbI_2(THF)_x + 2NaC_5H_5 \longrightarrow (C_5H_5)_2Yb + 2NaI \qquad 1.5$$

of $(C_5H_5)_3Sm$ with $KC_{10}H_8$.[32] The compound is pyrophoric and insoluble in common solvents. A more convenient synthetic route utilizes the THF-soluble SmI_2 in a manner similar to reaction 1.5.[31] Crystal structures of $(C_5H_5)_2Yb$ and $(C_5H_5)_2Sm(THF)$ have not been reported. The insolubility of both complexes hampered their structural and reactivity studies. Introduction of C_5Me_5 had a great impact on the development of divalent organolanthanide chemistry, as it did with early transition metals and the actinides. The C_5Me_5 ligand imparts stability, solubility and crystallinity to organometallic systems. Indeed, the bis-pentamethylcyclopentadienyl complexes of Sm^{+2} and Yb^{+2} are monomeric and arene-soluble. This led to the development of rich and unique chemistry.

$(C_5Me_5)_2Sm(THF)_2$ and $(C_5Me_5)_2Yb(THF)$ are readily prepared from $SmI_2(THF)_2$ and $YbBr_2(THF)_2$ in ether solvents.[33,34] The structure of the samarium complex consists of discrete monomeric units, the two C_5Me_5 ring centroids and the two THF ligands define a pseudo-tetrahedral geometry.[35] Solvent-free $(C_5Me_5)_2Sm$ is obtained by facile desolvation/sublimation of $(C_5Me_5)_2Sm(THF)_2$ at 75°C. The most striking feature of the structure of $(C_5Me_5)_2Sm$ is that two C_5Me_5 moieties are non-parallel. The (ring centroid)-Sm-(ring centroid) angle is 140.1° in contrast to the 180° angle found in ferrocene.[36] No substantial intermolecular interactions were found between monomeric units which could be the cause of the distortion. The unsolvated $(C_5Me_5)_2Yb$ also exhibits a bent metallocene structure both in the solid state and in the gas phase.[37,38] The surprising structures of $(C_5Me_5)_2Ln$ (Ln=Sm, Yb) may

contribute to the unusual and unique reactivities associated with these highly sterically unsaturated metal centers. Watson et al.[39] have measured the electrode potentials of the acetonitrile-solvated complexes $(C_5Me_5)_2Ln$ (Ln=Sm, Yb). The values are -2.41V (Sm) and -1.78V (Yb), which are 0.8-0.9V more negative than for the corresponding lanthanide perchlorate+3/+2 couples in acetonitrile. Therefore the reducing ability of the lanthanide(II) ions has been enhanced significantly by the addition of two good electron-donating C_5Me_5 ligands. The high reducing power of the divalent lanthanides, especially Sm^{+2}, coupled with the unique coordination environment, have important consequences on their reactivities.

$(C_5Me_5)_2Sm(THF)_2$ reacts with CO to give a tetrameric species[40], as shown in eq 1.6. The reaction involves reduction of six CO molecules by four electrons and then

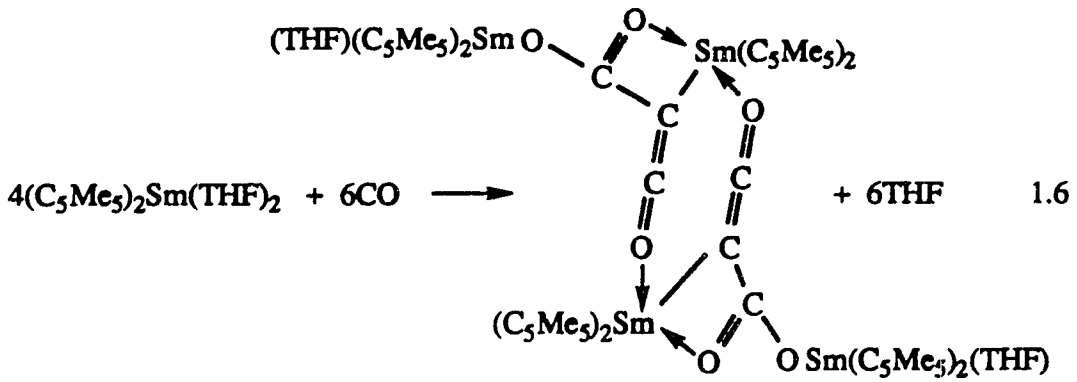

reductive homologation to yield two ketenecarboxylate units. A similar reaction does not occur with $(C_5Me_5)_2Yb$, indicating that reduction potential plays a dominant role in the observed reactivity.

$(C_5Me_5)_2Sm(THF)_2$ reacts with $C_6H_5C{\equiv}CC_6H_5$ to give a black Sm(III) compound as outlined in eq 1.7. Further treatment of $[(C_5Me_5)_2Sm]_2(C_6H_5C{\equiv}CC_6H_5)$ with CO results in a spectacular transformation to give a tetracyclic hydrocarbon (eq. 1.8). Although $(C_5Me_5)_2Yb(Et_2O)$ does not react

$$2(C_5Me_5)_2Sm(THF)_2 + C_6H_5C{\equiv}CC_6H_5 \longrightarrow [(C_5Me_5)_2Sm]_2(C_6H_5C{\equiv}CC_6H_5) \quad 1.7$$

$$[(C_5Me_5)_2Sm]_2(C_6H_5C{\equiv}CC_6H_5) \xrightarrow{2CO}$$

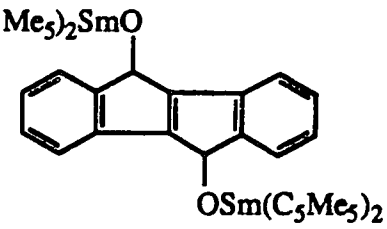

1.8

with $C_6H_5C{\equiv}CC_6H_5$, it interacts with the more electron-rich alkyne $CH_3C{\equiv}CCH_3$ to give a Lewis acid-base adduct $(C_5Me_5)_2Yb(CH_3C{\equiv}CCH_3)$. This represents the first example of η^2-alkyne complex of a lanthanide.[41]

$(C_5Me_5)_2Sm$ reacts rapidly with propene, butene and allylbenzene to give the allyl complexes $(C_5Me_5)_2Sm(\eta^3\text{-}CH_2CHCH_2)$, $(C_5Me_5)_2Sm(\eta^3\text{-}CH_2CHCHMe)$ and $(C_5Me_5)_2Sm(\eta^3\text{-}CH_2CHCHPh)$, respectively, in high yield.[42] The reaction of $(C_5Me_5)_2Sm$ with cyclooctatetraene unexpectedly gave the disproportionation product, $(C_5Me_5)_3Sm$, the first tris-C_5Me_5 metal complex.[13] $(C_5Me_5)_2Yb(OEt_2)$ polymerizes ethylene but it is unreactive toward propene or styrene.[23] It has been reported that $(C_5Me_5)_2Yb$ readily reacts with $(\eta^2\text{-}C_2H_4)Pt(PPh_3)_2$[43] to form the first η^2-olefin lanthanide compound, $(C_5Me_5)_2Yb(\eta^2\text{-}C_2H_4)Pt(PPh_3)_2$.

$(C_5Me_5)_2Sm(THF)_2$ also rapidly reacts with azobenzene in 1:1 or 2:1 molar ratio to yield dark green $(C_5Me_5)_2Sm(PhNNPh)(THF)$ and $[(C_5Me_5)_2Sm]_2(PhNNPh)$, respectively.[44] The dianion $PhNNPh^{-2}$ in the latter compound was stabilized by a cavity-like environment provided by two $(C_5Me_5)_2Sm$ moieties; other dianions stabilized by $(C_5Me_5)_2Sm(\mu\text{-}L)Sm(C_5Me_5)_2$ include L= O,[45] 2H,[46] S,[47] Se,[47] Te,[47] S_3,[47] Se_3,[47] Te_3,[47] N_2,[48] Te_2,[47] CC,[49] styrene,[42] HNNH,[50] PhNNPh,[44] Bi_2[51]. The shortest Sm-Sm distance (3.9Å) was found in $[(C_5Me_5)_2Sm(\mu\text{-}H)]_2$ and indicates that there is no Sm-Sm interaction in any of these

disamarium complexes. The arrangement of four C_5Me_5 ring centroids in these complexes defines either a tetrahedral or square planar geometry. With small bridging ligands, $(C_5Me_5)_2Sm(\mu\text{-}L)Sm(C_5Me_5)_2$ tends to form a structure in which four C_5Me_5 rings adopt a tetrahedral arrangement to minimize steric repulsion among the bulky C_5Me_5 rings (L=O, Figure 1.4). With larger bridging ligands, the four ring centroids define a square plane ($L=Te_2$, Figure 1.5).[52] The variable geometry is to be contrasted with the analogous transition metal complexes, $[(C_5Me_5)_2M(\mu\text{-}L)]_2$ (M=Ti, Zr), which favor a square planar arrangement of the four C_5Me_5 rings due to the strong and directional orbital interactions.[52,53] These findings are consistent with the notion that bonding in the lanthanide complexes is mostly ionic and that steric effects play a more important role than orbital considerations in determining molecular geometry.

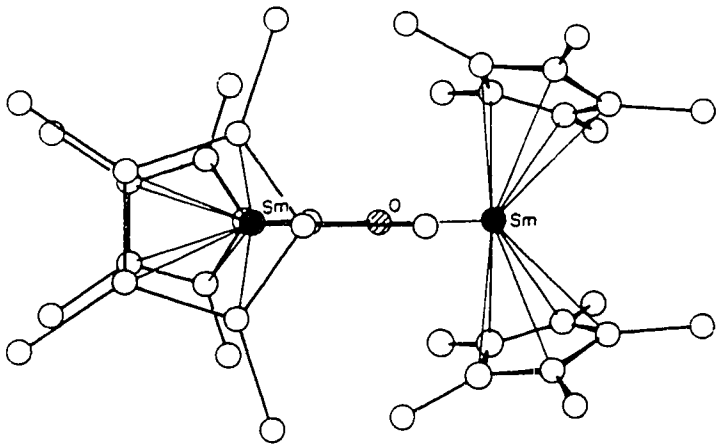

Figure 1.4 Molecular structure of $[(C_5Me_5)_2Sm]_2(\mu\text{-}O)$

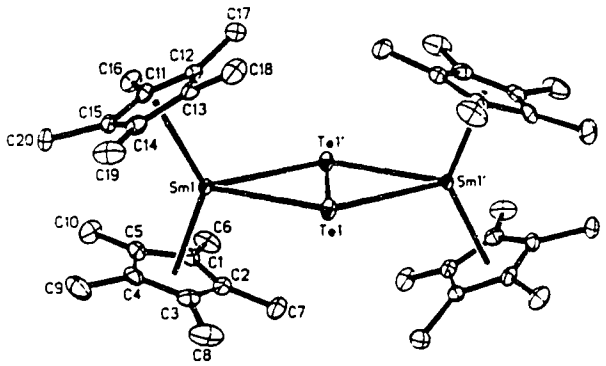

Figure 1.5 Molecular structure of $[(C_5Me_5)_2Sm]_2(\mu\text{-}Te_2)$

1.4. Complexes of the Lanthanides with Hydrotris(pyrazolyl)borate Ligands

1.4.1. The $Tp^{R,R'}$ Ligand System

The hydrotris(pyrazolyl)borate ligands were first introduced by Trofimenko in 1966.[54] A perspective view, with labeling scheme, of substituted hydrotris(pyrazolyl)borate ligands is shown in Figure 1.6. The designation used here

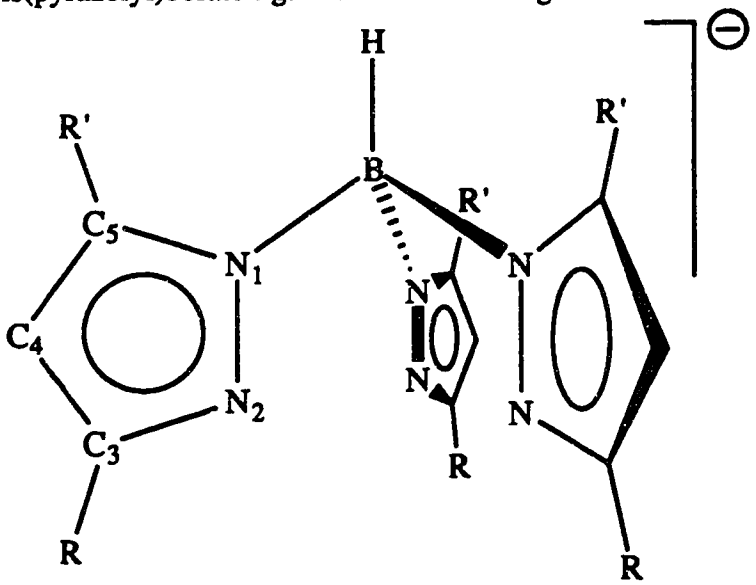

Figure 1.6 A perspective view of $Tp^{R,R'}$

follows Trofimenko's suggestion.[55] Therefore, the hydrotris(pyrazolyl)borate ligands are represented by the abbreviation $Tp^{R,R'}$ with the R and R' denoting the substituents on 3- and 5-positions of the pyrazolyl ring, respectively. Being uninegative and potentially tridentate, these ligands are formally analogous to the cyclopentadienyl ion. Indeed, they form many complexes that are stoichiometrically analogous to cyclopentadienyl or pentamethylcyclopentadienyl counterparts. But they also show differences in steric and electronic properties. A general comparison between $Tp^{R,R'}$ and C_5R_5 ligands, taken from a review by Trofimenko[55], in simplified form, is given in Table 1.1.

Table 1.1 Comparison of C_5R_5 and $Tp^{R,R'}$ Ligands

	C_5R_5	$Tp^{R,R'}$
	Common Features	
electrons donated	6	6
coordination sites occupied	3	3
charge	-1	-1
	Differentiating features	
symmetry of LM fragment	C_{5v}	C_{3v}
substitutable positions	5	10
Cone angle	<146°	>184°
monomeric LMX available? (X=halide)	no, (except Be)	yes

One of the unique features of the $Tp^{R,R'}$ ligands, which differentiates them from C_5R_5 ligand, is the extensive shielding of the coordinated metal ion by the substituents at the 3-position. This is shown by the values of the cone angles:[56] 100°

for C_5H_5 and 146° for C_5Me_5, compared to 184° for Tp, 224° for Tp^{Me2} and 244° for the bulky Tp^{tBu}.[55] It has been established from transition metal chemistry that the effective steric size of the $Tp^{R,R'}$ ligands decreases in the order: $Tp^{tBu} \approx Tp^{tBu,Me} > Tp^{Ph} > Tp^{Me2} > Tp^{Tn} > Tp$. The electron donating ability of the ligands has been inferred from variations in the infrared stretching frequencies of carbonyl groups and in the oxidation potentials of transition metal carbonyl anions containing $Tp^{R,R'}$ ligand and follows the trend:[57] $Tp^{tBu,Me} \approx Tp^{Me2} > Tp^{tBu} > Tp \approx C_5Me_5 > Tp^{Ph}$. It is clear from the above considerations that an important feature of the $Tp^{R,R'}$ ligands is the facile tunability of their steric size and electronic properties by judicious choice of appropriate substituents.

The substituted hydrotris(pyrazolyl)borate ligands are synthesized in a straightforward fashion via thermolysis of a mixture of an alkali metal tetrahydroborate and an excess pyrazole in a high boiling solvent or as a melt, eq 1.9. The pyrazoles in

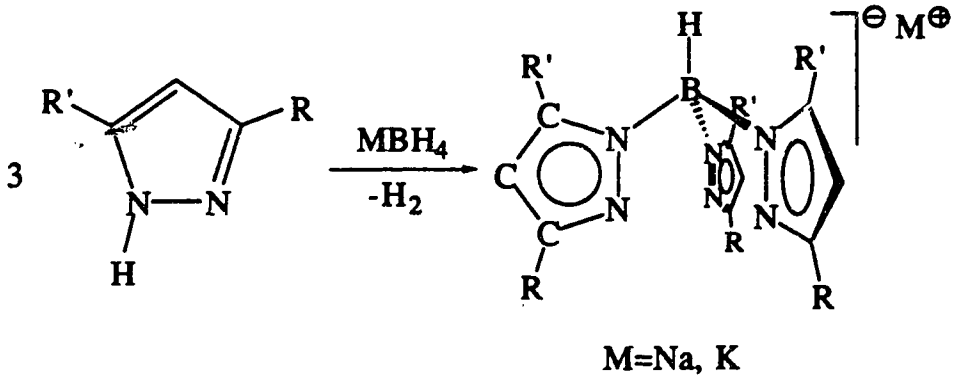

1.9

turn are prepared by cyclocondensation of the appropriate 1,3-diketone and hydrazine, eq 1.10. Substituents at the 3- and 5-positions are introduced during the synthesis of the diketone component, most often by a Claisen condensation of an ester and a ketone. When R and R' are different, the larger substituent tends to occupy the 3-position of the pyrazolyl rings to minimize steric repulsions between substituents. This

preference is most clearly manifested in the Tp^{tBu} and $Tp^{tBu,Me}$ ligands in which sterically very different substituents are present.

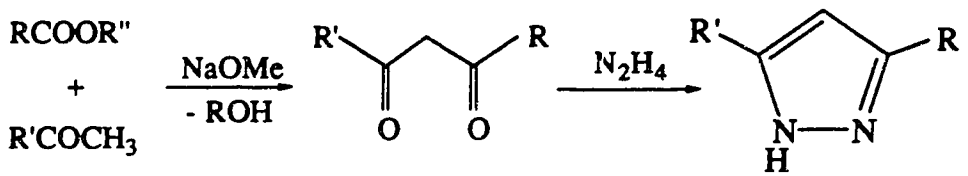

1.10

1.4.2. $(Tp)_3Ln$ Complexes

The first lanthanide pyrazolylborates were the $(Tp)_3Ln$ complexes prepared by Bagnall and Takats et al.[58] They were synthesized by simply mixing $LnCl_3(H_2O)_n$ with KTp in aqueous solution (eq 1.11).

$$LnCl_3(H_2O)_n + 3KTp \xrightarrow{H_2O} Tp_3Ln + 3KCl \qquad 1.11$$

$$Ln = La\text{-}Lu$$

These complexes are remarkable in that anhydrous complexes were obtained from water, and this is attributed to the ability of the Tp ligand to satisfy the high coordination number demanded by large lanthanide ions. The anhydrous nature of $(Tp)_3Ln$ complexes from aqueous reaction also suggests that these complexes will not behave as Lewis acids, which is in contrast to the corresponding triscyclopentadienyl lanthanide complexes. The $(Tp)_3Yb$ compound has been crystallographically characterized.[59] The Yb is surrounded in a bicapped trigonal prismatic arrangement, by eight pyrazolyl nitrogens from two tridentate and one bidentate Tp ligands. The spectroscopic data reveal that the complex is stereochemically rigid in solution and possesses a structure which is identical to the solid state form.[60]

1.4.3. $(Tp)_mLnCl_{3-m}$ (m=1, 2) and $(Tp)_2Ln$ Complexes

The mixed ligand complexes $TpLnCl_2(THF)_{1.5}$ (Ln=Er)[58,61] and $(Tp)_2LnCl(THF)$ (Ln=Er, Yb, Lu)[62] were prepared by reaction of $LnCl_3$ with KTp in THF in 1:1 and 1:2 molar ratio, respectively. However, complications were encountered when the synthesis was extended to the early lanthanides.[61] The pure Pr and Ce complexes could not be isolated This is reminiscent of the behaviour of the early lanthanides, attempted synthesis of the mono-cyclopentadienyl and bis-cyclopentadienyl derivatives failed also. In contrast to the tris-Tp compounds, the mixed complexes are moisture sensitive. The "mixed sandwich" complexes $TpLn(C_8H_8)$ (Ln=Er, Lu) was isolated by reaction of $TpLnCl_2(THF)_{1.5}$ with $K_2C_8H_8$ at -40°C.[61] The synthetic usefulness of $(Tp)_mLnCl_{3-m}$ (m=1, 2) compounds was plagued by ligand redistribution to $(Tp)_3Ln$ complexes. Only limited success has been achieved with certain types of ligands. Takats and co-workers[62] reported the synthesis of $(Tp)_2Ln(acac)$ (Ln=Yb, Lu; acac=dpm, tfac). Recently Jones and coworkers have prepared the full range of lanthanide complexes, $(Tp)_2Ln(X)$ (Ln=La-Lu; X=acac, ba, dbm).[63,64] These compounds are not only stable to moisture and air but also towards ligand redistribution. The crystal structures of $(Tp)_2Ce(acac)$ and $(Tp)_2Yb(acac)$ have been determined,[63] and revealed that both Ce and Yb are eight-coordinate with two tridentate Tp ligands and a bidentate acac group. The ^1H NMR spectra of the complexes exhibited only a single set of pyrazolyl ring resonances, implying that the molecules are fluxional in solution. The synthesis of $(Tp)_2LnY$ (Ln=Sm, Dy, Yb, Lu; Y=tropolonate, benzoate, acetate, oxalate) have also been reported.[65,66] Reger and coworkers[67] reported the synthesis and crystal structure of dimeric $[(Tp)_2Sm(\mu\text{-}O_2CPh)]_2$. More recently, Sella and coworkers reported the preparation of $(Tp^{Me2})_2Ln(OTf)$ (Ln=La, Ce, Pr, Nd, Sm, Eu, Gd, Ho, Yb).[68] For the early

lanthanides, these complexes are seven-coordinate with an η^1-bound triflate, while the compounds of late lanthanides are six-coordinate and the triflate acts as innocent counter-ion. The reduced coordination number is again consistent with the lanthanide contraction.

While this work was in progress, the preparation of the divalent complexes, $(Tp)_2Ln(THF)_n$ and $(Tp^{Me2})_2Ln$ (Ln=Sm, Yb, Eu) was reported by Jones and Evans[69], although the structure of the complexes was not determined. Marques has also communicated the synthesis of disolvated $(Tp)_2Sm(THF)_2$ and its oxidative-addition reactions with organic halides[70]. Finally, Sella and co-workers[71] reported the synthesis and structure of $(Tp^{Me2})_2Yb$.

1.5. Scope of the Thesis

Although divalent lanthanide chemistry has undergone a rapid growth during the past decade, major advances were limited to the bis-C_5R_5 ligand system. Recently there has been increasing interests to extend the scope of the ligand systems beyond C_5R_5 in anticipation of novel structures and reactivity patterns. It was our premise that the $Tp^{R,R'}$ ligand system was unique and well suited to divalent lanthanides. To begin the exploration, the following aspects were of interest:

(1) To establish the range of bis-ligand complexes, $(Tp^{R,R'})_2Ln$, as a function of the substituents R and R'.

(2) To explore the possibility of preparing half-sandwich type complexes, $(Tp^{R,R'})LnX$.

(3) To initiate reactivity studies on $(Tp^{R,R'})_2Ln$ and $Tp^{R,R'}LnX$ complexes, if their preparation was successful.

1.6. References

(1) Hampel, C. A. E. *The Encyclopedia of the Chemical Elements; Reinhold Publishing Corp.: New York,* **1968**.

(2) Cotton, F. A.; Wilkinson, G. *Advanced Inorganic Chemistry, 5th Edn. Wiley. New York* **1988**,

(3) Marks, T. J. *Prog. Inorg. Chem.* **1978**, *24*, 51.

(4) Yamamoto, A. *Organotransition Metal Chemistry, Wiley. New York 1986* **1986**,

(5) Birminham, J. M.; Wilkinson, G. *J. Am. Chem. Soc.* **1956**, *78*, 42.

(6) Rebizant, J.; Apostolidis, C.; Spirlet, M. R.; Kanellakopulos, B. *Acta Crystallogr., Sect. C* **1988**, *C44*, 614.

(7) Eggers, S. H.; Hinrichs, W.; Kopf, J.; Jahn, W.; Fischer, R. D. *J. Organomet. Chem.* **1986**, *311*, 313.

(8) Eggers, S. H.; Schultze, H.; Kopf, J.; Fischer, R. D. *Angew. Chem., Int. Ed. Engl.* **1986**, *25*, 656.

(9) Benetollo, F.; Bombieri, G.; Castellani, C. B.; Jahn, W.; Fischer, R. D. *Inorg. Chim. Acta* **1984**, *95*, L7.

(10) Ni, C.; Deng, D.; Qian, C. *Inorg. Chim. Acta* **1985**, *110*, L7.

(11) Spirlet, M. R.; Rebizant, J.; Apostolidis, C.; Kanellakopulos, B. *Inorg. Chim. Acta* **1987**, *139*, 211.

(12) Deacon, G. B.; Gatehouse, B. M.; Platts, S. N.; Wilkinson, D. L. *Aust. J. Chem.* **1987**, *40*, 907.

(13) Evans, W. J.; Gonzales, S. L.; Ziller, J. W. *J. Am. Chem. Soc.* **1991**, *113*, 7423.

(14) Hazin, P. N.; Huffman, J. C.; Bruno, J. W. *Organometallics* **1987**, *6*, 23.

(15) van der Heijden, H.; Schaverien, C. J.; Orphen, A. G. *Organometallics* **1989**, *8*, 255.

(16) Heeres, H. J.; Meetsma, A.; Teuben, J. H. *J. Chem. Soc., Chem. Commun.* **1988**, 962.

(17) Heeres, H. J.; Meetsma, A.; Teuben, J. H.; Rogers, R. D. *Organometallics* **1989**, *9*, 2637.

(18) Wayda, A. L.; Evans, W. J. *Inorg. Chem.* **1980**, *19*, 2190.

(19) Tilley, T. D.; Andersen, R. A. *Inorg. Chem.* **1981**, *20*, 3267.

(20) Jeske, G.; Lauke, H.; Mauermann, H.; Swepston, P. N.; Schumann, H.; Marks, T. J. *J. Am. Chem. Soc* **1985**, *107*, 8091.

(21) Evans, W. J.; Wayda, A. L.; Hunter, W. E.; Atwood, J. L. *J. Chem. Soc., Chem. Commun.* **1981**, 292.

(22) Evans, W. J.; Meadows, J. H.; Wayda, A. L.; Hunter, W. E.; Atwood, J. L. *J. Am. Chem. Soc.* **1982**, *104*, 2008.

(23) Watson, P. L.; Herskovitz, T. *ACS Symp. Ser.* **1983**, *212*, 459.

(24) Watson, P. L. *J. Am. Chem. Soc.* **1982**, *104*, 337.

(25) Watson, P. L.; Parshall, G. W. *Acc. Chem. Res.* **1985**, *18*, 51 (and references therein).

(26) Watson, P. L.; Roe, D. C. *J. Am. Chem. Soc.* **1982**, *104*, 6471.

(27) Watson, P. L. *J. Am. Chem. Soc.* **1983**, *105*, 6491.

(28) Morss, L. R. *Chem. Rev.* **1976**, *76*, 827.

(29) Varlashkin, P. G.; Peterson, J. R. *J. Less-Common Met.* **1983**, *94*, 333.

(30) Fischer, E. O.; Fischer, H. *J. Organomet. Chem.* **1965**, *3*, 181.

(31) Namy, J. L.; Girard, P.; Kagan, H. B. *Nouv. J. Chim.* **1981**, *5*, 479.

(32) Watt, G. W.; Gillow, E. W. *J. Am. Chem. Soc.* **1969**, *91*, 775.

(33) Watson, P. L. *J. Chem. Soc., Chem. Commun.* **1980**, 652.

(34) Evans, W. J.; Grate, J. W.; Choi, H. W.; Bloom, I.; Hunter, W. E.; Atwood, J. L. *J. Am. Chem. Soc.* **1985**, *107*, 941.

(35) Evans, W. J.; Bloom, I.; Hunter, W. E.; Atwood, J. L. *J. Am. Chem. Soc.* **1981**, *103*, 6507.

(36) Evans, W. J.; Hughes, L. A.; Hanusa, T. P. *Organometallics* **1986**, *5*, 1276.

(37) Andersen, R. A.; Boncella, J. M.; Burns, C. J.; Green, J. C.; Hohl, D.; Rosch, N. *J. Chem. Soc., Chem. Commun.* **1986**, 405.

(38) Burns, C. J. *Ph.D. Thesis, University of California, Berkeley* **1987**,

(39) Watson, P. L.; Tulip, T. H.; Williams, I. *Organometallics* **1990**, *9*, 1999.

(40) Evans, W. J.; Grate, J. W.; Hughes, L. A.; Zhang, H.; Atwood, J. L. *J. Am. Chem. Soc.* **1985**, *107*, 3728.

(41) Burns, C. J.; Andersen, R. A. *J. Am. Chem. Soc.* **1987**, *109*, 941.

(42) Evans, W. J.; Ulibarri, T. A.; Ziller, J. W. *J. Am. Chem. Soc.* **1990**, *112*, 2314.

(43) Burns, C. J.; Andersen, R. A. *J. Am. Chem. Soc.* **1987**, *109*, 915.

(44) Evans, W. J.; Drummond, D. K.; Chamberlain, L. R.; Doedens, R. J.; Bott, S. G.; Zhang, H. M.; Atwood, J. L. *J. Am. Chem. Soc.* **1988**, *110*, 4983.

(45) Evans, W. J.; Grate, J. W.; Bloom, I.; Hunter, W. E.; Atwood, J. L. *J. Am. Chem. Soc.* **1985**, *107*, 405.

(46) Evans, W. J.; Bloom, I.; Hunter, W. E.; Atwood, J. L. *J. Am. Chem. Soc.* **1983**, *105*, 1401.

(47) Evans, W. J.; Rabe, G. W.; Ziller, J. W.; Doedens, R. *Inorg. Chem.* **1994**, *33*, 2719.

(48) Evans, W. J.; Ulibarri, T. A.; Ziller, J. W. *J. Am. Chem. Soc.* **1988**, *110*, 6877.

(49) Evans, W. J.; Rabe, G. W.; Ziller, J. W. *J. Organomet. Chem.* **1994**, *483*, 21.

(50) Evans, W. J.; Kociok-Kohn, G.; Leong, V. S.; Ziller, J. W. *Inorg. Chem.* **1992**, *31*, 3592.

(51) Evans, W. J.; Gonzales, S. L.; Ziller, J. W. *J. Am. Chem. Soc.* **1991**, *113*, 3592.

(52) Evans, W. J.; Keyer, R. A.; Ziller, J. W. *J. Organomet. Chem.* **1993**, *450*, 115 and references therein.

(53) Lauher, J. W.; Hoffmann, R. *J. Am. Chem. Soc.* **1976**, *98*, 1729.

(54) Trofimenko, S. *J. Am. Chem. Soc.* **1966**, *88*, 1842.

(55) Trofimenko, S. *Chem. Rev.* **1993**, *93*, 943.

(56) Tolman, C. A. *Chem. Rev.* **1977**, *77*, 313.

(57) Kitajima, N.; Tolman, W. B. *Progr. Inorg. Chem. in press* **1995**,

(58) Bagnall, K. W.; Tempest, A. C.; Takats, J.; Masino, A. P. *Inorg. Nucl. Chem. Lett.* **1976**, *12*, 555.

(59) Stainer, M. V. R.; Takats, J. *Inorg. Chem.* **1982**, *21*, 4050.

(60) Stainer, M. V. R.; Takats, J. *J. Am. Chem. Soc.* **1983**, *105*, 410.

(61) Masino, A. P. *Ph.D. Thesis, University of Alberta* **1978**,

(62) Moffat, W. D.; Stainer, M. V. R.; Takats, J. *Inorg. Chim. Acta* **1987**, *139*, 75.

(63) Moss, M. A. J.; Jones, C. J.; Edwards, A. J. *J. Chem. Soc., Dalton Trans.* **1989**, 1393.

(64) Moss, M. A. J.; Jones, C. J. *Polyhedron* **1990**, *9*, 697.

(65) Moss, M. A. J.; Jones, C. J. *J. Chem. Soc. Dalton Trans.* **1990**, 581.

(66) Moss, M. A. J.; Jones, C. J. *Polyhedron* **1989**, *8*, 2367.

(67) Reger, D. L.; Knox, S. J.; Lindeman, J. A.; Lebioda, L. *Inorg. Chem.* **1990**, *29*, 416.

(68) Liu, S. Y.; Maunder, G. H.; Sella, A.; Stephenson, M.; Tocher, D. A. *Inorg. Chem.* **1995**, *in press*,

(69) Moss, M. H. J.; Kresinski, R. A.; Jones, C. J.; Evans, W. J. *Polyhedron* **1993**, *12*, 1953.

(70) Marques, N. *Rare Earths '92, Kyoto, Japan, June 1992; Abstract PIK-11* **1992**,

(71) Maunder, G. H.; Sella, A.; Tocher, D. A. *J. Chem. Soc., Chem. Commun.* **1994**, 885.

Chapter 2

Synthesis and Characterization of Divalent Lanthanide Hydrotris(pyrazolyl)borates: $(Tp')_2Ln$ ($Tp'=Tp^{Me2}$, Tp^{Ph}, Tp^{Tn}; Ln=Sm,Yb), a Structural Comparison

2.1. Introduction

The chemistry of divalent lanthanides has been extensively investigated during the past decade[1,2]. Our entry into this field was prompted by the remarkable reactivity of $(C_5Me_5)_2Ln$ (Ln=Sm, Yb) towards organic and inorganic substrates, as demonstrated especially by Evans[3-5], Andersen[6,7] and their co-workers. The high reactivity is mainly attributed to the strong reducing ability of Ln(II) and to the coordinative unsaturation of the metal centers. Since it is well recognized that the nature of the coordinated ligands plays an important role in determining coordination number, geometry, redox ability and reactivity of metal complexes, recent interest has focused on extending the scope of ligand systems beyond cyclopentadienyl and its analogues. Bis-ligand complexes of divalent lanthanides with alkoxide[8], amide[9,10], chalcogenate[11] and benzamidinate[12] have been reported and shown to possess interesting chemistry.

The hydrotris(pyrazolyl)borate ligand (Tp) and its functionalized derivatives ($Tp^{R,R'}$), which in a limited sense can be regarded as cyclopentadienyl analogues, offer a versatile series of such ligands where the steric size can be fine-tuned by judicious choice of the substituents. These ligands are more advantageous than other ligand systems since they offer steric and electronic control of the coordination environment of metal centers and have been widely used to achieve low coordination number, to enhance the stability of complexes, and to provide a protective pocket for isolation of unique metal complexes[13].

The poly(pyrazolyl)borate ligands have been found to bind to a wide range of metals. The most extensively used hydrotris(pyrazolyl)borate ligand in inorganic and organometallic chemistry is Tp^{Me2} because of its easy synthesis and formal analogy to C_5Me_5. Sandwich-type complexes of the alkaline earth metals, main group and transition metals are known and include, $(Tp^{Me2})_2M$ (M=Mg[14], Zn[15] , Cu[16], Fe[17], Pb[18], Ca, Sr, Ba[19]). One of the second-generation Trofimenko ligands is Tp^{Ph} with a steric demand larger than that of Tp^{Me2}. As a result, the number of bis-Tp^{Ph} complexes is very limited. Only two bis-hydrotris(3-phenylpyrazolyl)borato complexes of divalent transition metals, $(Tp^{Ph})_2Fe$ and $(Tp^{Ph})_2Mn$, have been reported and crystallographically characterized[20]. Interestingly, replacement of Tp with Tp^{Ph} in $(Tp^{R,R'})_2Fe$ had a dramatic effect on Fe^{III}/Fe^{II} reduction potential ; 0.58V and 1.09V, respectively. The steric demand of Tp^{Tn} would be expected to fit between those of Tp^{Me2} and those of Tp^{Ph}, but experimental findings[21] indicate that Tp^{Tn} is less sterically hindered than Tp^{Me2}. With large divalent lanthanides, formation of $(Tp')_2Ln$ ($Tp'=Tp^{Me2}$, Tp^{Ph}, Tp^{Tn}) should be feasible. The preparation of these complexes was undertaken with a view to study their reactivity and to establish how changes in size of the ligands may effect the coordination geometry of lanthanide centers.

While this work was in progress, Jones and Evans[22] reported the preparation of the divalent complexes $(Tp)_2Ln(THF)_n$ and $(Tp^{Me2})_2Ln$ (Ln=Sm, Yb, Eu), although no structure was reported. Marques has also communicated the synthesis of disolvated $(Tp)_2Sm(THF)_2$ and its oxidative-addition reactions with organic halides[23]. Sella and co-workers[24] reported the structure of $(Tp^{Me2})_2Yb$. In this chapter the synthesis and characterization of a series of bis-ligand complexes $(Tp')_2Ln$ (Ln=Sm, Yb; $Tp'=Tp^{Me2}$, Tp^{Ph}, Tp^{Tn}) is reported and a structural comparison made.

2.2. Synthetic Aspects

2.2.1. Synthesis of $(Tp^{Me2})_2Ln$ (Ln=Sm, 1; Yb, 2)

Addition of two equiv of KTp^{Me2} to a THF solution of LnI_2 afforded a deep purple precipitate and an almost colorless supernatant, eq 2.1. The insolubility of $(Tp^{Me2})_2Ln$ in THF was beyond expectation and attempts to separate the purple product from KI with repeated extraction of the mixture with THF were unsuccessful.

$$LnI_2 + 2KTp^{Me2} \xrightarrow{THF} \underset{\text{purple}}{(Tp^{Me2})_2Ln\downarrow} + 2KI\downarrow \qquad 2.1$$

Although Moss et al.[22] had reported that complexes **1** and **2** can be purified by sublimation under dynamic vacuum, in our hands this process gave products in low yields. A better synthetic strategy for preparation of pure **1** and **2** had to be developed. We found that complexes **1** and **2** could be synthesized more conveniently by using the sodium salt of the ligand (eq 2.2). The advantage here is that NaI is reasonably

$$LnI_2 + 2NaTp^{Me2} \xrightarrow{THF} \underset{\substack{\text{Ln=Sm, 1, purple} \\ \text{Yb, 2, purple}}}{(Tp^{Me2})_2Ln\downarrow} + 2NaI \qquad 2.2$$

soluble in THF, therefore pure **1** and **2** can be simply isolated by inverse filtration and yields are almost quantitative. Both **1** and **2** are air-sensitive, but interestingly not moisture-sensitive. Thus stirring a mixture of **1** with two equiv of H_2O in toluene resulted in no reaction in a couple of days. Compounds **1** and **2** are insoluble in common aliphatic, aromatic and ether type of solvents. They react with chlorinated solvents. Consequently, solution NMR is not accessible and characterization relies on elemental analysis, mass spectrometry and IR spectroscopy. The solid-state IR spectra of **1** and **2** are almost identical, indicating they have the same structure. The

characteristic B-H stretching bands are centered at ca. 2538 cm^{-1}. The formulation of **1** and **2** is consistent with elemental analysis, mass spectra and X-ray crystallographic data (vide infra). The highest intensity peak (100%) in the mass spectrum of **1** is the molecular ion at 746 $\{(Tp^{Me2})_2Sm\}^+$. Other fragments include 544 (41%) for $\{(Tp^{Me2})Sm(pz)\}^+$ and 96 (35%) for $(pzH)^+$. The molecular ion $\{(Tp^{Me2})_2Yb\}^+$ was observed only as 24.7% of the most intense peak, $(pzH)^+$.

2.2.2. Synthesis of $(Tp^{Ph})_2Ln$ and $(Tp^{Tn})_2Ln$ complexes (Ln=Sm, Yb)

The $(Tp')_2Ln$ (Ln=Sm, Yb; $Tp'=Tp^{Ph}$, Tp^{Tn}) were readily obtained by reaction of LnI_2 with KTp' in 1:2 molar ratio in THF, as outlined in eq 2.3. In contrast to

$$LnI_2 + 2KTp' \longrightarrow (Tp')_2Ln + 2KI \qquad 2.3$$

Ln=Sm, $Tp'=Tp^{Ph}$, **3**; $Tp'=Tp^{Tn}$, **5**
Yb, $Tp'=Tp^{Ph}$, **4**; $Tp'=Tp^{Tn}$, **6**

complexes **1** and **2**, all of these samarium and ytterbium compounds are soluble in THF and separation of bis-ligand complexes from KI is easily achieved by filtration. The compounds are intensely colored; the samarium complexes are dark green; the ytterbium compounds are dark red. The colors are not unusual, and resemble the corresponding cyclopentadienyl analogues. Mass spectra of the complexes display molecular ions $\{(Tp')_2Ln\}^+$ (Ln=Sm. Yb, $Tp'=Tp^{Ph}$, Tp^{Tn}) with the expected isotopic patterns. The solid-state IR spectra of **3-6** display H-B stretching bands which are at higher frequencies than those in free ligands. As an example, the B-H stretch in **3** is at 2476 cm^{-1} compared to 2422 cm^{-1} in KTp^{Ph}. In addition, IR spectra of compounds **5** and **6** exhibit no bands attributable to THF, suggesting the solvent-free nature, although Tp^{Tn} is less bulky than Tp^{Me2}.

The high solubility of complexes **3-6** allows NMR to be used as a tool for their characterization. The ^1H NMR spectra of **3** and **4**, are shown in Figure 2.1 and

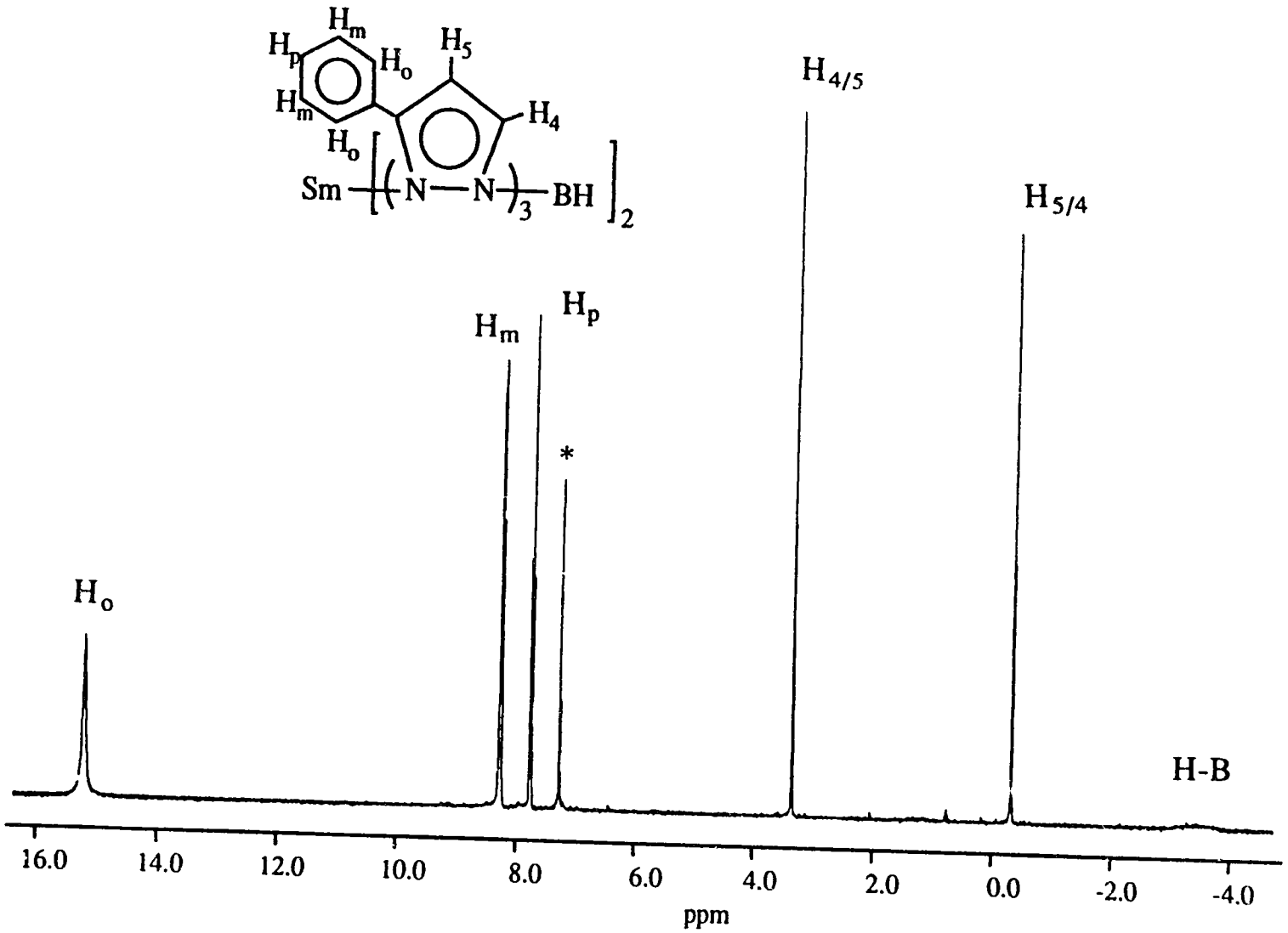

Figure 2.1 400MHz ^{1}H NMR spectrum of $(Tp^{Ph})_2Sm$ (3) in benzene-d_6. Here and elsewhere, the residual solvent proton resonance(s) is (are) marked with *.

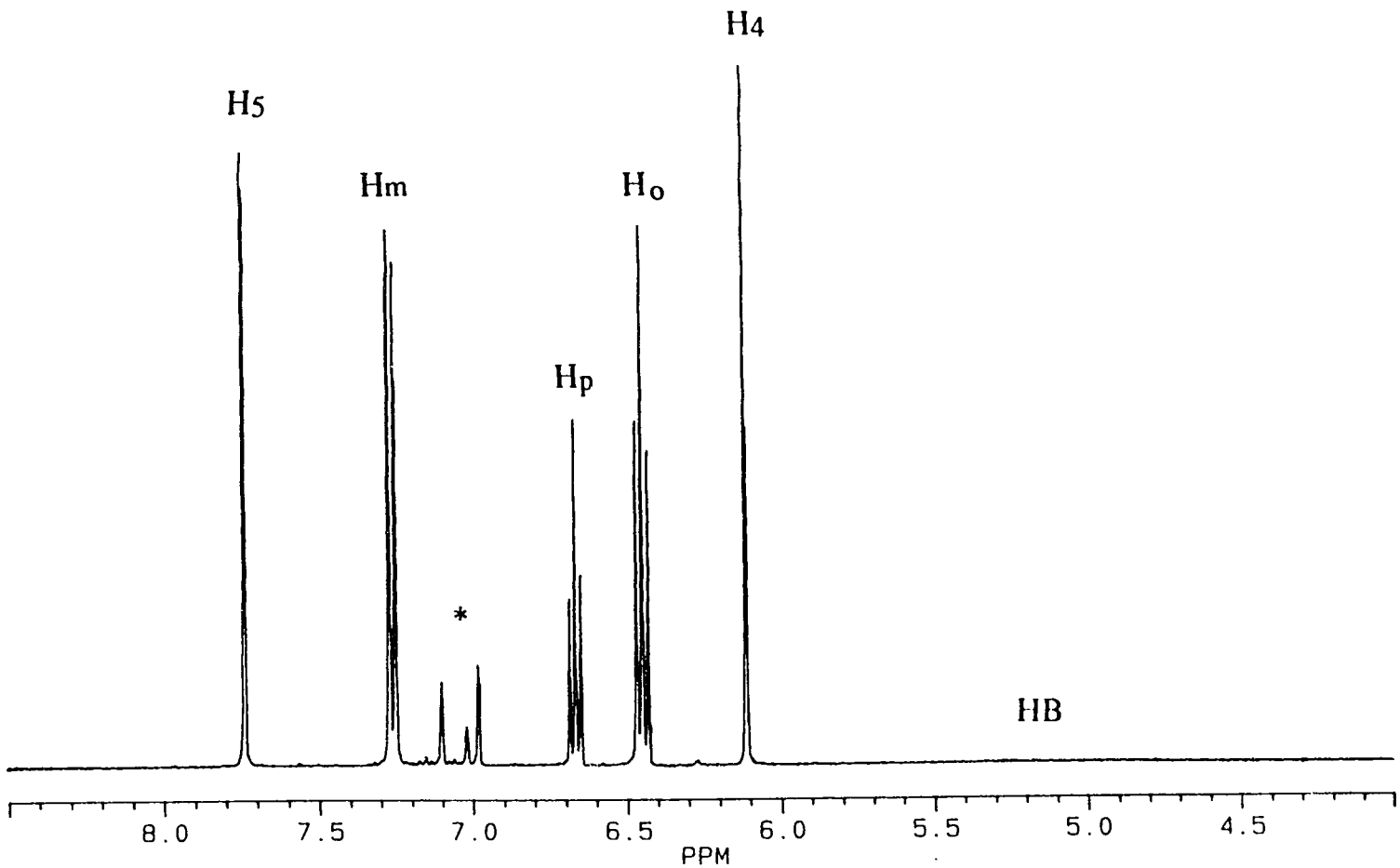

Figure 2.2 400MHz ^{1}H NMR spectrum of $(Tp^{Ph})_2Yb$ (**4**) in toluene-d8

Figure 2.2, respectively. They exhibit only one set of pyrazolyl group resonances, five signals with ratio of 1:1:2:2:1, indicating the presence of highly symmetric solution structure which is responsible for the magnetic equivalence of six pyrazolyl rings. This is to be contrasted with the situation with $(Tp^{Ph})_2Fe$ where fourteen proton resonances were observed.[20] It is possible that in the more sterically hindered iron complex the phenyl rings are not freely rotating causing the appearance of a more complex ^1H NMR spectrum. In the spectrum of the diamagnetic ytterbium complex, the signals exhibit the expected chemical shifts and coupling patterns. The doublet resonances at 7.75 ppm and 6.10 ppm, with coupling constant of 2 Hz, belong to two different pyrazolyl ring hydrogens. The signals at 7.30 (dd), 6.68 (tt), and 6.42 (t) ppm are assigned to ortho-, para-, meta-phenyl hydrogens, respectively, according to the coupling pattern and integration of the signals. In the spectrum of complex **4**, the resonances are subject to isotropic shift due to the paramagnetic samarium center. The isotropic shift consists of two components:[25,26] the contact and the pseudocontact shift. Because of weak interaction between lanthanide f-orbitals and ligand orbitals, the paramagnetic shift of lanthanide complexes is mainly induced via the pseudocontact mechanism, i.e., "through space" interaction between paramagnetic electron and the spin of the resonating nuclei. The magnitude of the shift is inversely proportional to the cube of the distance between metal atom and the observed nucleus (eq 2.4). In eq 2.4, $(\Delta\nu/\nu_o)_{pc}$ is the pseudocontact shift, D1 and D2 are the molecular magnetic anisotropies, r, θ and Ω are the polar coordinates of the NMR nucleus in the coordinate system defined by the magnetic axes of the complex.[25] By examining the

$$\left(\frac{\Delta\nu}{\nu_o}\right)_{pc} = D_1 \frac{(3\cos^2\theta - 1)}{r^3} + D_2 \frac{(\sin^2\theta \cos 2\Omega)}{r^3} \qquad 2.4$$

solid state structure of $(Tp^{Ph})_2Sm$, it is clear that the ortho-phenyl hydrogen is closer to Sm than meta- and para-phenyl hydrogens. Therefore we postulate that the ortho-phenyl hydrogens are much more affected, and on this basis the broad and much shifted singlet is assigned to the ortho-phenyl hydrogens. The hydrogens on the pyrazolyl rings are shifted to higher field, but remain doublets ($^3J = 2$ Hz).

The ^1H NMR spectra of complexes **5** and **6** reveal that all six pyrazolyl rings are equivalent at room temperature, which is similar to that observed in $(Tp^{Tn})_2Co$.[21]. No resonances are seen for coordinated THF. Thus, the coordination environment provided by the two Tp^{Tn} ligands is still too congested to allow THF to coordinate to the metal centers. In the ^1H NMR spectrum of paramagnetic complex **6**, the signal at 13.6 ppm exhibits the largest isotropic shift and is attributed to 3'-H proton on the thienyl ring due to its proximity to Sm (Figure 2.3). The other two protons (4'-H and 5'-H) on thienyl ring are less affected, consistent with their increasing distance from Sm.

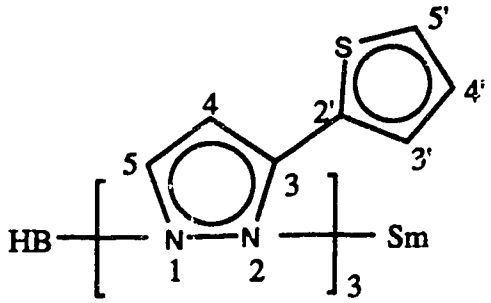

Figure 2.3 Diagram and numbering scheme of $(Tp^{Tn})_2Sm$

2.3. Solid State Structures of 1-4.

ORTEP views of $(Tp^{Me2})_2Sm$, $(Tp^{Me2})_2Yb$, $(Tp^{Ph})_2Sm$ and $(Tp^{Ph})_2Yb$ are shown in Figures 2.4-2.7, respectively. Tables 2.1 and 2.2 list the important bond lengths and bond angles. The crystals consist of discrete, well-separated monomeric

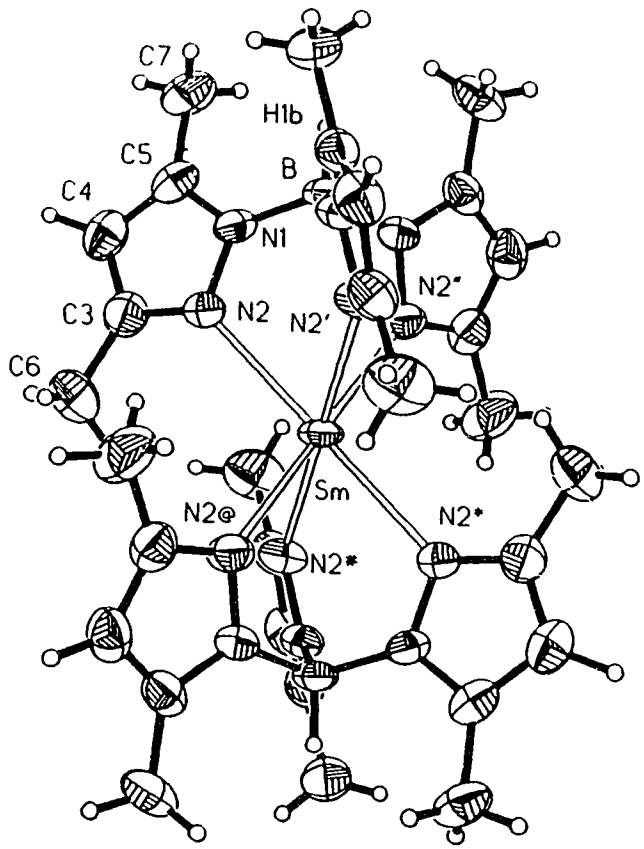

Figure 2.4 ORTEP view of $(Tp^{Me2})_2Sm$ (1)

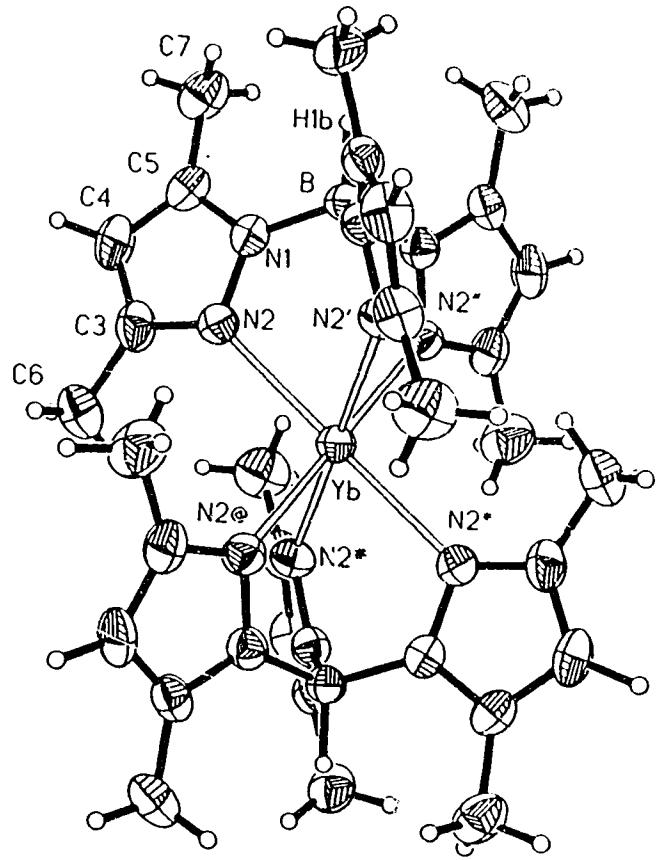

Figure 2.5 ORTEP view of $(Tp^{Me2})_2Yb$ (2)

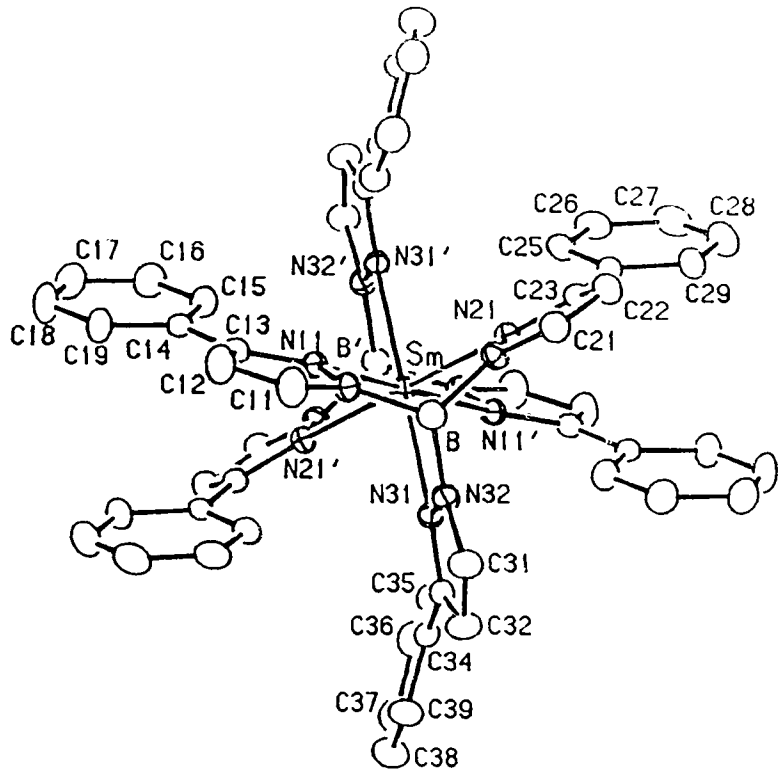

Figure 2.6 ORTEP view of $(Tp^{Ph})_2Sm$ (3)

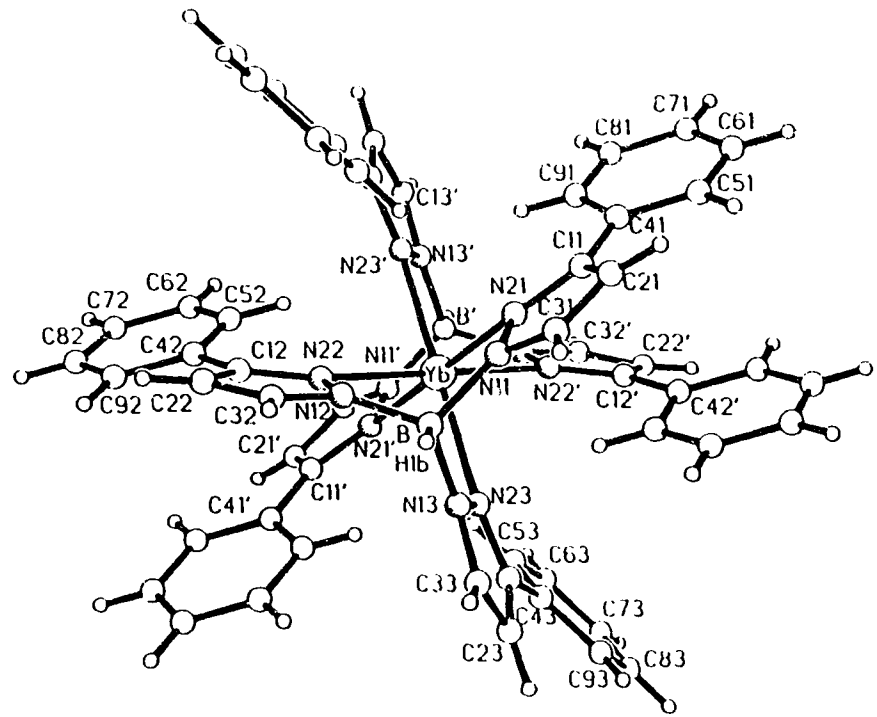

Figure 2.7 ORTEP view of $(Tp^{Ph})_2Yb$ (4)

Table 2.1 Selected Bond Lengths and Non-bonded Contacts (Å) for $(Tp^{Me2})_2Sm$ (**1**), $(Tp^{Me2})_2Yb$ (**2**), $(Tp^{Ph})_2Sm$ (**3**) and $(Tp^{Ph})_2Yb$ (**4**)

	1	**2**	**3**	**4**
Ln-N				
av	2.617(4)	2.482(5)	2.676(32)	2.545(24)
range			2.647(3)-2.711(3)	2.530(3)-2.573(3)
Ln--B	3.627(3)	3.474(4)	3.609(5)	3.435(4)

Table 2.2 Selected Bond Angles (deg) for $(Tp^{Me2})_2Sm$ (1), $(Tp^{Me2})_2Yb$ (2), $(Tp^{Ph})_2Sm$ (3) and $(Tp^{Ph})_2Yb$ (4)

	1	2	3	4
N-Ln-N (intra)				
av	75.5(1)	79.5(2)	77(2)	81(3)
range			75.19(8)-78.22(8)	78.4(1)-83.4(1)
N-Ln-N (inter)				
av	104.5(1)	100.5(2)	104(2)	99(3)
range			101.78(8)-104.81(8)	96.6(1)-101.6(1)
N-B-N				
av	110.9(2)	110.6(3)	112(2)	112(2)
range			110.7(3)-114.1(3)	110.2(3)-113.5(4)
Torsion Angles				
Ln-N-N-B				
av	21.0(3)	20.3(4)	10(2)	10(3)
range			7.6(4)-12.0(4)	5.6(4)-12.0(3)

units with no unusual intermolecular contacts. The complexes are all six-coordinate, with one Tp ligand occupying one face of a trigonally distorted octahedron and the other Tp ligand spanning the opposite face. The two tridentate Tp ligands adopt a staggered conformation about B-Sm-B axis. The solid-state structures of **1** and **2** have a crystallographically-imposed S_6–$\bar{3}$ symmetry with the Ln (Ln=Sm, **1**; Yb, **2**), both boron atoms and their covalently-bonded hydrogens lying on the crystallographic C_3 axis at (0, 0, 0) in the unit cell. They are isostructural with $(Tp^{Me2})_2Pb$[18] and $(Tp^{Me2})_2Ba$.[19] The $(Tp^{Me2})_2Mg$[14] complex has lower C_i symmetry and this is attributed to the smaller ionic radius of Mg, to accommodate two ligands around metal center a more distorted structure results. The structures of **3** and **4** have C_i symmetry. As observed in the main group complexes, $(Tp^{Me2})_2M$ (M=Mg, Pb, Ba), the planes defined by the nitrogen donor atoms from each $Tp^{R,R'}$ ligand in **1-4** are parallel. The "linear sandwich" structures of complexes **1-4** are in contrast to the "bent metallocene" arrangement found in $(C_5Me_5)_2Sm$[27] and the analogous Eu(II)[27] complex. The trigonal distortion of the coordination geometry is evidenced by the less than the ideal octahedral value of 90° for the intraligand N-Ln-N bond angles, while the interligand N-Ln-N bond angles (cis) are larger than 90°. The six substituents at 3-position from the two $Tp^{R,R'}$ ligands surround the Ln(II) ion around the equatorial girdle. Consequently, the Ln(II) ion is encapsulated and shielded from intermolecular interactions and from coordination of donor solvents like THF. The origin for the low solubility of **1** and **2** is not clear since no substantial intermolecular contacts are present in the solid state. A possible explanation may be, as Sella first pointed out,[24] due to the hexagonal close packed structures which lead to a high lattice energy.

2.4. Structural comparison

The Sm-N distances in **1** are all equal at 2.617(4)Å. This is almost identical to $R_3N:\rightarrow Sm$ distances 2.639(6)Å, 2.621(7)Å, 2.641(6)Å found in $[SmI(\mu\text{-}I)(N\text{-}MeIm)_3]_2$[28], but significantly longer than the Sm(II)-NR_2 distance 2.455(2)Å seen in $[\{(CH_3)_3Si\}_2NSm(\mu\text{-}I)(DME)(THF)]_2$[9]. The distance compares favorably to the corresponding distances found in $(Tp^{Me2})_2Mg$ (Mg-N 2.186(15)Å), $(Tp^{Me2})_2Pb$ (Pb-N 2.610(5)Å), and $(Tp^{Me2})_2Ba$ (Ba-N 2.760(1) Å)[29] after correcting for the difference in six-coordinate ionic radii (Sm(II), 1.17Å; Mg(II), 0.720Å; Pb(II), 1.19Å; Ba(II), 1.35Å)[30]. The Yb-N bond distance of 2.482(5)Å in **2** is 0.135Å shorter than the analogous distance in the samarium complex **1**, which is consistent with the literature difference of 0.14Å in the ionic radii of 6-coordinate Sm(II) and Yb(II).[30] The Sm-N distances in complex **3** are not equivalent and range from 2.671(2)Å to 2.711(3)Å, with average of 2.676(32)Å. This length is 0.06Å longer than that observed in $(Tp^{Me2})_2Sm$ and is as expected from the more bulky nature of the Tp^{Ph} ligand. It is interesting to note that the Sm-N bond length is slightly (0.04Å) longer than the corresponding distance in $(Tp^{Ph})_2Fe$, after correcting for the size difference between six-coordinate Sm(II) and six-coordinate, high spin Fe(II). Thus covalent bonding makes a contribution to the shortened Fe-N bond in the latter compound. The Yb-N distances in **4** range from 2.536(3)Å to 2.578(3)Å with an average of 2.545(24)Å. The difference of 0.13Å between **3** and **4** is almost identical to that found (0.14Å) with the Tp^{Me2} ligand.

The Ln---B distances in **1** and **3**, and **2** and **4** are almost identical. Clearly the longer Ln-N distances with Tp^{Ph} ligand are not accommodated by pulling the Tp^{Ph} ligand away from Ln(II) center along the Sm---B axis but by spreading the pyrazolyl rings further apart. This is evidenced by the slightly larger average intra-ligand N-B-N angles: 112(2)° in **3** vs 110.9(2)° in **1**.

The average intra-ligand N-Yb-N angles in **2** (79.5(2)°) and **4** (81(3)°) are significantly larger than those in **1** (75.5(1)°)and **3** (77(2)°). This can be explained by the larger size of Sm(II) compared to Yb(II). The tripodal Tp ligand provides a pocket-like environment around the metal. Therefore, the smaller the metal, the deeper the pocket becomes and the intra-ligand angle N-M-N gets larger. For instance in the following series of $(Tp^{Me2})_2M$ complexes the intraligand N-M-N angle increases (71.5(1)°, Ba; 75.2(1)°, Pb; 86.1(1)°, Mg) as the size of metal ion decreases, Ba > Pb >Mg.

The LnNNB torsional angles in the Tp^{Ph} complexes (**3** and **4**) are much smaller than those found in $(Tp^{Me2})_2Ln$, **1** and **2**. The reason for this difference may be that the lengthening of the Ln-N bonds in **3** and **4** reduces the distortion needed to accommodate six pyrazolyl rings surrounding the central metal atoms.

The phenyl rings in **3** and **4** are not coplanar with the pyrazolyl rings to which they are attached. The dihedral angles in the range of 11-31° for **3** and 21-28° for **4** are similar to those observed in $(Tp^{Ph})_2Fe$ (21°-31°), and in $Tp^{Ph}Co(NCS)(THF)$ (32.3°-36.6°)[31].

Finally, the Sm-o-phenyl distances (Sm-C15/C25/C35 are 3.7Å) are much shorter than the corresponding m- and p-phenyl distances and this has been used to assign the ortho-hydrogen in the ^1H NMR spectrum of **3**.

2.5. Conclusions

A series of divalent bis-hydrotris(pyrazolyl)borate lanthanide complexes, $(Tp')_2Ln$ (Ln=Sm, Yb; Tp'=Tp^{Me2}, Tp^{Ph}, Tp^{Tn}), have been synthesized. The sandwich type complexes are solvent-free. Compounds **1** and **2** are insoluble in THF. The complexes **3**, **4** , **5** and **6** are freely soluble in THF and they exhibit dynamic processes in solution which make all six pyrazolyl rings equivalent. These divalent

lanthanide complexes, especially the soluble ones, may provide new opportunities for achieving controlled reactivity at the metal center.

2.6. Experimental Section

2.6.1. General Techniques and Solvents

The compounds described below are extremely air sensitive. Therefore, both the synthesis and subsequent manipulations of these complexes were carried out under inert atmosphere with the use of a Vacuum Atmospheres HE-553-2 Dri Lab or a Schlenk double-manifold system. Glassware was routinely dried at 250°C and cooled in a nitrogen atmosphere prior to use. Hexane and pentane were washed with sulfuric acid, dried over $MgSO_4$, and distilled from sodium and CaH_2, respectively. Toluene and THF were distilled from sodium and potassium benzophenone ketyl, respectively. Benzene-d_6, toluene-d_8 and THF-d_8 were vacuum distilled from sodium-potassium alloy (1:3). All solvents were degassed prior to use.

2.6.2. Physical Measurements

Infrared (IR) spectra were recorded on a BOMEM MB-100 FT interferometer using samples pressed in KBr pellets. NMR samples were prepared in a glovebox and sealed under vacuum. Proton chemical shifts are relative to TMS and were calibrated against the residual protons in deuterated solvents (THF-d_8, δ 1.72; toluene-d_8, δ 2.09; benzene-d_6, δ 7.15), ^{11}B chemical shifts are reported relative to external $F_3B{\bullet}Et_2O$. ^1H and ^{11}B NMR spectra were recorded at 400 MHz and 128 MHz, respectively, on a Bruker AM-400 FT spectrometer. Mass spectra were obtained on a AEI MS-12 Spectrometer using electron ionization techniques operating at 70 eV. Elemental analyses were performed by the Microanalytical Laboratory, Department of Chemistry, University of Alberta.

2.6.3. Starting Materials and Reagents

The ligands KTp^{Me2},[15] $NaTp^{Me2}$,[15] KTp^{Ph},[31] KTp^{Tn},[21] and THF solution of SmI_2[32], solid of $YbI_2(THF)_{3.5}$[33], were prepared by literature methods. The lanthanide metals were purchased from CERAC Inc..

2.6.4. Synthetic Procedures

$(Tp^{Me2})_2Sm$ (1)

A solution of $NaTp^{Me2}$ (320 mg, 1.0 mmol) in ca. 20 mL of THF was added dropwise to 10.0 mL of 0.1 M SmI_2 in THF. A dark purple precipitate formed immediately. The mixture was stirred overnight at room temperature and then filtered. The precipitate was washed twice with 10 mL THF and dried in vacuum. The product was isolated as a purple solid (670mg, 90%). Single crystals of **1** suitable for X-ray diffraction were grown by slow diffusion of a THF solution of $NaTp^{Me2}$ into a THF solution of SmI_2 over several weeks. IR (KBr, cm^{-1}) 2540 (ν_{B-H}); MS (EI, 70ev, 200°C) m/z 746 (M^+); Anal. Calcd for $C_{30}H_{44}N_{12}B_2Sm$: C, 48.34; H, 5.91; N, 22.56. Found: C, 48.60; H, 5.98; N, 21.87.

$(Tp^{Me2})_2Yb$ (2)

In a similar fashion, $YbI_2(THF)_{3.5}$ (143 mg) and $NaTp^{Me2}$ (135 mg) were mixed and yielded purple **2** in 93% yield. X-ray quality crystals were obtained by the same method as for complex **1**. IR (KBr, cm^{-1}) 2537 (ν_{B-H}); MS (EI, 70ev, 250°C) m/z 769 (M^+); Anal. Calcd for $C_{30}H_{44}N_{12}B_2Yb$: C, 46.95; H, 5.78; N, 21.90. Found: C, 48.60; H, 5.98; N, 21.87.

$(Tp^{Ph})_2Sm$ (3)

A solution of KTp^{Ph} (192 mg, 0.40 mmol) in ca. 15 mL of THF was added dropwise to 2.0 mL of 0.1 M SmI_2 in THF. The mixture was stirred overnight at room temperature, then the THF solvent was removed under vacuum. The residue was extracted with 10 mL of toluene and filtered. Removal of toluene under vacuum yielded 3 as dark green powder (157 mg, 76%). Diffusion of pentane into the toluene solution afforded dark green crystals suitable for X-ray diffraction. The compound 3 melted at 180°C under dynamic vacuum without sublimation. IR (KBr, cm^{-1}) 2476 (ν_{B-H}); MS (EI, 70ev, 280°C) m/z 1034 (M^+); ^1H NMR (C_6D_6, 25°C, δ ppm) 15.10(s, 12H, *o*-Ph), 8.17(d, J=7Hz, 12H, *m*-Ph), 7.70(d, J=7Hz, 6H, *p*-Ph), 3.34(d, J=2Hz, 6H, pz), -0.22(d, J=2Hz, 6H, pz), -3.6(br s, 1H, HB); ^{11}B NMR (C_6D_6, 25°C, δ ppm) -27.75 (br. s); Anal. Calcd for $C_{54}H_{44}N_{12}B_2Sm$: C, 62.79; H, 4.26; N, 16.26. Found: C, 62.50; H, 4.69; N, 15.62.

$(Tp^{Ph})_2Yb$ (4)

In a similar fashion, $YbI_2(THF)_{3.5}$ (213 mg) and KTp^{Ph} (302 mg) were mixed and yielded dark green 4 in 80% yield. Diffusion of pentane into the toluene solution afforded dark red crystals suitable for X-ray diffraction. IR (KBr, cm^{-1}) 2458 (ν_{B-H}); MS (EI, 70ev, 250°C) m/z 1056 (M^+); ^1H NMR (C_6D_6, 25°C, δ ppm) 7.75(d, J=2Hz, 6H, pz), 7.30(dd, J=7, 1Hz, 12H, *m*-Ph), 6.68(tt, J=7, 1Hz, 6H, *p*-Ph), 6.42(td, J=7, 1Hz, 12H, *o*-Ph), 6.10(d, J=2Hz, 6H, pz); ^{11}B NMR (C_6D_6, 25°C, δ ppm) -0.18 (br. s); Anal. Calcd for $C_{54}H_{44}N_{12}B_2Sm$: C, 61.44; H, 4.17; N, 15.92. Found: C, 61.67; H, 3.90; N, 15.88.

$(Tp^{Tn})_2Sm$ (5)

A solution of KTp^{Tn} (494 mg, 0.99 mmol) in 10 mL of THF was added dropwise to 5.0 mL of 0.1 M SmI_2 in THF. The mixture was stirred overnight, then the THF was removed under vacuum. The residue was extracted with 20 mL of toluene and filtered. The filtrate was concentrated to ca. 5 mL and stored at -40°C overnight. Complex **5** was isolated as a dark green crystalline solid by filtration and drying under vacuum (327 mg, 61%). IR (KBr, cm^{-1}) 2434 (ν_{B-H}); MS (EI, 70ev, 250°C) m/z 1071 (M^+); ^1H NMR (toluene-d_8, 25°C, δ ppm) 13.63(s, 6H, thienyl), 8.12(d, J=5Hz, 6H, thienyl), 7.58(d, J=5Hz, 6H, thienyl), 3.50(d, J=2Hz, 6H, pz), -0.30(d, J=2Hz, 6H, pz), -3.14(br. s, 2H, B-H); ^{11}B NMR (toluene-d_8, 25°C, δ ppm) -28.30 (br. s); Anal. Calcd for $C_{49}H_{40}N_{12}B_2S_6Sm$: C, 50.29; H, 3.23; N, 14.67. Found: C, 50.14; H, 3.37; N, 14.15.

$(Tp^{Tn})_2Yb$ (6)

In a similar fashion, $YbI_2(THF)_{3.5}$ (106 mg) and KTp^{Tn} (155 mg) were mixed and yielded dark green **6** in 56% yield. IR (KBr, cm^{-1}) 2453 (ν_{B-H}); MS (EI, 70ev, 250°C) m/z 1091 (M^+); ^1H NMR (toluene-d_8, 25°C, δ ppm) 7.64(d, J=2Hz, 6H, pz), 6.93(dd, J=3, 1Hz, 6H, thienyl), 6.43(dd, J=5, 1Hz, 6H, thienyl), 6.13(dd, J= 5, 3Hz, 6H, thienyl), 6.12(d, J=2Hz, 6H, pz), 5.05(br. s, 2H, B-H); ^{11}B NMR (toluene-d_8, 25°C, δ ppm) -0.21(br. s); Anal. Calcd for $C_{49}H_{40}N_{12}B_2S_6Yb$: C, 46.20; H, 2.95; N, 15.34. Found: C, 46.09; H, 2.88; N, 14.73.

2.6.5. X-ray Structure Determinations

The crystals were placed in a capillary in the dry-box. The capillary was temporarily sealed with grease, and, once taken out of the dry-box, it was sealed with a torch. Complete X-ray structure determinations for compounds **1**, **2** and **4** were

carried out by Dr. V.W. Day at Department of Chemistry, University of Nebraska. The X-ray data collection and structure refinement for complex **3** were carried out by Dr. R. McDonald at the Structure Determination Laboratory, Department of Chemistry, University of Alberta. Summary of crystal data and general conditions of data collection and structure refinement is given in Table 2.3.

Table 2.3 Summary of Crystallographic Data for $(Tp^{Me2})_2Sm$ (1), $(Tp^{Me2})_2Yb$ (2), $(Tp^{Ph})_2Sm$ (3), $(Tp^{Ph})_2Yb$ (4)

Compound	1	2	3	4
Empirical formula	$C_{30}H_{44}N_{12}B_2Sm$	$C_{30}H_{44}N_{12}B_2Yb$	$C_{54}H_{44}N_{12}B_2Sm$	$C_{54}H_{44}N_{12}B_2Yb$
Crystal dimensions (mm)	0.25 x 0.38 x 0.38	0.28 x 0.36 x 0.36	0.51 x 0.22 x 0.16	
formula weight	744.72	767.43	1034.01	1056.69
Cell dimensions				
a (Å)	10.612(2)	10.510(4)	[illegible]	10.683(3)
b (Å)	10.612(2)	10.510(4)	[illegible]	11.029(3)
c (Å)	10.612(2)	10.510(4)	[illegible]	12.249(3)
α (deg)	63.30(2)	63.52(3)	[illegible]	63.51(2)
β (deg)	63.30(2)	63.52(3)	[illegible]	82.61(2)
γ (deg)	63.30(2)	63.52(3)	63.24 [illegible]	66.58(2)
Volume ($Å^3$)	906.8(4)	885(1)	1188.4	1183.2(6)
Z (formula units)	1	1	[illegible]	1
D(calcd), g cm^{-3}	1.360	1.440	1.443	1.482
μ(calcd), cm^{-1}	16.5	26.8	12.88	20.188
space group	S_6–$\bar{3}$	S_6–$\bar{3}$	$P\bar{1}$	$P\bar{1}$
radiation(l,Å)	Mo Ka	Mo Kα	Mo Kα	Mo Kα
scan type	ω	ω	θ-2θ	ω
2θ limits(deg)	55.0°	55.0°	50.0	50.7
temp, °C	20(1)	20(1)	23	25
Total no. reflection	2295	2264	4362	4555
No. unique reflection	1388	1372	4142	4332
No. with I>3σ(I)			3845	4249
R	0.029	0.035	0.033	0.024
R_W	0.037	0.043	0.039	0.032
GOF	0.848	0.98	1.246	0.836

2.7. References

(1) Evans, W. J. *Polyhedron* **1987**, *6*, 803.

(2) Schaverien, C. J. *Adv. Organomet. Chem.* **1994**, *36*, 283.

(3) Evans, W. J.; Ulibarri, T. A.; Ziller, J. W. *J. Am. Chem. Soc.* **1990**, *112*, 2314.

(4) Evans, W. J.; Gonzales, S. L.; Ziller, J. W. *J. Am. Chem. Soc.* **1991**, *113*, 9880.

(5) Evans, W. J.; Kohn, G. K.; Leong, V. S.; Ziller, J. W. *Inorg. Chem.* **1992**, *31*, 3592.

(6) Burns, C. J.; Andersen, R. A. *J. Am. Chem. Soc.* **1987**, *109*, 941.

(7) Berg, D. J.; Burns, C. J.; Andersen, R. A.; Zalkin, A. *Organometallics* **1989**, *8*, 1865.

(8) Evans, W.J.; Anwander, R.; Ansari, M.A.; Ziller, J.W. *Inorg. Chem.* **1995**, *34*, 5 and references therein.

(9) Evans, W. J.; Drummond, D. K.; Zhang, H. M.; Atwood, J. L. *Inorg. Chem.* **1988**, *27*, 575.

(10) Tilley, T. D.; Andersen, R. A.; Zalkin, A. *Inorg. Chem.* **1984**, *23*, 2271.

(11) Cary, D. R.; Arnold, J. *Inorg. Chem.* **1994**, *33*, 1791.

(12) Wedler, M.; Noltemeyer, M.; Pieper, U.; Schmidt, H. G.; Stalke, D.; Edelmann, F. T. *Angew. Chem. Int. Ed. Engl.* **1990**, *29*, 894.

(13) Trofimenko, S. *Chem. Rev.* **1993**, *93*, 943.

(14) Han, R.; Parkin, G. *J. Organomet. Chem.* **1990**, *393*, C43.

(15) Trofimenko, S. *J. Am. Chem. Soc.* **1967**, *89*, 6288.

(16) Kitajima, N.; Moro-oka, Y. *Acta Cryst.* **1988**, *C44*, 1876.

(17) Jesson, J. P.; Trofimenko, S.; Eaton, D. R. *J. Am. Chem. Soc.* **1967**, *89*, 3158.

(18) Reger, D. L.; Huff, M. F.; Rheingold, A. L.; Haggerty, B. S. *J. Am. Chem. Soc.* **1992**, *114*, 579.

(19) Belderrain, T. R.; Contreras, L.; Paneque, M.; Carmona, E. *J. Organomet Chem.* **1994**, *474*, C5.

(20) Eichhorn, D. M.; Armstrong, W. H. *Inorg. Chem.* **1990**, *29*, 3607.

(21) Calabrese, J. C.; Domaille, P. J.; Trofimenko, S.; Long, G. J. *Inorg. Chem.* **1991**, *30*, 2795.

(22) Moss, M. H. J.; Kresinski, R. A.; Jones, C. J.; Evans, W. J. *Polyhedron* **1993**, *12*, 1953.

(23) Marques, N. *Rare Earths '92, Kyoto, Japan, June 1992; Abstract PIK-11* **1992**,

(24) Maunder, G. H.; Sella, A.; Tocher, D. A. *J. Chem. Soc., Chem. Commun.* **1994**, 885.

(25) Jesson, J. P. *In NMR of Paramagnetic Molecules: Principles and Applications (Edited by G.N. La Mar, W. DeW. Horrocks, Jr. and R.H. Holm), Chap. 1 Academic Press, New York* **1973**,

(26) Stainer, M. V. R. *Ph.D. Thesis, University of Alberta, Edmonton* **1981**,

(27) Evans, W. J.; Hughes, L. A.; Hanusa, T. P. *Organometallics* **1986**, *5*, 1285.

(28) Evans, W. J.; Rabe, G. W.; Ziller, J. W. *Inorg. Chem.* **1994**, *33*, 3072.

(29) Dutremez, S. G.; Leslie, D. B.; Streib, W. E.; Chisholm, M. H.; Caulton, K. G. *J. Organomet. Chem.* **1993**, *462*, C1.

(30) Shannon, R. D. *Acta Cryst.* **1976**, *A32*, 751.

(31) Trofimenko, S.; Calabrese, J. C. *Inorg. Chem.* **1987**, *26*, 1507.

(32) Namy, J. L.; Girard, P.; Kagan, H. B. *Nouv. J. Chim.* **1981**, *5*, 479.

(33) Watson, P. L.; Tulip, T. H.; Williams, I. *Organometallics* **1990**, *9*, 1999.

Chapter 3

Reactivity Survey of $(Tp^{Me2})_2Sm$: Azobenzene, p-Quinone and Dioxygen Complexes

3.1. Introduction

In Chapter 2, we have shown that the hydrotris(pyrazolyl)borates are good ligands for binding divalent lanthanides and a series of bis-ligand complexes have been isolated and fully characterized. As described in Chapter 1, $(C_5Me_5)_2Ln(THF)_n$ (n=0-2) exhibit unique reactivity towards a variety of substrates. For example, Evans et al. have demonstrated that $(C_5Me_5)_2Sm(THF)_n$ readily reacts with unsaturated molecules such as PhN=NPh, CO, CH_3-CH=CH_2, PhC≡CPh, HC≡CPh etc,[1] to give the corresponding Sm(III) complexes. It was of interest to determine how the reactivity of these new bis-hydrotris(pyrazolyl)borate complexes compared to $(C_5Me_5)_2Sm(THF)_n$.

The highly insoluble $(Tp^{Me2})_2Sm$ (1) complex presented an interesting dilemma. Insoluble complexes usually have limited reactivity, but sometimes, as a result of specific coordination environment, show unique properties. For instance, Kagan et al.[2] have reported that insoluble Cp_2Sm promotes the pseudo-Barbier reaction between aliphatic and allylic halides and aldehydes or ketones more efficiently than SmI_2 does. Thus, although Jones and Evans et al.[3] reported that $(Tp)_2Sm(THF)_n$ does not react with CO even under 6 atm pressure and that the reaction with propene gives $(Tp)_3Sm$ as the only isolable metal complex, we found that the insoluble $(Tp^{Me2})_2Sm$ (1) readily reacts with reducible substrates. In this chapter the results of a reactivity survey of 1 are presented.

3.2. Reactivity Survey of $(Tp^{Me2})_2Sm$, 1

Despite its insoluble nature, we found that compound **1** is easily oxidized and readily reacts with various reducible substrates. The reactions are accompanied by spectacular color changes.

3.2.1. Reaction with $TlBPh_4$

Addition of one equivalent of $TlBPh_4$ to a stirred, purple slurry of complex **1** in THF resulted in immediate formation of colorless solution and black Tl precipitate. Subsequent filtration and crystallization gave the cationic complex $(Tp^{Me2})_2SmBPh_4$ (**7**) in good yield (eq 3.1). Complex **7** is soluble in polar solvents such as CH_2Cl_2, $CHCl_3$,

$$(Tp^{Me2})_2Sm + TlBPh_4 \xrightarrow{THF} \underset{\textbf{7}\text{, colorless crystals}}{[(Tp^{Me2})_2Sm][BPh_4]} + Tl \qquad 3.1$$

THF, and CH_3CN. Interestingly, compound **7** is colorless which is not common in trivalent samarium chemistry. Trivalent samarium complexes are normally red or yellow, although the colors are not intense. Compound **7** was characterized by elemental analysis, IR, NMR spectroscopies and the structure verified by X-ray analysis (Figure 3.4). The solid-state IR spectrum of the complex displays an H-B stretching band at 2560 cm^{-1} which is 20 cm^{-1} higher than that in the parent molecule **1**. This suggests a stronger interaction between metal center and ligand in the former complex.

3.2.2. Reaction with PhN=NPh

A slurry of **1** in toluene in the presence of one equivalent of azobenzene rapidly gave a green solution from which green crystals of $(Tp^{Me2})_2Sm(PhNNPh)$, **8**, could be isolated in 85% yield, eq 3.2. It is interesting to note that the same complex is obtained

$$Sm(Tp^{Me2})_2 + PhN{=}NPh \xrightarrow{toluene} \underset{\textbf{8}\text{, green crystals}}{Sm(Tp^{Me2})_2(PhN{=}NPh)} \qquad 3.2$$

when the reaction is carried out with two equivalents of **1** per molecule of azobenzene. With $(C_5Me_5)_2Sm$ both 1:1, $(C_5Me_5)_2Sm(\eta^2\text{-}N_2Ph_2)(THF)$, and 2:1, $[(C_5Me_5)_2Sm]_2(N_2Ph_2)$, complexes can be obtained[4]. The differences are clearly attributable to the sterically more demanding nature of the Tp^{Me2} ligand compared to the C_5Me_5 moiety. Apparently, the methyl groups of the pyrazolyl rings surrounding the samarium center effectively prohibit two $(Tp^{Me2})_2Sm$ units from approaching each other close enough to form a dinuclear compound such as $[(Tp^{Me2})_2Sm]_2(PhN{=}NPh)$. In a related phenomenon, $(Tp^{iPr2})Cu(I)$ reacts with dioxygen and forms the dinuclear species, $(Tp^{iPr2})Cu(O_2)Cu(Tp^{iPr2})$[5]. However, the reaction with $(Tp^{tBu,iPr})Cu(DMF)$ stops at the mononuclear stage, $(Tp^{tBu,iPr})Cu(O_2)$[6]. The slight increase in steric size from Tp^{iPr2} to $Tp^{tBu,iPr}$ is sufficient to prevent two Cu ions from closing within 4Å to form $(Tp^{tBu,iPr})Cu(O\text{-}O)Cu(Tp^{tBu,iPr})$. The bulkier nature of Tp^{Me2} is reflected further in the observation that the 1:1 complex with the latter ligand retains a coordinated THF, whereas compound **8** is obtained as a solvent-free complex. Compound **8** is air and moisture sensitive. It is soluble in polar solvents such as toluene, THF, diethyl ether and moderately soluble in hexane and heptane. Attempted sublimation under dynamic vacuum resulted only in decomposition.

The magnetic moment of **8** at room temperature, measured according to Evans' method[7], is $2.4\mu_B$, which is similar to the $2.2\mu_B$ observed in the compound $(C_5Me_5)_2Sm(PhN{=}NPh)(THF)$.[8] The room temperature magnetic moments of samarium complexes for a given oxidation state have been found to be within a narrow range, 1.36-$1.9\mu_B$ for Sm(III) and 3.5-$3.8\mu_B$ for Sm(II) compounds[9]. The present magnetic moment suggests that samarium ion in compound **8** is in the trivalent oxidation state.

The ^1H NMR spectrum of $(Tp^{Me2})_2Sm(PhN{=}NPh)$ is shown in Figure 3.1. The most striking feature of the spectrum is its complicated nature, which suggests that the molecule has low symmetry and that it is not subject to intramolecular or intermolecular

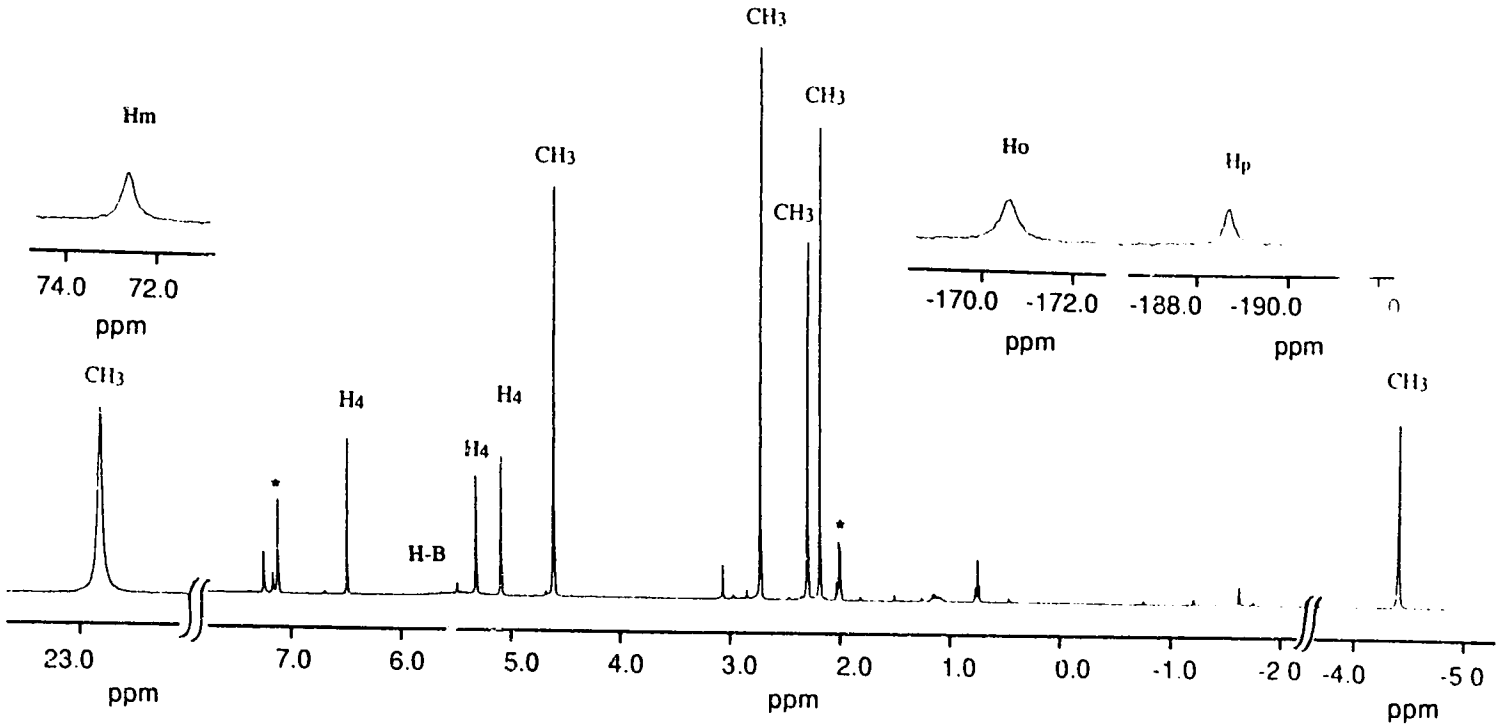

Figure 3.1. 400 MHz ^{1}H NMR spectrum of $(Tp^{Me2})_2Sm(PhN{=}NPh)$ (8) in toluene-d_8

exchange processes. The signals are isotropically shifted and the range of the proton chemical shifts spans 263 ppm.

A close inspection of the ^1H NMR spectrum indicates that of the maximum 26 signals, only 13 are seen in a ratio of 6:6:6:6:6:6:4:4:2:2:2:2:2. This suggests that the solution structure has C_2 symmetry and two pyrazolylborate ligands are equivalent. As required, the ^{11}B NMR spectrum exhibits one resonance. From integration, the following assignments of the signals can be made. The six resonances with relative intensity of 6 are assigned to six different methyl groups in each pyrazolylborate ligand. Three signals with relative intensity of 2 are attributed to the 4-position hydrogen of the pyrazolyl rings. The broad signal at 5.4 ppm is due to the two boron hydrogens. The drastically shifted resonances at 73.2, -170.3, -189.6 ppm are assigned to the azobenzene protons. The large chemical shifts of PhN=NPh moiety is probably due to radical anion nature of the azobenzene moiety and the associated contact shifts of the resonances. We note that ^1H NMR signals of azobenzene were not located in the related $(C_5Me_5)_2Sm(THF)(PhN{=}NPh)$ compound. The rigid solution structure of **8** is maintained even at the relatively high temperature of 90°C. The first solution rigid f-element hydrotris(pyrazolyl)borate complex was observed by Takats and Stainer[10] in $(Tp)_2Yb(\eta^2\text{-}Tp)$. Lanthanide complexes are held together by mostly ionic bond and are known to undergo ligand rearrangement. This can be seen from the growing number of crystallographically characterized molecules, $(Tp)_2Yb(L)$ (L=acac[11], dpm[12], tropolonate[13], benzoate[13]), $(Tp)_2YCl(H_2O)$[14], $(Tp)_2Ce(X)$ (X=acac, ba, dbm)[11], $(Tp^{Me2})_2Ln(OTf)$ (Ln=Nd, Yb)[15], $(Tp)_2Yb(\eta^2\text{-}Tp)$[10] and $(Tp^{Me2})_2Sm(PhN{=}NPh)$. With the exception of the latter two compounds, all molecules show fluxional behaviour in solution. In each of these molecules, the six pyrazolyl rings of two Tp ligands are equivalent at room temperature. The rigid solution structures observed in $(Tp)_2Yb(\eta^2\text{-}Tp)$ and $(Tp^{Me2})_2Sm(PhN{=}NPh)$ are probably due to the sterically congested coordination environment around the respective metal centers.

Contrary to $(Tp^{Me2})_2Sm$, $(Tp^{Tn})_2Sm$ is unreactive towards azobenzene. The reason may be the unfavorable steric repulsion between the azobenzene phenyl groups and thienyl rings in the expected product "$(Tp^{Tn})_2Sm(PhN{=}NPh)$".

3.2.3. Reaction with 2,6-di-tert-butyl-1,4-benzoquinone

Quinone transition metal complexes have been the subject of interest because of their electrochemical and magnetic properties.[16] To our knowledge, no lanthanide quinone complexes have been reported so far. Considering that the reduction potential of 2,6-di-tert-butyl-1,4-benzoquinone is more positive than azobenzene, we anticipated that $(Tp^{Me2})_2Sm$ should be able to reduce it to the monoanion stage. Indeed, addition of one equivalent of quinone to a slurry of $(Tp^{Me2})_2Sm$ in toluene led to immediate formation of a red solution, from which red crystals of **9** could be isolated in good yield, eq 3.3. The compound is soluble in aromatic and ether type of solvents, but only marginally soluble in

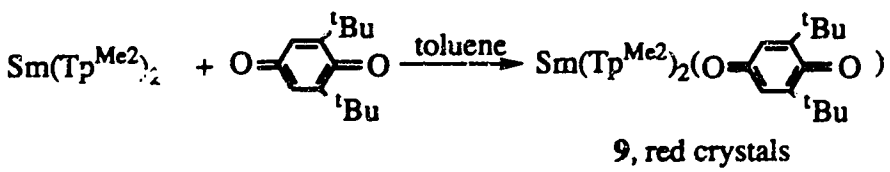

3.3

hexane. The complex has been characterized by analytic and spectroscopic methods and the structure verified by X-ray crystallography (Figure 3.3)

In contrast to compound **8**, the ^1H NMR spectrum of **9** (Figure 3.2) is simple and shows one single set of pyrazolyl ring resonances and one H-B signal, indicating that molecule is fluxional and results in the equivalence of the six pyrazolyl groups. Lowering the temperature causes the signals to broaden, and the chemical shifts change with temperature. No signal splitting is observed down to -100°C, which indicates that the activation barrier for this dynamic process is very low. The ^{11}B NMR spectrum of **9** exhibits one peak at -1.3 ppm, which is consistent with ^1H NMR results.

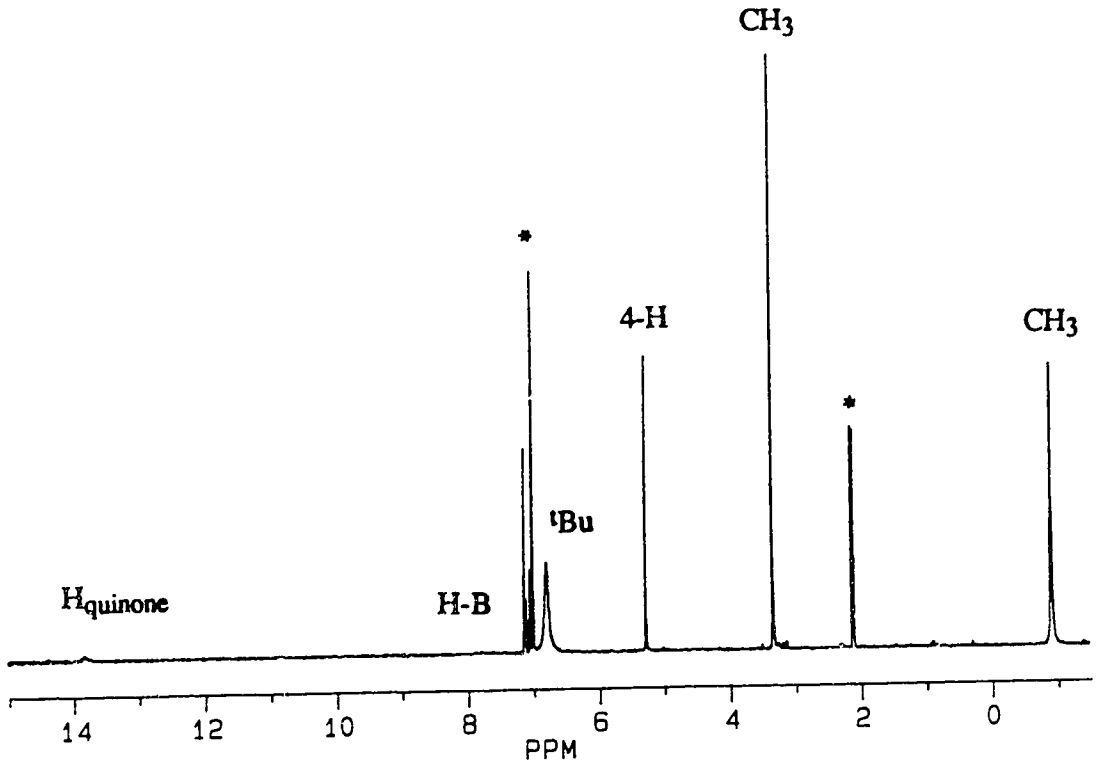

Figure 3.2. 400 MHz ^1H NMR spectrum of $(Tp^{Me2})_2Sm[OC_6H_2(^tBu)_2O]$ (**9**) in toluene-d_8

3.2.4. Reaction with Dioxygen

Metal-dioxygen chemistry is one of the most extensively investigated research fields during the past decades[17,18]. Among the numerous metal-dioxygen complexes known, the number of f-element dioxygen complexes are very limited[19-24]. To the best our knowledge, there is only one example of a structurally determined lanthanide dioxygen complex, $La_2\{N(SiMe_3)_2\}_4(\mu\text{-}\eta^2\text{-}O_2)(Ph_3PO)_2$[19], where dioxygen functions as a side-on bound peroxo ligand, bridging the two metal centers. Because of their high oxophilicity and electropositivity, f-element dioxygen complexes are usually not stable and decompose via oxygen-oxygen bond cleavage. It is well recognized that steric factors play a crucial role in the stability of f-element complexes. Well-demonstrated examples in lanthanide chemistry are the isolation of $(C_5Me_5)_2Sm(\mu\text{-}L)Sm(C_5Me_5)_2$ (L=olefin,, HNNH, N_2, Bi_2, Te_2)[25] where the cage-like environment provided by four C_5Me_5 ligands has allowed

the stabilization and isolation of unique series of dinuclear species. Recently it was found that the highly hindered hydrotris(3-tert-butylpyrazolyl)borate (Tp^{tBu}), hydrotris(3-tert-butyl-5-methylpyrazolyl)borate ($Tp^{tBu,Me}$), hydrotris(3-tert-butyl-5-isopropylpyrazolyl)borate ($Tp^{tBu,iPr}$) ligands[26,27] have profound influence on the nature of the isolated metal complexes. Theopold et al.[28] and Kitajima et al.[6] have isolated the first symmetrically side-on bonded superoxo-Co(II) and Cu(II) complexes, $(Tp^{tBu,Me})Co(\eta^2\text{-}O_2)$, and $(Tp^{tBu,iPr})Cu(\eta^2\text{-}O_2)$, respectively. The successful isolation of mononuclear dioxygen adducts was directly attributed to the bulky tert-butyl substituents on the ligands which prevented further reaction and formation of binuclear complexes.

Although reactions of $(C_5Me_5)_2Sm(THF)_n$ with chalcogens have been reported[25] and the oxide complex, $[(C_5Me_5)_2Sm]_2(\mu\text{-}O)$,[29] has been isolated, no intact dioxygen complex has appeared.

Since we have shown that reaction of **1** with azobenzene gives only the mononuclear complex **8** and that formation of $[(Tp^{Me2})_2Sm]_2(PhN{=}NPh)$ is sterically unfavorable, it was of considerable interest to test the reaction with O_2.

When a purple slurry of **1** in toluene was stirred at -78°C under an atmosphere of dioxygen, the solid slowly dissolved and after ca. 3 h yielded an intensely colored red solution, eq 3.4. Since **1** is completely insoluble in toluene the formation of a colored

$$\underset{\text{purple solid}}{Sm(Tp^{Me2})_2} + O_2 \xrightarrow[\text{toluene}]{-78°C} \text{red solution} \xrightarrow[\text{r.t.}]{\text{warm up}} \underset{\textbf{10}\text{, green solid}}{Sm(Tp^{Me2})_2(O_2)} \quad 3.4$$

solution is a vivid demonstration of a reaction between **1** and O_2. Warming the solution to room temperature, while removing the excess dioxygen, resulted in a color change from red to pale green. Solvent removal, followed by crystallization from toluene gave analytically pure **10** as a pale green solid.

The formulation of the green solid is in complete accord with elemental analysis and spectroscopic data. The complex is soluble in polar solvents such as toluene, THF, CH_3CN and $CHCl_3$ and aromatic solvents like toluene, but only slightly soluble in aliphatic hydrocarbons. The solid compound is thermally robust. It does not undergo any visible change up to 130°C under a dynamic vacuum. The ^1H NMR spectrum is deceptively simple and exhibits only a single set of pyrazolyl resonances, three signals in a 3:3:1 ratio. The pattern of the signals remains temperature invariant down to -100°C. The ^{11}B NMR spectrum displays one peak. Although uninformative as to the molecular structure, the NMR features established that the Tp^{Me2} ligand remained intact in the molecule. The highest mass peak in the mass spectrum corresponded to the (M^+-O_2) fragment. The UV spectrum of the compound in CH_2Cl_2 solution exhibited an intense absorption at 240 nm ($\varepsilon = 4.8 \times 10^3$ M^{-1} cm^{-1}), slightly shifted from the characteristic band of KO_2, 250(1) nm (ε = 2686(29) M^{-1} cm^{-1}),[30] and first hinted at the possible presence of the superoxide ligand in compound **10**. However, the complex is ESR-silent down to -176°C. Good evidence for O_2^- coordination came from the Raman spectrum of the complex. As shown in Figure 3.3, all bands, except the peak at 1124 cm^{-1}, remain unchanged in a sample prepared with $^{18}O_2$. This band is in the region associated with the stretching of the superoxo ligand[31,32] and, as expected, the band shifts to lower frequency (1059 cm^{-1}) upon isotopic substitution. The observed shift of 65 cm^{-1} is exactly as predicted for a pure O-O stretch from the change in reduced mass.

Binding of O_2^- to samarium is strong. The ligand is not displaced by donor solvents such as THF or CH_3CN. However, preliminary reactivity studies show that it can participate in oxygen transfer reactions, delivering one oxygen atom to triphenylphosphine; the nature of the resultant samarium complex is under investigation.

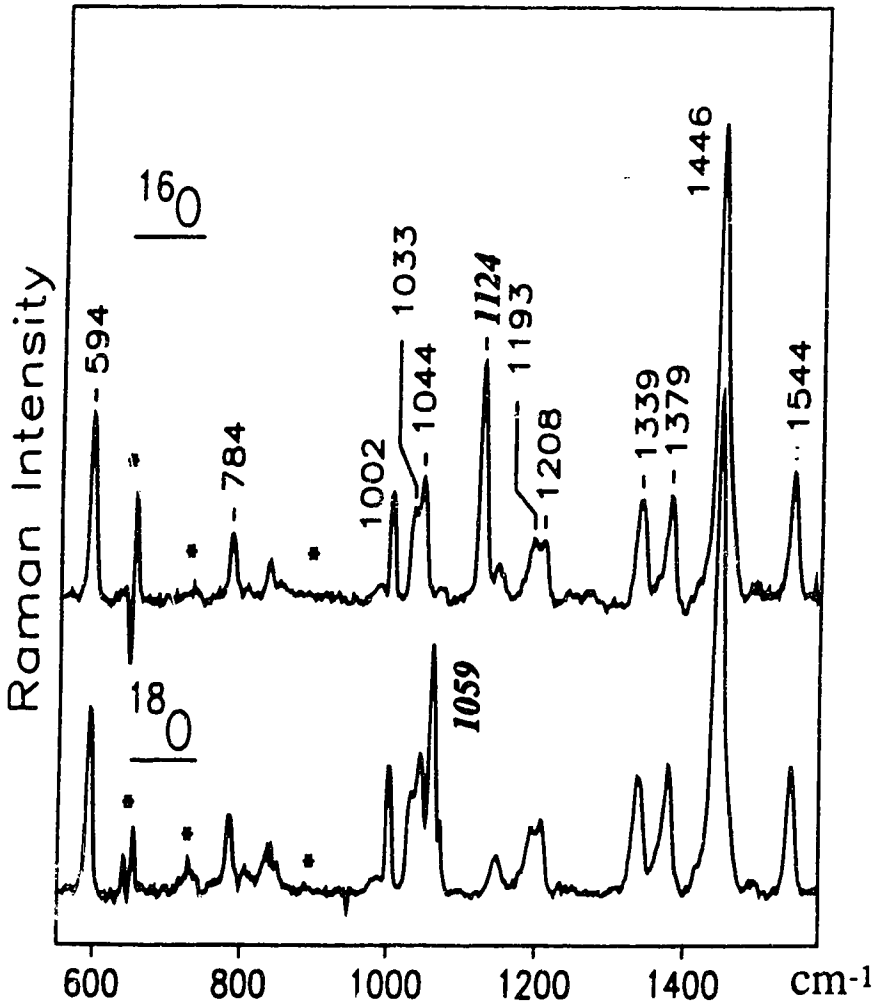

Figure 3.3. Raman spectra of $(Tp^{Me2})_2Sm(\eta^2\text{–}^{16}O_2)$ (top) and $(Tp^{Me2})_2Sm(\eta^2\text{–}^{18}O_2)$ (bottom). Spectral features marked with an asterisk are artifacts arising from substraction of the CD_2Cl_2 solvent spectrum.

3.2.5. Reactions with TCNQ, TCNE and DMAD

Complex **1** also reacted with TCNQ, TCNE and DMAD to yield colored solids, but pure compounds could not be isolated.

3.2.6. Reactions with HC≡CPh, HC≡CH, PhC≡CPh, CO, $H_2C{=}CH_2$, $CH_3CH{=}CH_2$

In contrast to $(C_5Me_5)_2Sm(THF)_n$, samarium compound **1** is unreactive toward HC≡CPh, HC≡CH, PhC≡CPh, CO, $CH_3CH{=}CH_2$.

3.3 Solid-State Structures of 7, 8, 9 and 10

Perspective views of the structures are shown in Figures 4-7, respectively. Important interatomic distances and angles are presented in Table 1. The Tp^{Me2} ligands in each of these molecules are coordinated to samarium in classic η^3-bonding mode. This is as expected for complex **7** but in view of the well known variable (η^3, η^2 and even η^1) coordination modes of the $Tp^{R,R'}$ ligand systems,[33,26] and the sterically congested nature of the parent complex, $(Tp^{Me2})_2Sm$, the structures of **8**, **9** and **10** are remarkable. It indicates that even with the bulky Tp^{Me2} ligand the "bent metallocene" type structure is accessible and provides further experimental evidence for the calculated shallow potential energy surfaces for the bending motion in the series of $(C_5H_5)_2M$ complexes[34] (M = Ln(II), and alkaline earth metals). Viewing the molecules as analogous to $(C_5Me_5)_2Sm(X)(Y)$, the plane defined by three nitrogen donor atoms from each Tp^{Me2} ligand is equivalent to the C_5Me_5 ring. The dihedral angles between planes are 173(1)° (**7**), 152(1)° (**8**), 146.2(5)° (**9**) and 144.1(4)° (**10**). However the nature of the ligand redistribution appears to be different for Tp^{Me2} and C_5Me_5 ligand systems. Slippage and twisting of the former ligands occur in the transformation of **1** into **7**, **8**, **9** and **10** whereas only simple bending of the two C_5Me_5 ligands is required to give the " bent metallocene " type structure in $(C_5Me_5)_2M$ complexes.

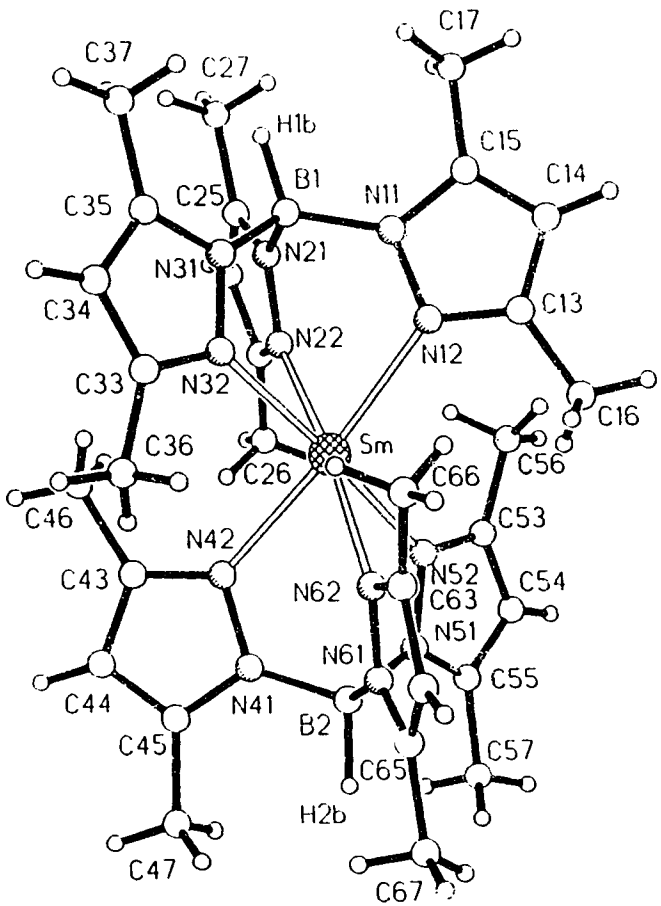

Figure 3.4. ORTEP view of $(Tp^{Me2})_2SmBPh_4$ (7)

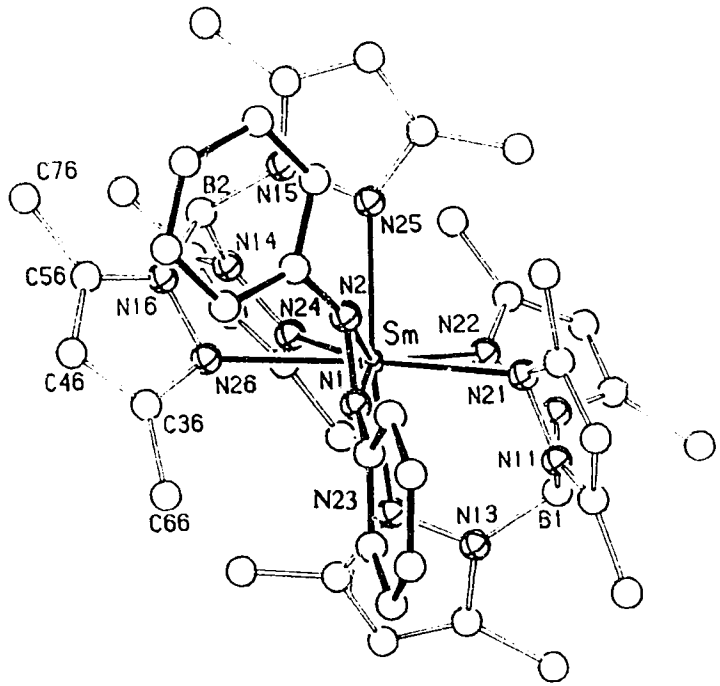

Figure 3.5. ORTEP view of $(Tp^{Me2})_2Sm(PhN{=}NPh)$ (8)

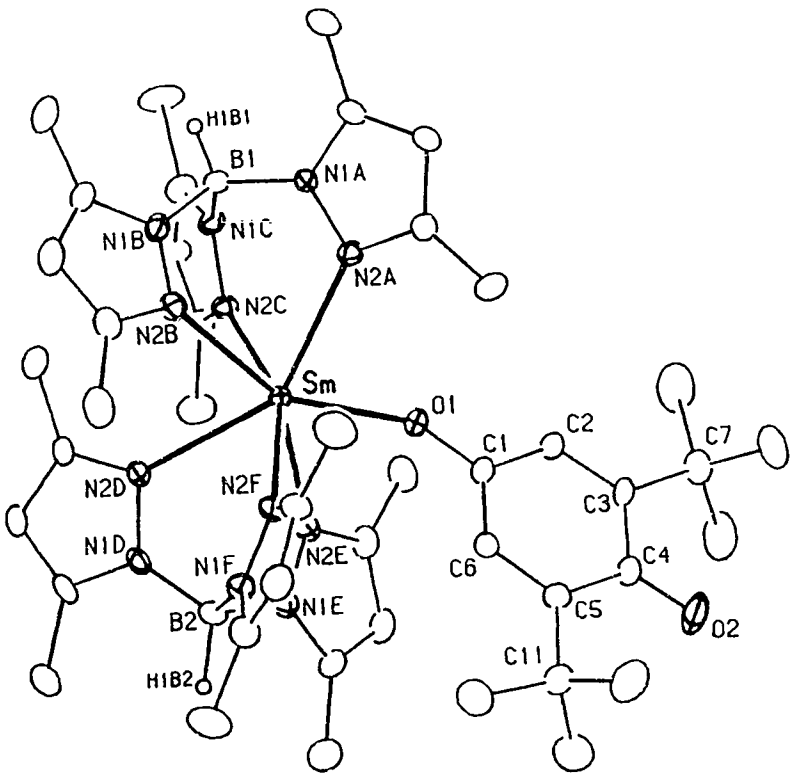

Figure 3.6. ORTEP view of $(Tp^{Me2})_2Sm[OC_6H_2(^tBu)_2O]$ **(9)**

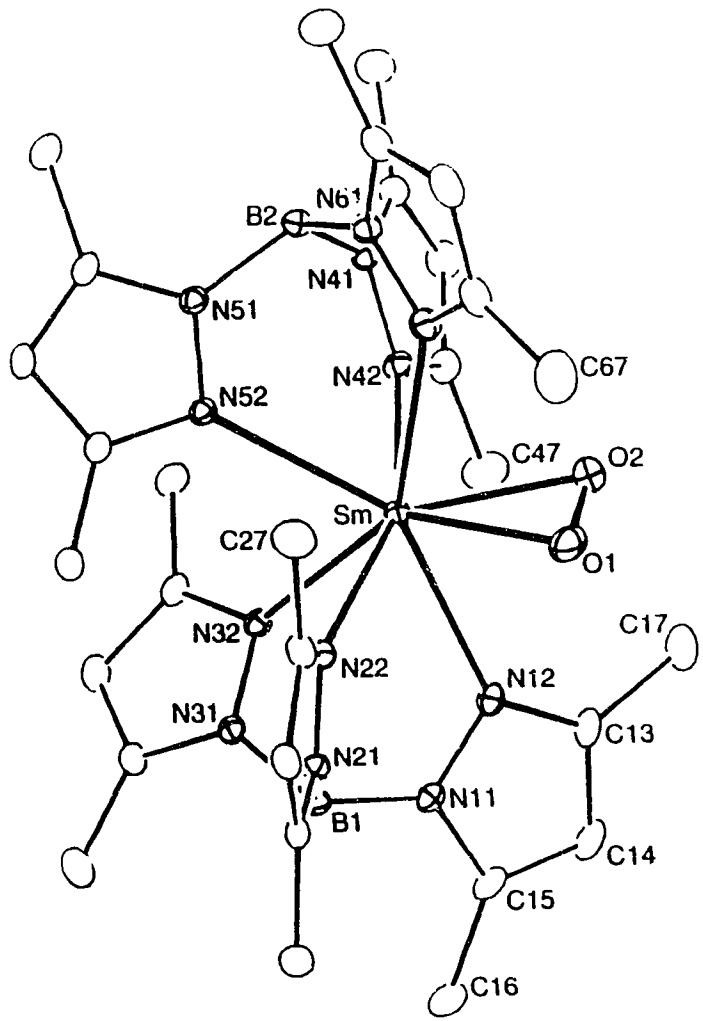

Figure 3.7. ORTEP view of $(Tp^{Me2})_2Sm(O_2)$ **(10)**

Table 3.1 Selected Interatomic Distances and Angles (deg) for $(Tp^{Me2})_2SmBPh4$ (7), $(Tp^{Me2})_2Sm(PhN{=}NPh)$ (8), $(Tp^{Me2})_2Sm(OC_6H_2(^tBu)_2O)$ (9) and $(Tp^{Me2})_2Sm(O_2)$ (10)

	7	8	9	10
		Distances		
Sm-N(pz)	2.407(12)-2.485(12)	2.512(8)-2.669(10)	2.475(8)-2.612(8)	2.488(3)-2.647(3)
av	2.44(3)	2.59(6)	2.55(6)	2.58(7)
Sm-L		2.418(8) (N1)	2.213(5) (O1)	2.329(3) (O1)
		2.386(8) (N2)		2.321(3) (O2)
N=N		1.332(12)		
O=O				1.319(5)
C1-O1			1.300(11)	
C4-O2			1.247(12)	
		Angles		
N-Sm-N (intra)	76.9(4)-80.2(4)	67.6(3)-89.9(3)	71.5(2)-80.2(3)	69.4(1)-80.1(1)
av	78(1)	77(9)	76(4)	76(4)
B-Sm-B	173(1)	152(1)	146.2(5)	144.1(4)

The coordination number of the samarium varies in the series. Complexes of **8** and **10** are eight coordinate while compounds **7** and **9** are six and seven-coordinate, respectively. The samarium atom in **7** is surrounded by six pyrazolyl nitrogens in slightly distorted octahedral fashion. The coordination geometry of **8** is best described as a distorted pentagonal bipyramidal with N12 and N42 occupying the axial sites and N22, N32, N52, N62 and the mid-point of the PhN=NPh ligand spanning the equatorial positions. The distances to the axial pyrazolyl nitrogens (ave 2.493(5)Å) are shorter than to the equatorial nitrogens (ave 2.62(2)Å) and reflect the less congested nature of the former sites. The same is true for complexes **9** and **10**. The average Sm-N (pz) distance in **7** is 2.44 Å, which is 0.11Å shorter than that found in the seven-coordinate complex **9**. This is as expected from the change in coordination number and the larger positive charge of Sm(III) in the cationic complex **7**, both contributing to a reduction in ionic radius. The difference in Sm-N bond distances between **1** and **7** is 0.18Å, which is comparable to the difference in ionic radius of Sm^{+2} and Sm^{+3} (0.20Å)[41]. The consistency reveals that the tabulated values of the ionic radii are also valid in the Tp system. The average Sm-N (pz) distances in the eight-coordinate complexes **8** and **10** are equivalent within experimental error. The difference between these distances and those in the seven-coordinate **9** (0.03-0.04Å) is less than expected from the increase in coordination number (0.06Å) and this is attributed to the small bite angles of η^2-PhNNPh and η^2-O_2 in complexes **8** and **10**, respectively.

The azobenzene moiety in **8** is coordinated to Sm in η^2-fashion, with Sm-N (azo) distance of 2.386(8)Å and 2.418(8)Å which are comparable to those (2.390(10)Å-2.450(10)Å) found in $(C_5Me_5)_2Sm(N_2Ph_2)(THF)$.[4] These distances are ca. 0.07Å longer than Sm-N single bond distance of 2.331(3)Å seen in $(C_5Me_5)_2Sm(NHPh)(THF)$[35] but ca. 0.15Å shorter than N:→Sm dative bond distance of 2.563(6)Å, 2.596(6)Å found in $[Sm(N\text{-}MeIm)_8]I_3$.[36] As observed in $(C_5Me_5)_2Sm(THF)(PhN{=}NPh)$,[4] the metrical parameters of the coordinated PhN=NPh moiety are different from those of free

azobenzene. The N-N bond distance at 1.332(12)Å is equivalent to those found in $(C_5Me_5)_2Sm(THF)(PhN{=}NPh)$, which is longer than 1.253Å[37] found in cis-azobenzene, but shorter than 1.45Å, the N-N single bond distance of hydrazine. In contrast to free PhN=NPh, the phenyl rings are no longer coplanar, the dihedral angle is 67.7°.

The Sm-O distance in **9** at 2.213(5)Å is slightly longer than the similar distance in $(C_5Me_5)_2Sm(OC_6Me_4H)$,[38] 2.13(1)Å, consistent with more congested nature of the Sm center in the pyrazolylborate complex. Coordination of quinone via O1 causes the C1-O1 distance to lengthen to 1.300(11)Å, compared to C4-O2 (1.247(12)Å). The latter distance is typical for C=O double bond. The Sm-O1-C1 angle is 154.5°.

In complex **10**, the dioxygen ligand is bonded to samarium in a symmetrical, side-on fashion; the Sm-O distances, 2.329(3) and 2.321(3)Å are nearly identical. The O-O bond distance is 1.319(5)Å, and is consistent with the superoxo formulation of the O_2 ligand. This bond distance is somewhat longer than the corresponding distances in $(Tp^{tBu,Me})Co(\eta^2\text{-}O_2)$ (1.262(8)Å)[28] and $(Tp^{tBu,iPr})Cu(\eta^2\text{-}O_2)$ (1.22(3)Å)[6] but in the range of the values found in NaO_2 (1.33(6)Å)[39] and KO_2 (1.28(7)Å).[40] The isolation and stability of **10** is a direct consequence of the unique environment provided by the two Tp^{Me2} ligands. It can be seen in the Figure 3.7 that the two Tp^{Me2} ligands, in particular the methyl groups C17 and C67 provide a protective cradle which shields the O_2^- ligand.

As mentioned before complexes **9** and **10** are highly fluxional in solution while **8** possesses a rigid solution structure, yet all three have approximately C_2 symmetry in the solid state. The rigidity of the solution structure of **8** is obviously due to the presence of phenyl substituents of the azobenzene moiety.

3.4. Conclusion

Despite its insolubility, $(Tp^{Me2})_2Sm$ (**1**) is easily oxidized and readily reacts with reducible substrates such as $TlBPh_4$, azobenzene, 2,6-di-tert-butyl-1,4-benzoquinone, dioxygen, TCNQ, TCNE and DMAD. In the case of the former four reagents, the

resultant metal complexes **7**, **8**, **9**, and **10**, have been fully characterized, including crystal structures. The influence of different steric size of $(Tp^{Me2})_2Sm$ and $(C_5Me_5)_2Sm$ is clearly evidenced by the reaction with Ph_2N_2. In contrast to the reaction of $(C_5Me_5)_2Sm(THF)_n$ with PhN=N[illegible] where PhN=NPh can be reduced to the monoanion or dianion, depending on the stoichiometric ratio of the reactants, the similar reaction with samarium complex [illegible]ly gives complex **8**, even in the presence of excess of **1**. Interestingly, the more soluble $(Tp^{Tn})_2Sm$ is unreactive towards azobenzene, which indicates that steric effects play a key role governing the reactivity of $(Tp^{R,R'})_2Ln$ complexes. Reactions with quinone and O_2 also results in single electron reduction and formation of the first lanthanide quinone complex, **9**, and the first example of a lanthanide superoxo complex **10**, respectively. The stabilization of complex **10** is attributed to the protective pocket provided by two Tp^{Me2} ligands. The successful isolation of superoxo complex **10** presages formation of related E_2 (E_2=OH, Te_2) complexes. On the other hand, the steric bulk of the Tp^{Me2} ligand also inhibits reactivity. Thus, unlike $(C_5Me_5)_2Sm(THF)_n$, complex **1** does not react with CO, olefinic or acetylenic substrates.

3.5. Experimental Section

3.5.1. Starting Materials and Methods

Azobenzene, 2,6-di-tert-butyl-1,4-benzoquinone, 7,7,8,8-tetracyanoquinodimethane (TCNQ), tetracyanoethylene (TCNE), (Aldrich) were sublimed before use. Phenylacetylene and dimethyl acetylenedicarboxylate (DMAD) were dried and vacuum-distilled prior to use (molecular sieves 4Å). Propene (Aldrich) was condensed into a pressure-vessel and dried over molecular sieves (4Å) before use; CO (Matheson) was used as received and the acetone stabilizer in HC≡CH (Matheson) was removed by passing the gas through a dry-ice/acetone trap. The preparation of $(Tp^{Me2})_2Sm$ has been described as in Chapter 2. $TlBPh_4$ was prepared from the reaction of Tl_2SO_4 with $NaBPh_4$ in aqueous solution.

Raman Spectra were excited with 25 mW of 457.9 nm light and detected with a CCD detector coupled to a single monochromator. Total accumulation time was 5 minutes for each sample. Frequencies are accurate to ±1.5 cm^{-1}.

When listing NMR chemical shifts below, the number in parentheses following assignment refers to the line width of the signal at half-height in Hz.

3.5.2. Synthesis of the Compounds

$[(Tp^{Me2})_2Sm][BPh_4]$, 7

Solid $TlBPh_4$ (61 mg, 0.11 mmol) was added in several portions to a slurry of **1** (84 mg, 0.11 mmol) in 8 mL of THF. A black precipitate of Tl metal formed and the solution became colorless. The mixture was stirred for 2 hours and filtered. The filtrate was concentrated to 3 mL and placed at -40°C overnight. Colorless crystals of **7** were isolated by filtration and dried under vacuum (60 mg, 50%). Single crystals suitable for X-ray studies were grown by vapor diffusion of hexane into THF solution of **7**. IR(KBr, cm^{-1}) 2560 (ν_{B-H}); MS (EI, 70ev, 200°C) m/z 746 (M^+-BPh_4); ^1H NMR (THF-d_8, 25°C, δ ppm) 9.60(br. s, 2H, B-H), 7.12(m, 8H, Ph), 6.70(m, 8H, Ph), 6.60(m, 4H, Ph), 5.25(s, 6H, H-pz), 3.70(s, 18H, Me-pz), 3.54(s, 2H, THF), 1.70(s, 2H, THF), -2.16(br., [illegible] Me-pz); ^{11}B NMR (THF-d_8, 25°C, δ ppm) 3.41(br. s, $HBpz_3$), -6.10(s, BPh_4); Anal. Calcd for $C_{56}H_{68}N_{12}B_3O_{0.5}Sm$: C, 61.17; H, 6.18; N, 15.29 Found: C, 60.91; H, 6.57; N, 15.80.

$(Tp^{Me2})_2Sm(PhN{=}NPh)$, 8

An orange solution of PhN=NPh (43 mg, 0.236 mmol) in ca. 5 mL of toluene was added dropwise to a purple slurry of $(Tp^{Me2})_2Sm$ (175 mg, 0.235 mmol) in ca. 5 mL of toluene. The solid dissolved and a dark green solution was obtained. After 4 hours stirring, the solution was concentrated to ca. 2 mL and placed at -40°C overnight. A dark green solid was isolated (192 mg, 88%). IR (KBr, cm^{-1}) 2533 (ν_{B-H}); MS (EI, 70 eV,

270°C) 744 ($M^+ - N_2Ph_2$); ^{1}H NMR (toluene-d_8, 25°C, δ ppm) 73.19 (s, 4H, *m*-Ph). 23.21 (s, 6H, pz-Me), 6.35 (s, 2H, pz-H), 5.40 (br, 2H, B-H), 5.20 (s, 2H, pz-H), 5.00 (s, 2H, [illegible]), 4.55 (s, 6H, pz-Me), 2.75 (s, 6H, pz-Me), 2.40 (s, 6H, pz-Me), 2.20 (s, 6H, pz-Me), -4.55 (s, 6H, pz-Me) -170.30 (s, 4H, *o*-Ph), -189.55 (s, 2H, *p*-Ph); ^{11}B NMR (toluene-d_8, 25°C, δ ppm) -7.30(s), Anal. Calcd for $C_{42}H_{54}N_{14}B_2Sm$: C, 54.41; H, 5.83; N, 21.16. Found: C, 54.43; H, 5.93; N, 21.56.

Attempted preparation of $[(Tp^{Me2})_2Sm]_2(PhN{=}NPh)$

A solution of PhN=NPh (52 mg, 0.285 mmol) in ca. 10 mL of toluene was added dropwise to a slurry of $(Tp^{Me2})_2Sm$ (429 mg, 0.576 mmol) in ca. 10 ml of toluene. The mixture turned dark green immediately. After stirring overnight, the mixture was filtered. A large amount of unreacted $(Tp^{Me2})_2Sm$ (221mg) remained. The toluene was removed from the filtrate under vacuum and a dark green solid was obtained (207mg, 80%). Spectroscopic analysis showed that solid was identical to **8**.

$(Tp^{Me2})_2Sm[OC_6H_2(^tBu)_2O]$, 9

A solution of 2,6-di-tert-butyl-1,4-benzoquinone (205 mg, 0.930 mmol) in ca. 3 mL of toluene was added dropwise to a slurry of $(Tp^{Me2})_2Sm$ (692 mg, 0.930 mmol) in ca. 5 ml of toluene. Solid **1** slowly dissolved and a red solution was obtained at the end of the addition. After stirring the solution for 4 hours, the toluene was removed under vacuum. The residue was washed with ca. 3 mL of hexane , and then it was dissolved in ca. 3 mL of a mixture of toluene/hexane (2:1). Cooling the solution at -40°C for 2 days gave red crystals of **9** (550mg, 0.570mmol, 62%). IR (KBr, cm^{-1}) 2548 (ν_{B-H}); MS (EI, 70 eV, 220°C) 744$(M - C_{14}H_{20}O_2)^+$; ^{1}H NMR (toluene-d_8, 25°C, δ ppm) 13.80 (s, 2H, quinone, 28), 7.7 (br. s, 2H, B-H, 146), 6.77 (s, 18H, quinone, 20), 5.26 (s, 6H, pz-H), 3.33 (s, 18H, pz-Me), -0.92 (s, 18H, pz-Me); ^{11}B NMR (toluene-d_8, 25°C, δ ppm) -1.3(s, 320), Anal. Calcd for $C_{51}H_{72}N_{12}O_2B_2Sm$: C, 57.94; H, 6.86; N, 15.90. Found: C, 57.73; H, 6.91; N, 15.88.

$(Tp^{Me2})_2Sm(O_2)$, 10

A purple slurry of $(Tp^{Me2})_2Sm$ (620 mg, 0.833 mmol) in 15 mL of toluene was placed in a 100 mL Schlenk flask. After degassing by three freeze-pump-thaw cycles, the flask was filled with 1 atm of dioxygen. The mixture was stirred at -78°C. The solid slowly dissolved and after ca.3 hours stirring, a red solution was obtained. The solution was allowed to slowly warm to room temperature, while excess dioxygen was removed. The color of the solution slowly changed from red to green. Following removal of toluene, a green powder was obtained. Recrystallization from toluene gave analytically pure $(Tp^{Me2})_2Sm(O_2)$ (482 mg, 75%) as pale green crystals. IR (KBr, cm^{-1}) 2545 (ν_{B-H}); Raman (CD_2Cl_2, cm^{-1}) 1124 ($\nu_{16O-16O}$), 1059 ($\nu_{18O-18O}$); MS (EI, 70 eV, 240°C) 744($M^+ - O_2$); ^1H NMR (toluene-d_8, 25°C, δ ppm) 9.58 (s, 18H, pz-Me), 5.82 (s, 6H, pz-H), 5.3 (br. s, 2H, B-H), 3.10 (s, 18H, pz-Me); ^{11}B NMR (toluene-d_8, 25°C, δ ppm) -5.3(s), Anal. Calcd for $C_{37}H_{52}N_{12}O_2B_2Sm$ (10•toluene): C, 51.15; H, 6.03; N, 19.34 Found: C, 51.22; H, 6.07; N, 19.52.

^{31}P NMR Study of the Reaction of 10 with PPh_3

A mixture of the samarium complex (20 mg, 0.023 mmol) and triphenylphosphine (6 mg, 0.023 mmol) was dissolved in 0.6 mL of toluene-d_8. Within 20 minutes after mixing, 15% of the PPh_3 was converted to $OPPh_3$, as calculated from ^{31}P NMR. Conversion of PPh_3 to $OPPh_3$ was completed over a period of 9 h.

Attempted Reactions with CO, HC≡CH, $CH_2=CH_2$, $CH_3CH=CH_2$, HC≡CPh and PhC≡CPh

A slurry of $(Tp^{Me2})_2Sm$ in toluene was placed under 1 atm of CO, HC≡CH, $CH_2=CH_2$, $CH_3CH=CH_2$. The mixture were stirred at room temperature overnight; in no case was any reaction seen. The complex also did not react with excess HC≡CPh and PhC≡CPh.

Reactions with TCNQ, TCNE and DMAD

Complex $(Tp^{Me2})_2Sm$ reacts with one equiv of TCNQ or TCNE in THF to give a red and a green precipitate, respectively. The precipitates were not characterized. Attempts to obtain single crystals by diffusion of THF solutions of TCNQ or TCNE into $(Tp^{Me2})_2Sm$ in THF were not successful.

$(Tp^{Me2})_2Sm$ readily reacts with DMAD in THF to give a red solution, but subsequent crystallization did not give a pure compound.

Reaction of $(Tp^{Tn})_2Sm$ (5) with PhNNPh

A solution of azobenzene (27 mg, mmol) in 5 mL of toluene was added to a green solution of $(Tp^{Tn})_2Sm$ in 5 mL of toluene. No obvious color change was observed. After stirring overnight, the toluene was removed under vacuum and the residue was washed with 4 mL hexane. The precipitate was redissolved in 4 mL toluene. Dark green crystals were obtained after diffusion of hexane vapor into the toluene solution over a period of one week (80 mg, 43%). Spectroscopic data showed that the crystals were identical to the starting material.

3.5.3. X-ray Structure Determinations

Preparation of X-ray quality crystals of **10** proved to be challenging and after numerous unsuccessful attempts, they were finally obtained by slow crystallization of **10** from a 1:1 mixture of hexane/dimethoxyethane at -40°C. Crystals of **7**, **8**, **9** and **10** were handled as described in Chapter 2. Complete X-ray structure determinations for compounds **7**, **8** and **9** were carried out by Dr. V.W. Day at Department of Chemistry, University of Nebraska. The X-ray data collection and structure refinement for complex **10** was carried out by Dr. R. McDonald at Structure Determination Laboratory, Department of Chemistry, University of Alberta. Summary of crystal data and general conditions of data collection and structure refinement are given in Table 3.2.

Table 3.2 Summary of Crystallographic Data for $(Tp^{Me2})_2SmBPh_4$ (7), $(Tp^{Me2})_2Sm(PhN{=}NPh)$ (8), $(Tp^{Me2})_2Sm(C_{14}H_{20}O_2)$ (9), $(Tp^{Me2})_2Sm(O_2)\cdot C_4H_{10}O_2$ (10)

Compound	7	8	9	10
Empirical formula	$C_{54}H_{64}N_{12}B_3Sm$	$C_{42}H_{54}N_{14}B_2Sm$	$C_{51}H_{72}N_{12}O_2B_2Sm$	$C_{34}H_{54}N_{12}O_4B_2Sm$
Crystal dimensions (mm)		0.28 x 0.30 x 0.42		0.48 x 0.13 x 0.10
formula weight	1063.72	926.96	1055.69	866.86
Cell dimensions				
a (Å)	10.045(2)	14.094(3)	10.924(4)	10.531(2)
b (Å)	15.411(3)	17.540(3)	15.040(5)	11.025(1)
c (Å)	21.047(4)	18.723(4)	18.785(6)	18.129(2)
α (deg)	90.93(2)	90.00	89.96(3)	100.297(7)
β (deg)	90.15(2)	103.98(3)	105.71(3)	97.423(9)
γ (deg)	98.46(2)	90.00	108.8693)	100.571(9)
Volume ($Å^3$)	3222	4491(2)	2799(2)	2007.1(8)
Z (formula units)	2	4	2	2
D(calcd), g cm^{-3}	1.097	1.371	1.254	1.434
μ(calcd), cm^{-1}	9.512	13.4	10.971	15.17
space group	$P\bar{1}$	$P2_1/n$	$P\bar{1}$	$P\bar{1}$
radiation(l,Å)	Mo Kα	Mo Kα	Mo Kα	Mo Kα
scan type	ω	ω	ω	θ-2θ
2θ limits(deg)	43.0	45.8	45.8	50.0
temp, °C	25	20(1)	25	-50
Total no. reflection	7644	6691	7948	7281
No. unique reflection	7389	6199	7668	6987
No. with I>3σ(I)	3820	3196	4847	5526
R	0.052	0.040	0.044	0.034
R_w	0.057	0.046	0.051	0.042
GOF	1.087	0.929	1.008	1.298

3.6. References

(1) Evans, W. J.; Ulibarri, T. A.; Chamberlain, L. R.; Ziller, J. W.; Jr. Alvarez, D. *Organometallics* **1990**, *9*, 2124 and references therein.

(2) Namy, J. L.; Collin, J.; Zhang, J.; Kagan, H. B. *J. Organomet. Chem.* **1987**, *328*, 81.

(3) Moss, M. A. J.; Kresinski, R. A.; Jones, C. J.; Evans, W. J. *Polyhedron* **1993**, *12*, 1953.

(4) Evans, W. J.; Drummond, D. K.; Chamberlain, L. R.; Doedens, R. J.; Bott, S. G.; Zhang, H. M.; Atwood, J. L. *J. Am. Chem. Soc.* **1988**, *110*, 4983.

(5) Kitajima, N.; Koda, T.; Hashimoto, S.; Kitagawa, T.; Moro-oka, Y. *J. Am. Chem. Soc.* **1991**, *113*, 5664.

(6) Fujisawa, K.; Tanaka, M.; Moro-oka, Y.; Kitajima, N. *J. Am. Chem. Soc.* **1994**, *116*, 12079.

(7) Evans, D. F. *J. Chem. Phys.* **1959**, 2003.

(8) Evans, W. J.; Drummond, D. K.; Chamberlain, L. R.; Doedens, R. J.; Bott, S. G.; Zhang, H. C.; Atwood, J. L. *J. Am. Chem. Soc.* **1988**, *110*, 4983.

(9) Evans, W. J.; Foster, S. E. *J. Organomet. Chem.* **1992**, *433*, 79.

(10) Stainer, M. V. R.; Takats, J. *J. Am. Chem. Soc.* **1983**, *105*, 410.

(11) Moss, M. A. J.; Jones, C. J.; Edwards, A. J. *Polyhedron* **1988**, *7*, 79.

(12) Moffat, W. D.; Stainer, M. V. R.; Takats, J. *Inorg. Chim. Acta* **1987**, *139*, 75.

(13) Moss, M. A. J.; Jones, C. J. *J. Chem. Soc. Dalton Trans.* **1990**, 581.

(14) Reger, D. L.; Lindeman, J. A.; Lebioda, L. *Inorg. Chim. Acta* **1987**, *139*, 71.

(15) Liu, S. Y.; Maunder, G. H.; Sella, A.; Stephenson, M.; Tocher, D. A. *Inorg. Chem.* **1995**, in press.

(16) Pierpont, C. G.; Lange, C. W. *Prog. Inorg. Chem.* **1994**, *41*, 331.

(17) Martell, A. E.; Sawyer, D. T.; Eds. *Oxygen Complexes and Oxygen Activation by Transition Metals; Plenum Press: New York* **1988**,

(18) Klotz, I. M.; Kurtz, J., D.M. Guest Eds. *Metal Dioxygen Complexes, Chem. Rev.* **1994**, *94*, Number 3.

(19) Bradley, D. C.; Ghotra, J. S.; Hart, F. A.; Hursthouse, M. B.; Reithby, P. R. *J. Chem. Soc., Dalton* **1977**, 1166.

(20) Rose, D.; Chang, Y. D.; Chen, Q.; Zubieta, J. *Inorg. Chem.* **1994**, *33*, 5167.

(21) Doyle, G. A.; Doodgame, D. M. L.; Sinden, A.; Williams, D. J. *J. Chem. Soc., Chem. Commun.* **1993**, 1170.

(22) Charpin, P. P.; Folcher, G.; Lance, M.; Vigner, M. N. D. *Acta Cryst.* **1985**, *C41*, 1302.

(23) Haegele, R.; Boeyens, J. C. A. *J. Chem. Soc., Dalton* **1977**, 648.

(24) Alcock, N. W. *Chem. Comm.* **1966**, 537.

(25) Evans, W. J.; Rabe, G. W.; Ziller, J. W.; Doedens, R. J. *Inorg. Chem.* **1994**, *33*, 2719 and references therein.

(26) Trofimenko, S. *Chem. Rev.* **1993**, *93*, 943.

(27) Hasinoff, L.; Takats, J.; Zhang, X. W.; Bond, A. H.; Rogers, R. D. *J. Am. Chem. Soc.* **1994**, *116*, 8833.

(28) Egan, J. W., Jr.; Haggerty, B. S.; Rheingold, A. L.; Sendlinger, S. C.; Theopold, K. H. *J. Am. Chem. Soc.* **1990**, *112*, 2445.

(29) Evans, W. J.; Grate, J. W.; Bloom, I.; Hunter, W. J.; Atwood, J. L. *J. Am. Chem. Soc.* **1985**, *107*, 405.

(30) Kim, S.; DiCosimo, R.; Fillippo, J. S., Jr. *Anal. Chem.* **1979**, *51*, 679.

(31) Loehr, T. M. *In Oxygen Complexes and Oxygen Activation by Transition Metals; Martell, A.E.; Sawyer, D.T.; Eds., Plenum Press: New York,* **1988**, 33.

(32) In the Raman spectrum of solid KO_2, this band is observed at 1143 cm^{-1}.; Bate, J. B.; Brooker, M. H.; Boyd, G. E. *Chem. Phys. Lett.* **1972**, *16*, 391.

(33) Trofimenko, S. *Prog. Inorg. Chem.* **1986**, *34*, 115.

(34) Kaupp, M.; Schleyer, P. V. R.; Dolg, M.; Stoll, H. *J. Am. Chem. Soc.* **1992**, *114*, 8202.

(35) Evans, W. J.; Keciok-Kohn, G.; Leong, V. S.; Ziller, J. W. *Inorg. Chem.* **1992**, *31*, 3592.

(36) Evans, W. J.; Rabe, G. W.; Ziller, J. W. *Inorg. Chem.* **1994**, *33*, 3072.

(37) Mostad, A.; Romming, C. *Acta Chem. Scand.* **1971**, *25*, 3565.

(38) Evans, W. J.; Hanusa, T. P.; Levan, K. R. *Inorg. Chim. Acta* **1985**, *110*, 191.

(39) Templeton, D. H.; Dauben, C. H. *Acta Cryst.* **1950**, *72*, 2251.

(40) Kassatochkin, W.; Kotow, W. *J. Chem. Phys.* **1936**, *4*, 458.

(41) Shannon, R. D. *Acta Cryst.* **1976**, *A32*, 751.

Chapter 4

Consequence of Steric Control Provided by Highly HinderedHydrotris(3-tert-butyl-5-methylpyrazolyl)borate ($Tp^{tBu,Me}$) Ligand: Stabilization and Isolation of a Series of Monomeric, Half-sandwich Ln(II) Complexes

4.1. Introduction

The last decade has witnessed an explosive growth in the organometallic chemistry of the Ln(II) elements[1]. However, the development of this chemistry remained mainly focused on the preparation and reactivity studies of bis-ligand complexes. Among the numerous divalent lanthanide compounds, the number of mono-ligated LLn(II) complexes is surprisingly small, and the divalent lanthanide hydrocarbyl and hydride complexes were unknown prior to our investigations. A problem associated with potential mono-ligated precursor complexes, LLnX (X=halide), is ligand redistribution and formation of bis-ligand complexes LnL_2 and LnX_2. This is particularly problematic for the large lanthanide ions. For example, Evans *et al.* have reported the preparation and structure of $[(C_5Me_5)Sm(\mu\text{-}I)(THF)_2]_2$[2] and $[(Me_3Si)_2NSm(\mu\text{-}I)(DME)(THF)]_2$,[3] but the complexes tend toward ligand redistribution to $SmI_2(THF)_2$ and SmL_2. Schumann *et al.*[4] have synthesized $Cp'YbCl(L)_2$ ($Cp' = C_5H_5$, C_5Me_5; L = THF, 1/2 DME) but, to our knowledge, there are no reports on attempted derivatization of the complexes, except for the mixed ligand complex, $(C_5Me_5)Yb\{Sn(CH_2{}^tBu)_3\}(THF)_2$, reported by Cloke, Lawless *et al.*[5] The lack of suitable starting material is a serious impediment for the development of this area of organo-lanthanide chemistry.

The utility of pyrazolylborate ligands in the synthesis of bis-ligand complexes of divalent lanthanide has been established in Chapter 2. In this chapter, we report our

successful stabilization and isolation of the first monomeric, half-sandwich complexes of $(Tp^{tBu,Me})LnI(THF)_n$ by using the strategy of steric control via substitution in the 3-position of the pyrazolyl rings. We also show that these complexes are excellent precursors for the synthesis of $(Tp^{tBu,Me})LnER$ type compounds. A preliminary account of this work has appeared.[6]

4.2. The Precursor Complexes $(Tp^{Me2})YbI(THF)_2$ and $(Tp^{tBu,Me})LnI(THF)_n$

4.2.1. Synthetic Aspects

The hydrotris(3,5-dimethylpyrazolyl)borate (Tp^{Me2}) ligand is one of the most extensively used "Trofimenko ligands" in inorganic and organometallic chemistry.[7] It provides better solubility and more steric congestion than the unsubstituted Tp ligand, a situation which somewhat parallels the behaviour of pentamethylcyclopentadienyl (C_5Me_5) compared to the cyclopentadienyl (C_5H_5) ligand. Considering that Tp^{Me2} is more sterically demanding than C_5Me_5, we postulated that one Tp^{Me2} ligand might be able to stabilize mono-ligated $(Tp^{Me2})LnX$ complexes toward ligand redistribution reactions. To our satisfaction, the reaction of YbI_2 with one equiv of KTp^{Me2} in THF yielded, after simple work-up, half-sandwich $(Tp^{Me2})YbI(THF)_2$ (**11**) as an orange crystalline solid in high yield, eq 4.1. Extension of the reaction to samarium failed. Addition of KTp^{Me2} to an equimolar amount of SmI_2 led to an immediate precipitation

$$YbI_2(THF)_n + KTp^{Me2} \xrightarrow{THF} \underset{\mathbf{11}\ (70\%)}{(Tp^{Me2})YbI(THF)_2} + KI \qquad 4.1$$

of purple $(Tp^{Me2})_2Sm$. The formation of $(Tp^{Me2})_2Sm$ may involve the intermedicacy of $(Tp^{Me2})SmI(THF)_n$ which is subjected to ligand redistribution to give the final product, as outlined in eq. 4.2. The difference in stability toward ligand redistribution

$$SmI_2 + KTp^{Me2} \xrightarrow[-KI]{THF} \left[(Tp^{Me2})SmI(THF)_n \right] \xrightarrow{THF} (Tp^{Me2})_2Sm + SmI_2 \qquad 4.2$$

is attributed to the size difference between Yb(II) and Sm(II).

Although complex **11** is isolable, it slowly undergoes ligand redistribution at room temperature in THF to give $(Tp^{Me2})_2Yb$ and YbI_2 over a period of days. The ligand redistribution reaction is faster in toluene or at elevated temperature. As a result complex **11** appeared not to be a good precursor for other mono-ligated ytterbium complexes. Indeed, reaction of **11** with $NaN(SiMe_3)_2$ gave $(Tp^{Me2})_2Yb$ and $Yb[N(SiMe_3)_2]_2$, with no evidence of formation of the mixed ligand complex.

Clearly, to enhance the stability of the mono-hydrotris(pyrazolyl)borate lanthanide complex, steric crowding around the metal center must be increased. This can be done by introducing a bulky group in the 3-position of the pyrazolyl ring. Parkin *et al.*[8,9] have reported the successful isolation of monomeric $(Tp^{tBu})MR$ (M=Zn, Mg; R=alkyl) by using Tp^{tBu} as the supporting ligand. The ligand we chose was $Tp^{tBu,Me}$ which has similar steric size as Tp^{tBu}, but the methyl group on the 5-position increase the solubility of the complexes and also plays an important role in protecting the B-N bonds from cleavage.[7] It was with considerable relief that we observed that the reaction of LnI_2 with one equivalent of $KTp^{tBu,Me}$ in THF afforded $(Tp^{tBu,Me})LnI(THF)_n$ (Ln=Sm, n=2, **12**; Ln=Yb, n=1, **13**) in high yield, as shown in eq 4.3. Both samarium and ytterbium compounds are freely soluble in THF and

$$LnI_2(THF)_n + KTp^{tBu,Me} \xrightarrow{THF} (Tp^{tBu,Me})LnI(THF)_n + KI \qquad 4.3$$

Ln=Sm, n=2: dark green
Yb, n=1: yellow

toluene, but only sparingly soluble in hydrocarbon solvents. The formulation is consistent with elemental analysis, NMR, IR spectroscopic data and X-ray analysis.

The THF molecules in $(Tp^{tBu,Me})SmI(THF)_2$ are very labile and can be removed by repeated cycles of dissolution in toluene and removal of the solvent under vacuum. The plausible equilibria in toluene are shown in eq 4.4. The ^1H NMR of **12**

$$\underset{\mathbf{12}}{(Tp^{tBu,Me})SmI(THF)_2} \xrightleftharpoons{-THF} (Tp^{tBu,Me})SmI(THF) \xrightleftharpoons{-THF} \underset{\mathbf{14}}{(Tp^{tBu,Me})SmI} \qquad 4.4$$

in toluene-d[illegible] concentration-dependent, and this is consistent with the operation of equation [illegible] [illegible]ation of solvent free $(Tp^{tBu,Me})SmI$, **14** was corroborated by the absence of THF signals in ^1H NMR and IR spectra and elemental analysis. Compound **14** is much less soluble in toluene than compound **12**. Addition of THF to complex **14** reforms compound **12**. Unfortunately, it has proved impossible to grow X-ray quality crystals of compound **14**. Therefore, the structure of the complex remains unknown. The ^1H NMR spectrum of **14** in toluene-d_8 shows only one set of pyrazolyl group resonances. As the temperature is lowered, the signals broaden and then the chemical shifts change, however, no signal splitting was observed down to -100°C.

Interestingly, the THF molecule of ytterbium compound **13** could not be removed. Similar phenomenon had also been observed with the $(C_5Me_5)_2Ln(THF)_n$ complexes. The unsolvated $(C_5Me_5)_2Sm$ is readily obtained by desolvation/sublimation at 85°C,[10] while $(C_5Me_5)_2Yb(THF)_2$ only loses one THF molecule at 90°C.[10] The marked difference in binding ability of f-elements to THF is attributed to changes in the charge/ionic radius ratio. The larger ratio for ytterbium(II) results in a stronger electrostatic interaction with THF. Therefore, removing THF from Yb(II) is much more difficult than doing the same from a Sm(II) center.

Contrary to the ytterbium complex **11**, compounds **12**, **13** and **14** are quite stable in solution with respect to ligand redistribution reaction and formation of $(Tp^{tBu,Me})_2Ln$ and LnI_2. Even after heating **12**, **13** and **14** in toluene-d_8 at 80°C, no bis-ligand complexes were observed as monitored by ^1H NMR. The inertness of $(Tp^{tBu,Me})LnI(THF)_n$ towards ligand redistribution must be a direct consequence of the sterically very demanding nature of $Tp^{tBu,Me}$ ligand which disfavors the formation of $(Tp^{tBu,Me})_2Ln$, even with larger sized Sm(II) ion.

4.2.2. Oxidation of $(Tp^{tBu,Me})SmI(THF)_2$

It is interesting to note that complex **12**, unlike $(Tp^{Me2})_2Sm$, is not oxidized by $TlBPh_4$. However, the oxidation can be effected by the stronger oxidizing reagent $AgBPh_4$, eq 4.5. This suggests that the reducing ability of samarium is dependent on the coordination environment, the more electron rich complex, $(Tp^{Me2})_2Sm$, has a

$$(Tp^{tBu,Me})SmI(THF)_2 + AgBPh_4 \xrightarrow{THF} \underset{\textbf{15}\text{, colorless}}{[(Tp^{tBu,Me})SmI(THF)_2][BPh_4]} + Ag \qquad 4.5$$

stronger reducing power than that of complex **12**. Compound **15** is only soluble in polar solvents such as THF, CH_3CN, CH_2Cl_2 and $CHCl_3$. The compound is colorless, which is not as expected since most of trivalent samarium complexes are yellow, orange and red.[11]

The IR spectrum of complex **15** shows a B-H stretch at 2571 cm^{-1} which is ca. 50 cm^{-1} higher than that in complex **12** due to stronger interaction between metal center and ligand in the former compound. ^1H NMR of **15** exhibits only one set of pyrazolyl rings resonances, indicating fluxionality of the molecule in solution.

4.2.3. Molecular structures of complexes 11, 13, 15

The crystal structures of ytterbium complexes **11**, **13** and samarium complex **15** have been determined by X-ray diffraction techniques. ORTEP drawings are given in Figures 4.1-4.3, respectively. Selected bond lengths and bond angles are presented in Table 4.1. All structures comprise well-separated monomeric units with no unusual intermolecular contacts. The $Tp^{R,R'}$ ligand is coordinated to the metal center *via* η^3-bonding mode. The variations in coordination number can be accounted for by changes in ligand size and the charge to ionic radius ratio. Thus, the coordination number of complex **13** is one less than compound **11** due to the bulkier $Tp^{tBu,Me}$ ligand. The increased coordination number of **15** compared to **13** is consistent with the larger charge to radius ratio of Sm(III) compared to Yb(II).

Complex **11** is six-coordinate, with the ytterbium center coordinated in a distorted octahedral fashion by three nitrogens of the Tp^{Me2} ligand occupying one triangular face and two THF and one I ligands occupying the opposite triangular face. The molecule has a crystallographically-imposed C_s symmetry. The ytterbium complex **13** is five-coordinate and the coordination geometry is best described as a distorted trigonal bipyramidal with N6 and O(THF) occupying axial sites, the N6-Yb-O angle is 145.8(2)°. Five-coordinate ion is not as common for lanthanide complexes as four and six coordinate species. The only other example of a crystallographically characterized five coordinate divalent lanthanide complex is $Yb(OAr)_2(THF)_3$[12] (Ar=2,4,6-$^tBu_3C_6H_2$) with a distorted square pyramidal coordination geometry around Yb. Preliminary data on complex **15** indicate that the samarium center in $(Tp^{tBu,Me})SmI(THF)_2^+$ (**15**) is also six-coordinate. However, the coordination geometry of samarium, unlike that of ytterbium in **11**, is a distorted bicapped tetrahedral with the two THF ligands capping two tetrahedral faces. The most

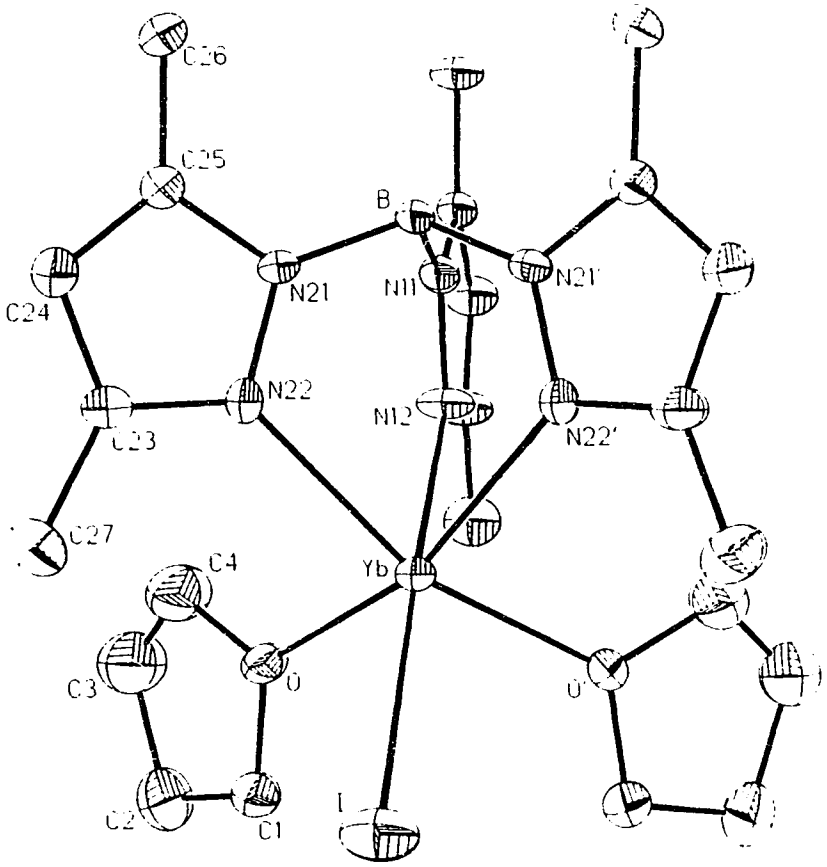

Figure 4.1 ORTEP view of $(Tp^{Me2})YbI(THF)_2$ (**11**)

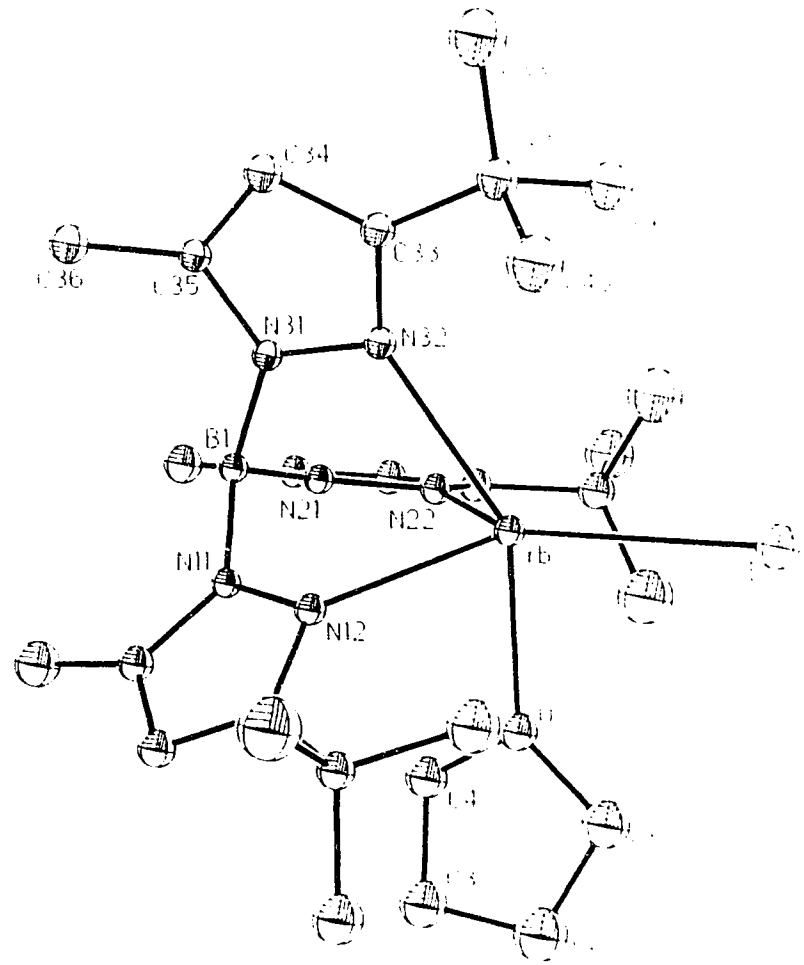

Figure 4.2 ORTEP view of $(Tp^{tBu,Me})YbI(THF)$ (**13**)

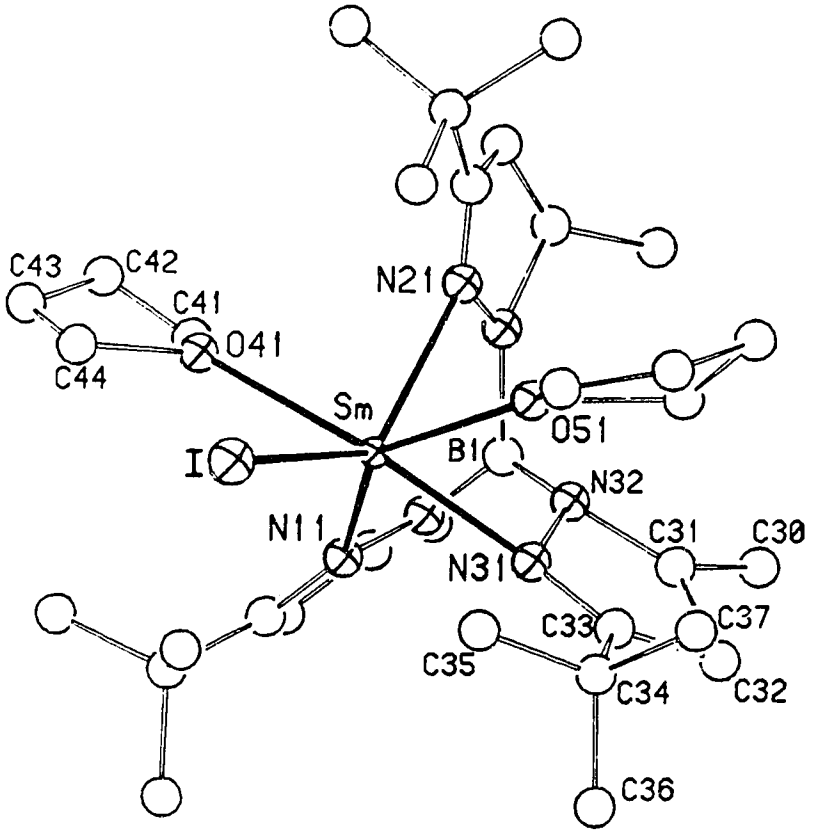

Figure 4.3 ORTEP View $[(Tp^{tBu,Me})SmI(THF)_2][BPh_4]$ **(15)**

Table 4.1 Selected Bond Lengths (Å) and Bond Angles (deg) for $(Tp^{Me2})YbI(THF)_2$ (**11**) and $(Tp^{tBu,Me})YbI(THF)$ (**13**)

	11	**13**
	Distances	
Yb-N	2.53 (2) (Yb-N2)	2.431 (6) (Yb-N2)
	2.49 (1) (Yb-N4)	2.434 (7) (Yb-N4)
		2.493 (6) (Yb-N6)
Yb-I	3.065 (2)	3.0536 (8)
Yb-O(THF)	2.40 (1)	2.447 (6)
	Angles	
N-Yb-N	77.9 (6) (N2YbN4)	92.4 (2) (N2YbN4)
	77.6 (7) (N4YbN4a)	75.3 (2) (N2YbN6)
		75.8 (2) (N4YbN6)
I-Yb-N	173.1 (5) (IYbN2)	133.6 (2) (IYbN2)
	107.3 (4) (IYbN4)	132.1 (2) (IYbN4)
		121.5 (1) (IYbN6)
I-Yb-O(THF)	89.6 (3)	92.7 (2)

common geometry for six-coordinate complexes is octahedral and the observed bicapped tetrahedral arrangement represents the first example in lanthanide chemistry.

The Yb-O(THF) distance in **11**, 2.40(1)Å, compares favorably with that in $(C_5Me_5)_2Yb(THF)(C_7H_8)_{0.5}$[13] (Yb-O 2.412(5)Å). The Yb-I distance of 3.065(2)Å, is comparable to 3.237(1) Å for terminal Sm-I distance found in the six-coordinate Sm(II) complex $[SmI(\mu\text{-}I)(N\text{-}MeIm)_3]_2$[14] after a correction for the difference in ionic radii between Sm(II) and Yb(II) (0.15Å). The average Yb-N distance in **11** (2.50(4)Å) is comparable to that in the related six-coordinate complex $(Tp^{Me2})_2Yb$ (2.482(5)Å,[15] 2.480(4)Å[16]), but slightly longer than that in **13** (2.453(8)Å), consistent with the reduced coordination number of the latter compound. However, the Yb-I and Yb-O distances in **11** and **13** are similar, if anything the Yb-O length in **11** is slightly shorter. The apparent inconsistency between the two measurements may be attributed to the size difference between the two ligands. Steric repulsion between the ^{t}Bu moiety of the bulky $Tp^{tBu,Me}$ ligand and coordinated THF and iodide prevents the expected reduction in bond distances on going from six-coordinated **11** to five coordinated **13**.

4.3. Derivatization of $(Tp^{tBu,Me})LnI(THF)_n$

4.3.1. Synthetic Aspects

The $(Tp^{tBu,Me})LnI(THF)_n$ complexes have proven to be excellent precursors to a variety of new half-sandwich, divalent lanthanide compounds. Their synthetic utility is clearly documented in Scheme 4.1. The reactions occur readily at low temperature and give, after appropriate work-up, pure products. Precipitation of NaI or KI, provides the principal driving force for these simple metathesis reactions.

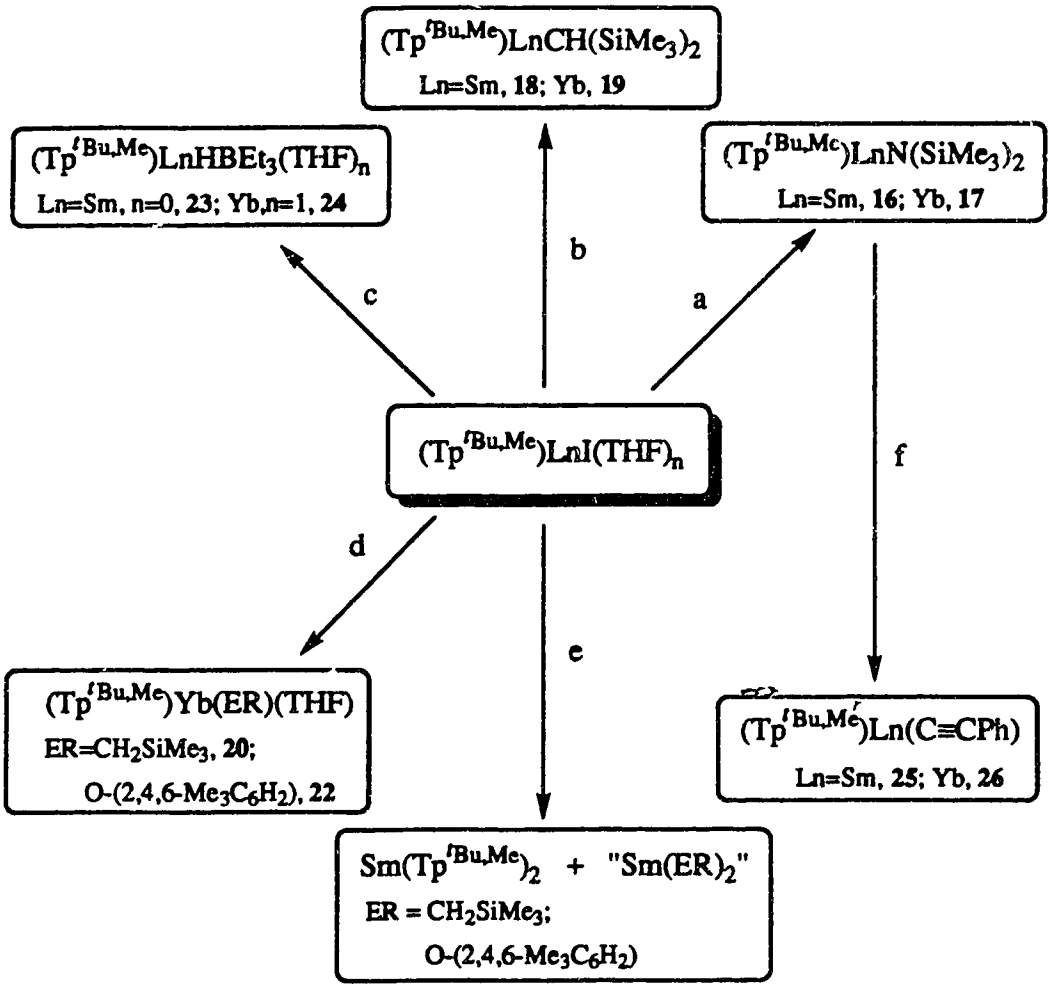

Scheme 4.1 Reagents and conditions (at -50°C): a, NaN(SiMe$_3$)$_2$, toluene; b, KCH(SiMe$_3$)$_2$, diethyl ether; c, NaHBEt$_3$, toluene; d and e, KER, diethyl ether or THF; f, HC≡CPh, hexane

Our initial attempts involved the bulky, lipophilic bis(trimethylsilyl)amido ligand, $(Me_3Si)_2N^-$, because it has been widely utilized to prepare well defined, hydrocarbon-soluble complexes with low coordination number in transition metal and f-element chemistry.[18] To our pleasure, monomeric, pentane-soluble amide complexes (Tp^{tBu,Me})Ln[N(SiMe$_3$)$_2$] (Ln=Sm, dark green, **16**; Yb, orange, **17**) were easily obtained by addition of NaN(SiMe$_3$)$_2$ to (Tp^{tBu,Me})LnI(THF)$_n$ (Ln=Sm, n=0; Yb,

n=1) at -50°C in toluene. Complexes of **16** and **17** are the first monomeric, solvent-free and salt-free divalent lanthanide amide compounds. The formulation of compounds **16** and **17** is consistent with elemental analysis, mass spectra, IR, ^{1}H, ^{11}B and ^{171}Yb NMR spectroscopies. ^{1}H NMR spectrum of samarium compound **16** exhibits isotropically shifted signals due to the paramagnetic center of samarium.

Considering the importance of the metal-carbon bond in the broad range of stoichiometric and catalytic organometallic reactions, one of the ultimate goals was the preparation of Ln(II) hydrocarbyl complexes. An added incentive was the fact that these complexes were unknown at the time our studies were initiated. The common way to generate a Ln-C bond in organo-lanthanide chemistry is metathesis of a Ln-X bond with lithium alkyls. However, initial studies showed that $LiCH(SiMe_3)_2$, Li^tBu and LiPh were unsuitable since the reactions with the samarium **14** gave intractable, arene-insoluble red-brown material. Another way of introducing a hydrocarbyl moiety to metal center is by reaction of the metal halide with Grignard reagents. However, the reaction of $(Tp^{tBu,Me})SmI(THF)_2$ with CH_3MgCl gave $(Tp^{tBu,Me})MgCH_3$ and $SmICl(THF)_2$, eq. 4.6, the latter was not isolated.

$$(Tp^{tBu,Me})SmI(THF)_2 + CH_3MgCl \longrightarrow (Tp^{tBu,Me})MgCH_3 + \text{"}SmICl(THF)_2\text{"} \qquad 4.6$$

With the above two failures in mind, the use of $KCH(SiMe_3)_2$ and KCH_2SiMe_3 was attempted. It was hoped that precipitation of KI would provide the driving force and the more electropositive K^+ would give a better chance for transmetallation. It was indeed gratifying to see that the low temperature reaction of $(Tp^{tBu,Me})LnI(THF)_n$ with an equimolar amount of $KCH(SiMe_3)_2$ in diethyl ether, followed by recrystallization from the same solvent, gave monomeric, hexane-soluble crystalline solids of $(Tp^{tBu,Me})Ln(CH(SiMe_3)_2)$ (Ln=Sm, dark green, **18**; Yb, orange,

19). The complexes represented the first isolated divalent lanthanide alkyl complexes. Since then, Lappert et al. and Smith et al. have reported the synthesis and crystal structures of $Yb\{C(SiMe_3)_3\}_2$[19], $[Yb\{C(SiMe_3)_3\}I(OEt_2)]_2$[19], and $[Yb\{C(SiMe_3)_3\}(\mu\text{-}OEt)(OEt_2)]_2$[20]. Complexes **18** and **19** are thermally stable and no visual decomposition was observed after storage for weeks in the solid state at room temperature. The ^1H NMR spectra of the complexes show only one set of pyrazolyl group resonances. The equivalence of the two $SiMe_3$ moieties of $CH(SiMe_3)_2$ is maintained down to -100°C. The $CH(SiMe_3)_2$ methyne proton is a singlet with Yb satellites, the $^2J_{Yb\text{-}H}$ coupling constant is 24 Hz.

In a similar fashion, addition of KCH_2SiMe_3 in diethyl ether to ytterbium complex **13** at -50°C, after simple workup, affords the desired hexane-soluble orange $(Tp^{tBu,Me})Yb(CH_2SiMe_3)(THF)$ in good yield. The monomeric, mono-solvated nature of compound **20** is consistent with analytical and spectroscopic data and was verified by X-ray crystallographic study (see later). The THF molecule in **20** is not displaced by diethyl ether during the reaction, suggesting that THF ligand is needed for coordinative saturation. Variable temperature ^1H NMR reveals that the molecule is fluxional and all three pyrazolyl rings are equivalent down to -100°C. The methylene resonance of the CH_2SiMe_3 unit is a singlet with Yb satellites ($^2J_{Yb\text{-}H}$ =18 Hz). Unfortunately reaction of samarium complex **14** with the less sterically hindered KCH_2SiMe_3 led to the unexpected formation of $(Tp^{tBu,Me})_2Sm$, a product of ligand redistribution, as shown in eq. 4.7. Hence the ligand environment provided by

$$(Tp^{tBu,Me})SmI + KCH_2SiMe_3 \longrightarrow \{(Tp^{tBu,Me})SmCH_2SiMe_3\} \longrightarrow (Tp^{tBu,Me})_2Sm + \text{"}Sm(CH_2SiMe_3)_2\text{"} \quad 4.7$$

one $Tp^{tBu,Me}$ ligand, one CH_2SiMe_3 and THF molecules is able to stabilize ytterbium(II) ion but not the larger samarium(II) ion. The marked difference in stability

must be due to the difference in ionic radii. It is more difficult to stabilize the larger Sm(II) atom than Yb(II), therefore it is more prone to undergo ligand redistribution.

Similar problems were encountered with aryloxide derivatives. Addition of one equiv of potassium 2,4,6-trimethylphenyloxide to compound **11** in toluene at low temperature, followed by recrystallization from the same solvent yielded orange crystals of monomeric $(Tp^{tBu,Me})Yb(O\text{-}2,4,6\text{-}Me_3C_6H_2)(THF)$ in good yield. Given the similar ionic radii and $E_{1/2}$ of Yb(II) and U(III), this is in sharp contrast with the behaviour of U(III) where reaction of $(Tp^{Me2})UI_2(THF)_2$ with $KO\text{-}2,4,6\text{-}Me_3C_6H_2$ at low temperature led to redox reaction, and formation of a U(IV) complex, $(Tp^{Me2})U(O\text{-}2,4,6\text{-}Me_3C_6H_2)_3$.[21] The different chemistry between Yb(II) and U(III) may be due to the fact that the redox product, $(Tp^{tBu,Me})Yb(O\text{-}2,4,6\text{-}Me_3C_6H_2)_2$, would be too crowded to exist. The ytterbium complex **22** is soluble in toluene and THF but very sparingly soluble in hydrocarbons. Attempts to prepare the samarium analogue again failed. The reaction of **14** with one equiv of $KO\text{-}2,4,6\text{-}Me_3C_6H_2$ in THF gave $(Tp^{tBu,Me})_2Sm$, the ligand redistribution product.

Lanthanide hydride complexes have played a fundamental role in catalytic processes such as olefin polymerization, hydrogenation and hydroamination.[22,23] An often used route to preparing such complexes involves reaction of metal halides with hydride donors such as MH, $MAlH_4$ and $MHBEt_3$ (M=Li, Na, K). Alkali trialkylborohydrides, which are soluble in common solvents, have been widely used in organic chemistry as hydride donors.[24] The utility of these hydrides in organometallic synthesis has also been established. Ephritikhine et al.[25] have reported the successful synthesis of $(\eta^5\text{-}C_5H_4SiMe_3)_3UH$ by reaction of $(\eta^5\text{-}C_5H_4SiMe_3)_3UCl$ with $KHBEt_3$. Although trivalent lanthanide hydrides have been well established, the preparation of divalent lanthanide hydrides remained elusive.[26] In an attempt to prepare hydrides, reaction of complexes **13** and **14** with $KHBEt_3$ was carried out.

Addition of one equiv of $KHBEt_3$ to a toluene solution of $(Tp^{tBu,Me})LnI(THF)_n$ (Ln=Sm, n=0; Yb, n=1) at -50°C followed by filtration and crystallization from hexane afforded dark green (Sm, **23**) and orange (Yb, **24**) crystalline solids in good yield. Characterization of the complexes surprisingly revealed the retention of BEt_3 fragment. The complexes **23** and **24** are hydrocarbon-soluble. They are highly air-sensitive but thermally stable. No significant decomposition of compound **23** in solution was observed up to 100°C as monitored by ^1H NMR. The compound doesn't sublime under dynamic vacuum and melts at 110°C.

The IR spectra of solids display two H-B stretches: one at 2550 cm^{-1} for the ytterbium complex and 2548 cm^{-1} for the samarium compound; the other at 1935 cm^{-1} for ytterbium and 1936 cm^{-1} for samarium. The bands at higher frequencies are typical for terminal H-B stretch of a pyrazolylborate ligand while the signal at ca. 1936 cm^{-1} is 25 cm^{-1} lower than that of H-B vibrational stretch of $NaHBEt_3$, and perhaps indicative of B-H-Ln interaction.

^1H NMR spectra of complexes **23** and **24**, shown in Figure 4.4 and Figure 4.5 respectively, are simple, consisting of only a single set of pyrazolyl group resonances and one set of ethyl group resonances. The peaks of the ethyl groups in samarium complex **23** are shifted to much higher field from their diamagnetic positions found in the ytterbium complex and provide further indication for $HBEt_3$ coordination. The ^{11}B NMR spectra of both **23** and **24** show two signals, consistent with the presence of a $HBEt_3$ moiety. In the spectrum of the ytterbium complex, the signal at lower field (-8.3 ppm) is a broad singlet with no resolvable B-H coupling, the higher field resonance (-10.2 ppm) is a doublet with a reduced B-H coupling constant of 46 Hz compared to that of 65 Hz observed in $NaHBEt_3$. The presence of the hydride bridge between Yb and BEt_3 was confirmed by ^{171}Yb NMR and $^{171}Yb\{^1H\}$ experiments. The proton coupled spectrum is a doublet, $^1J_{Yb\text{-}H}$ =200 Hz, which

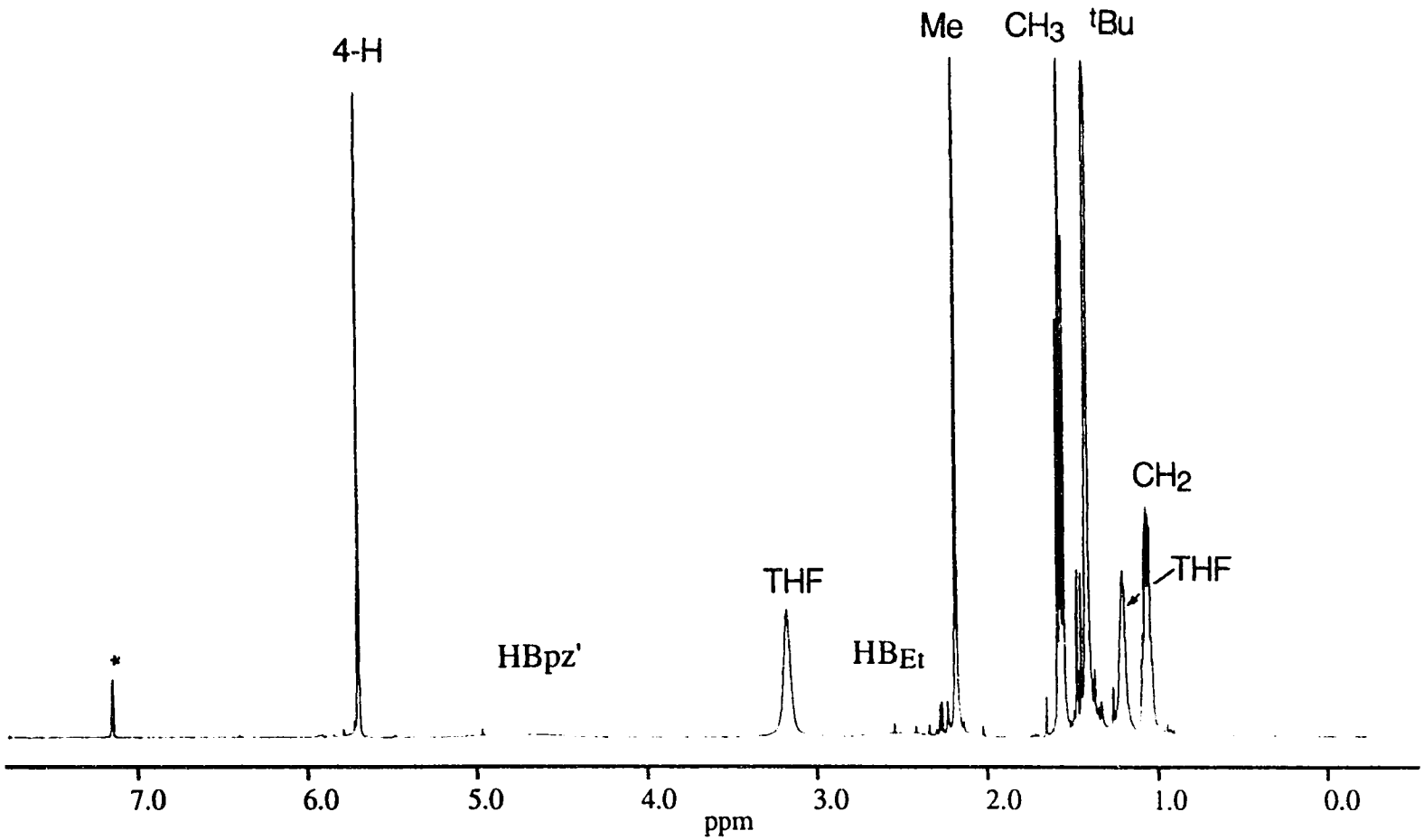

Figure 4.4 400 MHz ^{1}H NMR spectrum of $(Tp^{tBu,Me})Yb[HB(CH_2CH_3)_3](THF)$ (**24**) in benzene-d_6

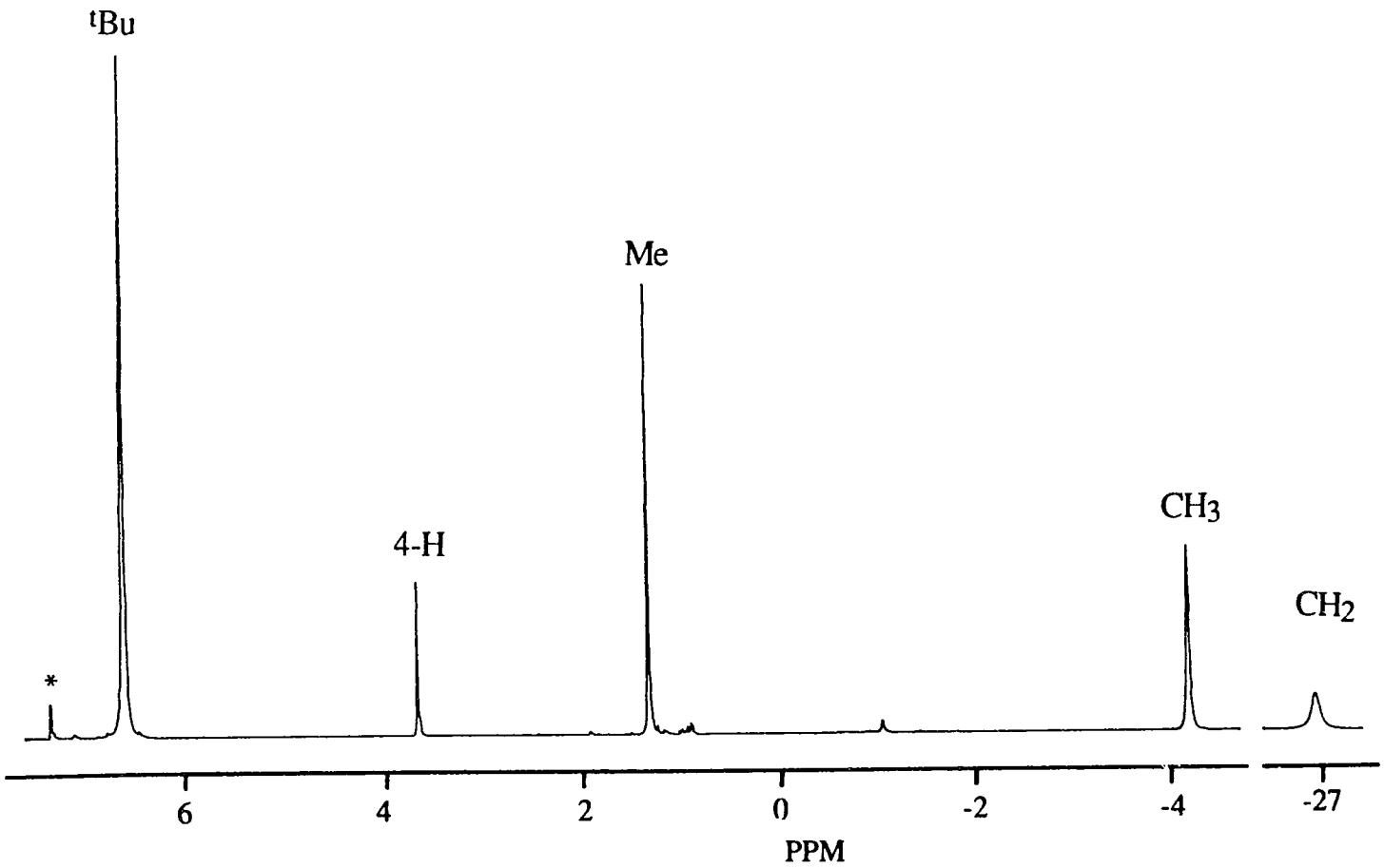

Figure 4.5 400 MHz ^{1}H NMR spectrum of $(Tp^{tBu,Me})Sm[HB(CH_2CH_3)_3]$ (**23**) in benzene-d_6

collapses to a singlet when the B-H signal at 2.55 ppm is irradiated. Upon irradiation of this B-H signal, the higher field ^{11}B doublet is also collapsed to a singlet, which lends further support for the presence of bridging B-H-Yb unit. The observed ^{171}Yb-^{1}H coupling constant, is similar to the 170 Hz reported by Green for $[\{(C_5H_5)_2NbH_2\}_2Yb\cdot diglyme]$[27]. The ^{11}B NMR spectrum of the samarium complex **23** exhibits two dramatically different signals at -33.6 ppm and -278 ppm. The chemical shift of the lower field signal is similar to that observed in the samarium complex **12** (-28.2 ppm). Therefore the drastically high-field shifted signal is attributed to the Et_3B-H-Sm unit as a result of it being much closer to the paramagnetic Sm(II) center.

The hydride of the bridging Ln-H-BEt_3 is not reactive. Preliminary reactivity studies show that complexes **23** and **24** do not react with phenylacetylene, ethylene or propylene. However, the amide complexes $(Tp^{tBu,Me})Ln[N(SiMe_3)_2]$ readily undergo simple metathetical reactions with HC≡CPh in hexane at low temperature to give $(Tp^{tBu,Me})Ln(C{\equiv}CPh)$ (Ln=Sm, dark brown, **25**; Yb, dark reddish brown, **26**) in good yields. This contrasts to the behavior of $(C_5Me_5)_2Yb(OEt_2)$, and $(C_5Me_5)_2Sm(THF)_2$, toward HC≡CPh. The samarium complex $(C_5Me_5)_2Sm(THF)_2$ undergoes electron transfer reaction to afford $(C_5Me_5)_2Sm(C{\equiv}CPh)(THF)$[28] in excellent yield, while the ytterbium complex $(C_5Me_5)_2Yb(OEt_2)$ undergoes both simple metathetical and electron transfer reactions to form a mixed-valence complex$[(C_5Me_5)_2Yb]_2(\mu\text{-}C{\equiv}CPh)_4Yb$.[29] Interestingly, Evans et al. reported that the $(C_5Me_5)_2Ln[N(SiMe_3)_2]$ complexes are unreactive towards HC≡CPh even at 100°C in the non-coordinating solvent toluene, but the metalation reaction does take place in THF.[30]

4.3.2. Crystallographic Studies

ORTEP drawings of the molecules, with numbering schemes, are shown in Figures 4.6 - 4.10, respectively. Important bond lengths and angles are presented in Table 4.2 for **17** and **19**, Table 4.3 for **20**, **22** and **24**, respectively. All five compounds contain monomeric, discrete units, with molecules separated by normal van der Waals contact.

Table 4.2 Selected Bond Lengths (Å) and Angles (deg) for $(Tp^{tBu,Me})Yb[N(SiMe_3)_2]$ (**17**), $(Tp^{tBu,Me})Yb[CH(SiMe_3)_2]$ (**19**)

	17	**19**
	Distances	
Yb-N	2.475 (5) (Yb-N3)	2.482 (4) (Yb-N2)
	2.438 (4) (Yb-N5)	2.471 (4) (Yb-N4)
	2.467 (5) (Yb-N7)	2.454 (4) (Yb-N6)
ave	2.46 (2)	2.47 (1)
Yb-Y	2.382 (5) (Yb-N1)	2.552 (5) (Yb-C1)
Yb--C	3.064 (5) (Yb--C1)	3.070 (Yb--C7)
	Angles	
N-Yb-N	92.3 (1) (N3YbN5)	94.12(13) (N2YbN4)
	76.2 (2) (N3YbN7)	76.18 (14) (N2YbN6)
	75.2 (2) (N5YbN7)	78.32 (14) (N4YbN6)
N-Yb-Y	125.4 (2) (N1YbN3)	119.6 (2) (C1YbN2)
	120.3 (2) (N1YbN5)	129.1 (2) (C1YbN4)
	149.1 (1) (N1YbN7)	142.4 (2) (C1YbN6)

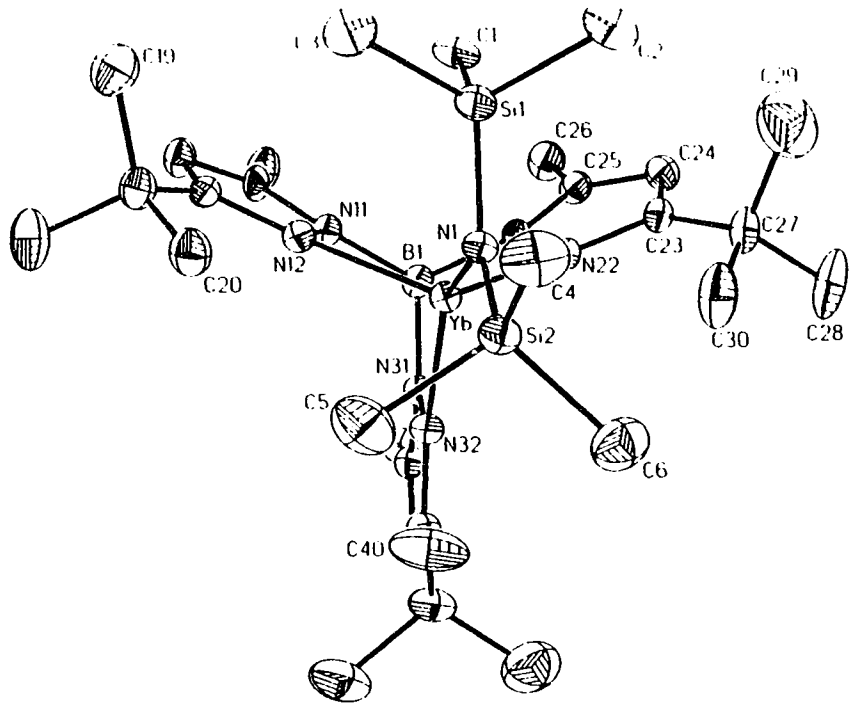

Figure 4.6 ORTEP view of $(Tp^{tBu,Me})Yb[N(SiMe_3)_2]$ (17)

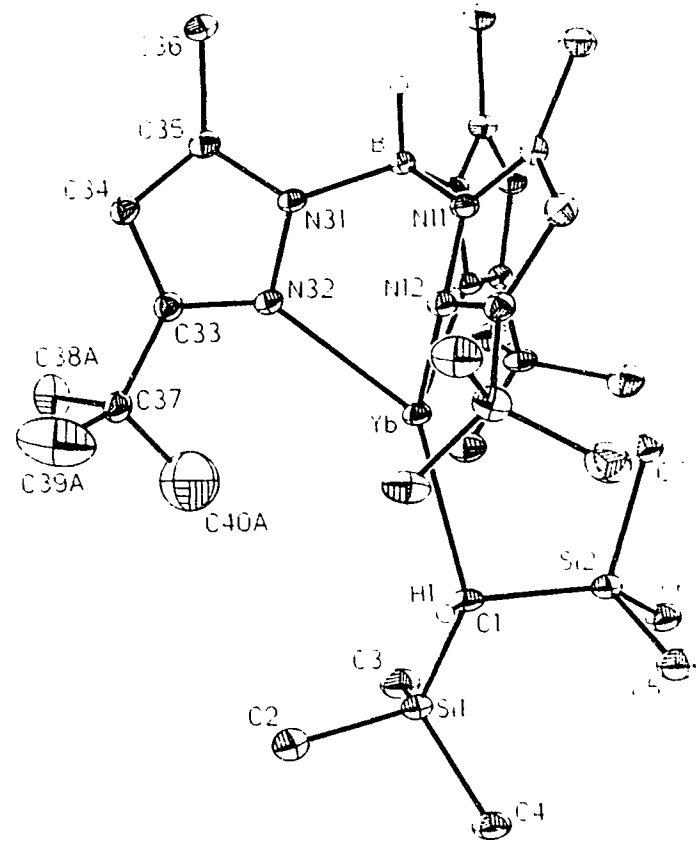

Figure 4.7 ORTEP view of $(Tp^{tBu,Me})Yb[CH(SiMe_3)_2]$ (19)

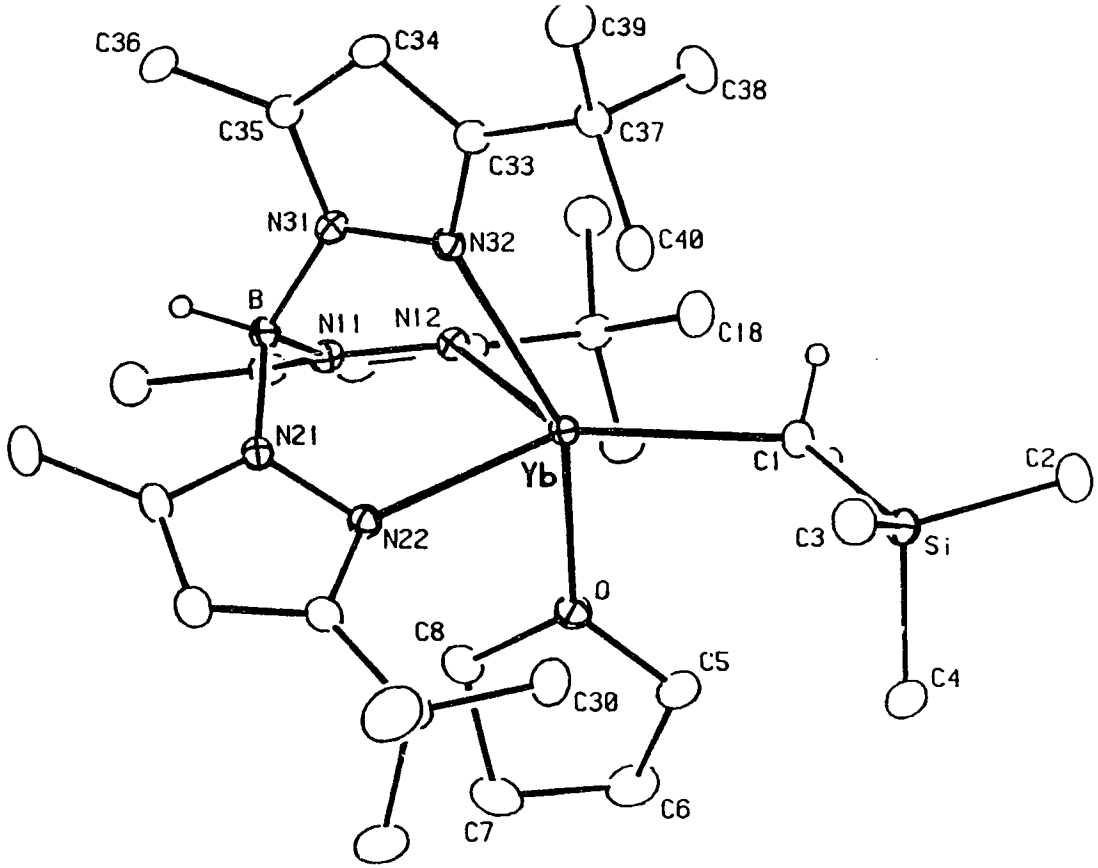

Figure 4.8 ORTEP view of $(Tp^{tBu,Me})YbCH_2SiMe_3(THF)$ **(20)**

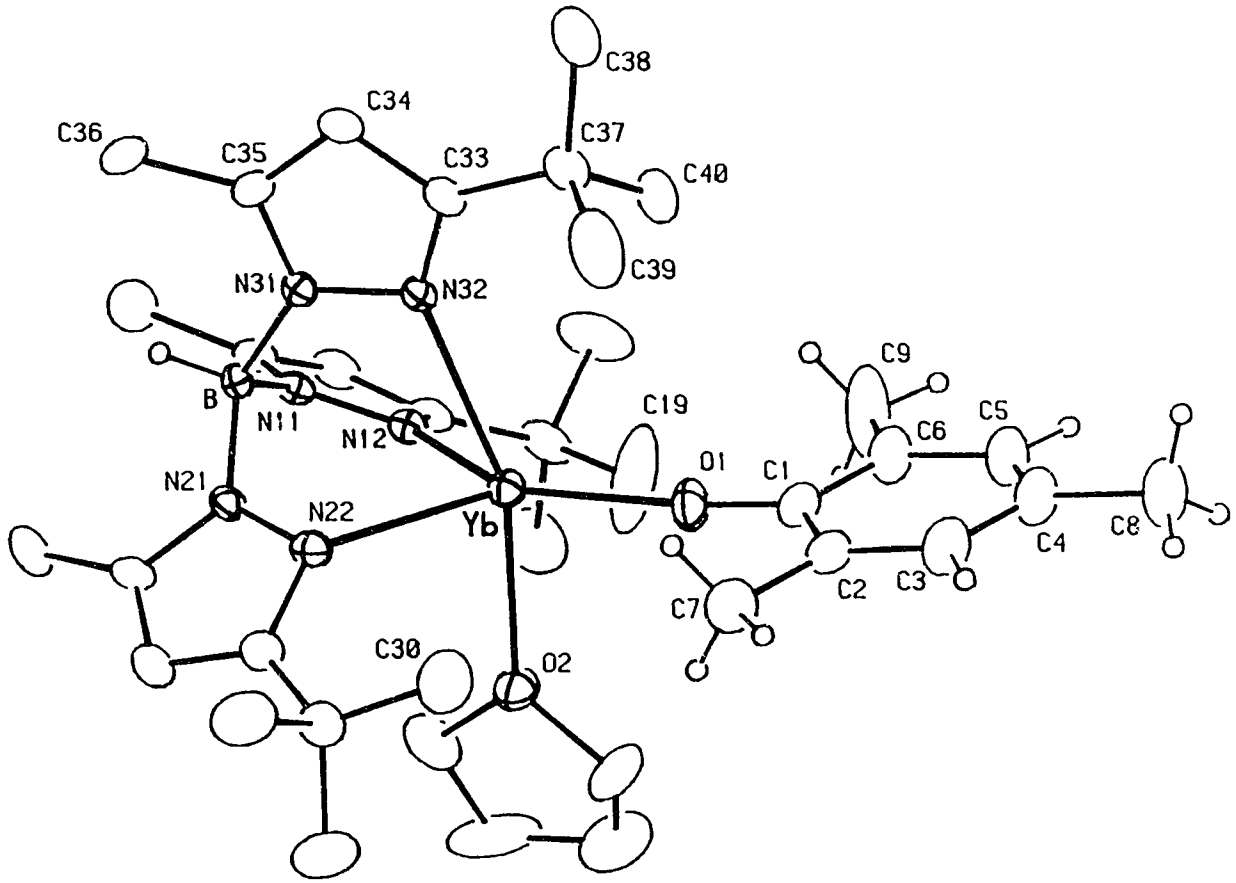

Figure 4.9 ORTEP view of $(Tp^{tBu,Me})Yb[O(2,4,6\text{-}Me_3C_6H_2)](THF)$ (22)

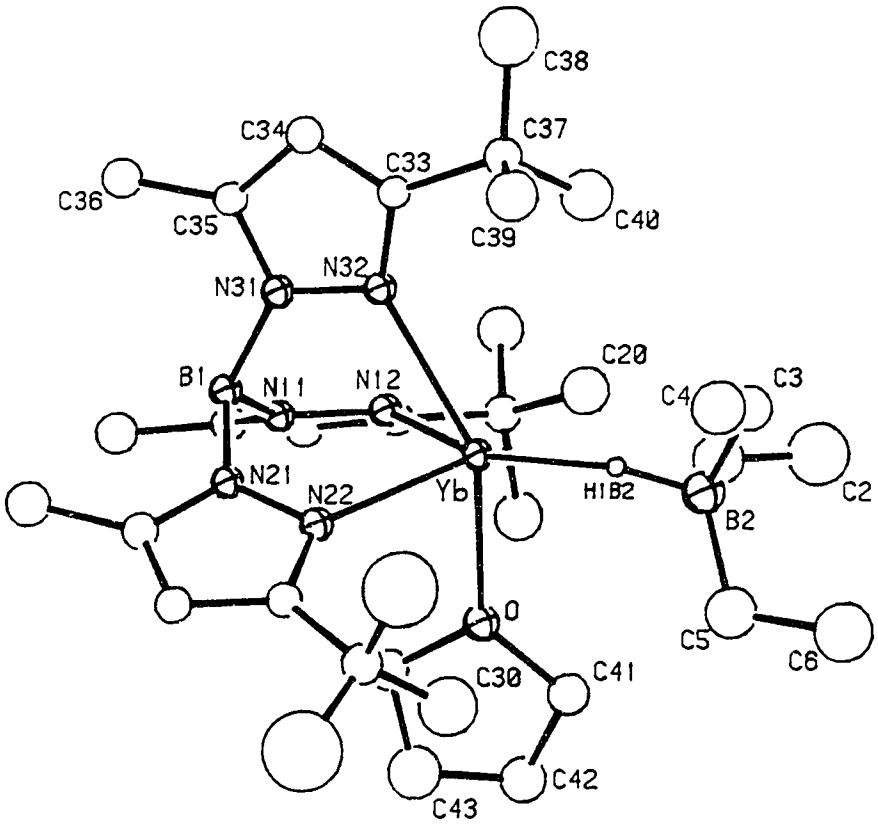

Figure 4.10 ORTEP view of $(Tp^{tBu,Me})Yb[HB(CH_2CH_3)_3](THF)$ **(24)**

Table 4.3 Selected Bond Lengths (Å) and Angles (deg) for $(Tp^{tBu,Me})Yb(CH_2SiMe_3)(THF)$ (**20**), $(Tp^{tBu,Me})Yb[O\text{-}(2,4,6\text{-}Me_3C_6H_2)](THF)$ (**22**) and $(Tp^{tBu,Me})Yb(HBEt_3)(THF)$ (**24**)

	20	**22**	**24**
		Distances	
Yb-N12	2.500 (3)	2.525 (6)	2.480 (8)
-N22	2.477 (3)	2.501 (5)	2.451 (8)
-N32	2.517 (3)	2.467 (5)	2.524 (7)
Yb-X	2.528 (4) (Yb-C1)	2.177 (5) (Yb-O1)	2.12 (Yb-H1B2)
Yb-O(THF)	2.484 (3)	2.395 (5) (Yb-O2)	2.481 (7)
		Angles	
N12-Yb-N22	90.14 (9)	90.0 (2)	92.4 (2)
N12-Yb-N32	77.08 (9)	77.1 (2)	74.9 (2)
N22-Yb-N32	76.5 (1)	78.7 (2)	78.8 (2)
N-Yb-X	128.8 (1) (N12YbC1)	133.9 (2) (N12YbO1)	152.1 (N12YbH1)
	140.2 (1) (N22YbC1)	135.7 (2) (N22YbO1)	115.4 (N22YbH1)
	115.5 (1) (N32YbC1)	112.4 (2) (N32YbO1)	111.2 (N32YbH1)

X-ray analysis reveals that the hydrotris(pyrazolyl)borate ligand is bonded to Yb center in an η^3-fashion. The complexes **17** and **19** are four-coordinate and **20, 22** and **24** are five-coordinate. The average Yb-N(pz) distances in complexes **17, 19** are slightly shorter than those in **20, 22, 24,** as expected from the reduced coordination number of the former compounds. A common feature of all five structures is that they exhibit unsymmetrical ($Tp^{tBu,Me}$)Yb ligation, one intraligand N-Yb-N angle is substantially larger, in the 92.3(1)-92.4(2)° range, than the other two, in the 75.2(2)-78.8(2)° range. As will be shown, the origin of this distortion is steric. Structural comparison of the complexes will be divided according to the coordination number of the ytterbium center.

Molecular Structures of Compounds 17 and 19

The coordination geometries of both compounds are distorted tetrahedral. The distortion is manifested by $E(SiMe_3)_2$ ligand (E = N , CH) being off the B---Yb axis by 18.6° for **17** and 15.0° for **19**. Although steric repulsions may be largely responsible for this, the role of electronic factors will be addressed also.

The ytterbium-amido nitrogen distance in **17** is 2.382(5)Å. This distance is similar to those found in other ytterbium(II) complexes containing the $N(SiMe_3)_2$ ligand; 2.331(13)Å in $Yb[N(SiMe_3)_2]_2(dmpe)$[31] and 2.38(2)Å in $NaYb[N(SiMe_3)_2]_3$[32] for the terminal amido ligand. As expected, these distances are shorter than the bridging Yb-N distances seen in $Yb[N(SiMe_3)_2]_2(AlMe_3)_2$[33] (2.510(2)Å and 2.573(2)Å), and those in $NaYb[N(SiMe_3)_2]_3$ (2.45(2) and 2.47(2)Å). Compound **19** represented the first structurally characterized Yb(II)-hydrocarbyl complex. The length of the Yb-C1 sigma bond, 2.552(5)Å is comparable to those found in $Yb(CH(SiMe_3)_2)_3Cl^-$[34], after correction for the difference in ionic radii between four-coordinate Yb(II) and Yb(III) ions, and is also close to those found in

most recently structurally characterized complexes containing Yb(II)-C σ-bonds: $Yb(C(SiMe_3)_3)_2$[19] (2.490(8)Å, 2.501(9)Å), $[Yb(C(SiMe_3)_3)I(OEt_2)]_2$[19] (2.47(2)Å), and $[Yb(C(SiMe_3)_3)(\mu\text{-}OEt)(OEt_2)]_2$[20] (2.573(13)Å). The Yb-C1 distance is also somewhat longer than Yb(II)-carbene distance observed in $(C_5Me_4Et)_2Yb$(1,3,4,5-tetramethylimidazol-2-ylidene)[35]. The shorter Yb(II)-C distance found in the carbene complex is consistent with its high thermal, air and moisture stability compared to other Yb(II) complexes.[35]

The steric unsaturation and electronic demand of the ytterbium center in both compounds are compensated by secondary interactions between ytterbium and one of methyl groups of $E(SiMe_3)_2$ (E = N, CH) ligand. This interaction is clearly evidenced from the very different Yb-C-Si angles: Yb-C1-Si1 = 133.0(3)° and Yb-C1-Si2 = 99.1(2)°. The distortion results in short Yb---C1/C7 contacts of 3.064(5)Å and 3.070(7)Å, in **17** and **19** respectively. These distances are substantially less than 3.7Å, the sum of the Yb(II) metallic and van der Waals radius of the CH_3 moiety. Finally, it is noteworthy that the position of the C1-H atom of **19** could be refined. The $CH(SiMe_3)_2$ moiety is almost planar and the hydrogen is pointing toward the metal (Yb-C1-H1 = 92(3)°) and this results in short Yb-H distances (Yb-H1 = 2.77(5)Å). Similar α-CH agostic interactions have been observed for a number of trivalent lanthanide and actinide hydrocarbyls,[36] and reflect the high electron deficiency of the compound. In the case of the amido complex **17**, π-donation from the planar $N(SiMe_3)_2$ nitrogen fulfills this demand.

Molecular Structures of Compounds 20, 22 and 24

The replacement of the bulky $E(SiMe_3)_2$ (E=N, CH) by smaller ligands (CH_2SiMe_3, $HBEt_3$ and OAr) allows for an increase in the coordination number of ytterbium from four to five. Coordination of THF relieves the electron deficiency and

steric unsaturation at Yb(II). As a result, no secondary interactions are seen between Yb and methyl or α-C hydrogens. The geometries of the three complexes are distorted trigonal bipyramidal with two pyrazolyl nitrogens (N12 and N22) and the ER ligand occupying the equatorial positions. The THF molecule lies in the cleft between two pyrazolyl rings and causes the corresponding N-Yb-N angle to open up significantly compared to the other two N-Yb-N angles. The Yb-O(THF) distances 2.484(3)Å and 2.481(7)Å in complexes **20** and **24** respectively are identical, but are significantly longer than that in **22** (2.395(5)Å), perhaps the flat aryloxide ligand allows for the closer approach of THF in this molecule. The average Yb-N(pz) distance in the three structures are similar.

The Yb-C1-Si angle of 135.7(2)° in compound **20** is similar to that found in $(C_5H_5)_2Lu(CH_2SiMe_3)THF$[37] where no secondary interaction between Lu and hydrocarbon group was found. The Yb-C1 bond length 2.528Å is close to that found in **19**, but longer than 2.344(18)Å and 2.314(18)Å found in $[Li(THF)_3]Lu(\eta^5\text{-}C_5Me_5)(CH_2SiMe_3)[CH(SiMe_3)_2]Cl$[38] and 2.376(17)Å found in $(C_5H_5)_2Lu(CH_2SiMe_3)THF$.[37] The two α-hydrogens of the (trimethylsilyl)methyl ligand are pointing away from Yb center. Thus no α-agostic Yb-H--C interactions are present in **20**. The bond lengths and angles in CH_2SiMe_3 ligand are unexceptional compared to those found in other (trimethylsilyl)methyl complexes.[39]

The Yb-O1 (aryloxide) distance of 2.177(5)Å is close to the corresponding values, 2.21(1)Å and 2.22(1)Å, seen in five-coordinate $Yb(OAr)_2(THF)_3$[12] and compares favorably to 2.075(6)Å and 2.046(6)Å found in five-coordinate $Y_2(OC_6H_3Me_2\text{-}2,6)_6(THF)_2$[40], after correction for the difference in ionic radii between Yb(II) and Y(III) (0.12Å)[41]. The Yb-O2(THF) distance is ca. 0.22 Å longer than Yb-O1 (aryloxide). This bond length difference is in the 0.2-0.3 Å range observed for other ytterbium aryloxide complexes.[12] The shortening is as expected

from the strong interaction between Yb(II) and the anionic π-donor ligand. The Yb-O1-C angle 173.3(5)° is at the long end of the range 119(1)°-177.8(8)° observed in ytterbium aryloxide complexes. The distances of ytterbium to methyl groups C7 and C9 are 4.35Å and 4.24Å respectively, which reveals the absence of secondary interactions.

The X-ray analysis also revealed that $HBEt_3$ moiety is coordinated to Yb(II) center *via* a Yb-H-BEt_3 linkage, which corroborates the IR and NMR results. Although there are numerous metal complexes containing M-H-B unit,[42] to our knowledge this is the first example of a metal complex with a coordinated triethylborohydride ligand. The calculated Yb-H1 distance of 2.12Å is comparable to those of 2.2(1)Å and 2.4(1)Å found in $(CH_3CN)_6Yb(\mu\text{-}H)_2B_{10}H_{12}$[43] and 2.32(8)-2.33(7)Å in $[\{(C_5H_5)_2NbH_2\}_2Yb\cdot diglyme]$[27] but ca. 0.2Å longer than the bridging Yb-H-Yb distances of 1.903(4)Å, and 2.10(3)Å in $[\{MeSi(\eta^5\text{-}C_5H_4)_2Yb(THF)\}_2(\mu\text{-}H)(\mu\text{-}Cl)]$[44]. The Yb-H-BEt3 linkage is bent and Yb-H1-B2 angle is 151°. This is in contrast with the almost linear hydride bridging observed in $[Zn(\eta^1\text{-}GaH_4)Cl(pmdeta)]$(Zn-H-Ga 177(3)°)[45]. However, bent linkage was seen in the copper complex containing an $\eta^1\text{-}BH_4$ ligand, $[Cu(\eta^1\text{-}BH_4)(triphos)]$ [triphos = 1,1,1-tris{[(diphenylphosphino)methyl]ethane}][46].

4.4. ^{171}Yb NMR Studies

A unique feature of the Yb(II) species lies in the availability of ^{171}Yb NMR spectroscopy. The ^{171}Yb isotope has a nuclear spin 1/2, it is 14.27% natural abundant and has a receptivity four times larger than that of ^{13}C and therefore it can be readily observed. Recently, ^{171}Yb NMR has been used as a structural and mechanistic probe.[47] We have successfully utilized ^{171}Yb NMR to confirm the presence of an agostic Ln-H-B interaction in $(Tp^{tBu,Me})_2Yb$ (see Chapter 5) and the persistence of the

bridging Yb-H-BEt_3 linkage in solution. The ^{171}Yb NMR data for the Yb complexes are listed in Table 4.4. The ^{171}Yb chemical shifts are in the range, 400-1000 ppm, with $(Tp^{tBu,Me})Yb(CH_2SiMe_3)(THF)$ (985 ppm) having the lowest field resonance and $(Tp^{tBu,Me})Yb(HBEt_3)(THF)$ (413 ppm), the highest field resonance. Although it is difficult to assess quantitatively the shielding contribution to the ^{171}Yb chemical shift from the different ligands, for the present series the following order holds: hydrocarbyl > amide > iodide > aryloxide > triethylborohydride. A similar order has been observed for the yttrium chemical shift in a series of three-coordinate

Table 4.4 ^{171}Yb NMR Chemical Shifts

Complex	δ (ppm)
$(Tp^{tBu,Me})Yb(CH_2SiMe_3)(THF)$	985
$(Tp^{tBu,Me})YbCH(SiMe_3)_2$	865
$(Tp^{tBu,Me})YbN(SiMe_3)_2$	711
$(Tp^{tBu,Me})YbI(THF)$	689
$(Tp^{tBu,Me})Yb(C{\equiv}CPh)$	673
$(Tp^{tBu,Me})Yb(OAr)(THF)$	600
$(Tp^{tBu,Me})Yb(HBEt_3)(THF)$	413

organoyttrium complexes[1], $Y[CH(SiMe_3)_2]_3$ (895.0 ppm), $Y[N(SiMe_3)_2]_3$ (570 ppm), $Y(OAr)_3$(Ar=2,6-$^tBu_2C_6H_2$-4-Me (170.8 ppm).

4.5. Conclusions

Reaction of SmI_2 with one equivalent of KTp^{Me2} gave $(Tp^{Me2})_2Sm$, the result of a ligand redistribution reaction, instead of the sought after "$(Tp^{Me2})SmI$". The same

reaction with the smaller Yb(II) ion gave the desired half-sandwich complex, $(Tp^{Me2})YbI(THF)_2$ (**11**) in good yield. However, compound **11** is not stable and tends to ligand redistribute to $(Tp^{Me2})_2Yb$ and YbI_2 in non-coordinating solvents at room temperature. The use of the more sterically demanding ligand $Tp^{tBu,Me}$ finally allowed the stabilization and isolation of monomeric, arene-soluble, half-sandwich complexes $(Tp^{tBu,Me})LnI(THF)_n$ (Ln=Sm, n=2; Yb, n=1), which are inert to ligand redistribution reaction. These complexes, and especially the ytterbium compound, are excellent precursors to other mixed-ligand divalent lanthanide complexes. Noteworthy are the synthesis of the hydrocarbyl species, $(Tp^{tBu,Me})Ln[CH(SiMe_3)_2]$ (Ln=Sm, Yb) and $(Tp^{tBu,Me})Yb(CH_2SiMe_3)(THF)$, which represent the first examples of crystallographically characterized divalent lanthanide complexes containing Ln-C σ bond. Unfortunately, ligand redistribution reactions still plague the larger Sm(II) ion and no mixed-ligand derivatives could be isolated with the moderately bulky ligands such as $OC_6H_2Me_3$ and CH_2SiMe_3. One of the ligand rearrangement products, $(Tp^{tBu,Me})_2Sm$, has been isolated and its solid structure and unprecedented solution behaviour for f-element chemistry will be discussed in Chapter 5. In the solid state, complexes **20**, **22** and **24** are five-coordinate while **17** and **19** are four-coordinate but exhibit secondary interaction between the Yb center and one of the methyl groups from the $E(SiMe_3)_2$ (E=CH, N) moiety. The successful isolation of hydrocarbyl complexes opens the way to the preparation of hydride complexes. Indeed, preliminary experiments show that both ytterbium complexes **23** and **24** undergo slow hydrogenolysis to form orange crystalline solids. The identity of these species is of obvious interest.

4.6. Experimental Section

4.6.1. Starting Materials and Reagents

$KHB(3\text{-}^{t}Bu,5\text{-}Mepz)_3$ ($KTp^{tBu,Me}$) and was prepared by a modification of Trofimenko's method[48]. $AgBPh_4$ was prepared from $NaBPh_4$ and $AgNO_3$ according to the literature.[49] HC≡CPh was dried and vacuum-distilled before use (molecular sieves, 4Å). $KCH(SiMe_3)_2$ and KCH_2SiMe_3 were synthesized by reaction of corresponding lithium salt with $KO^{t}Bu$ in Hexane.[18] $NaN(SiMe_3)_2$ was purchased from Aldrich and sublimed before use. 1 M solution of $NaHBEt_3$ in toluene from Aldrich was used as received. KO-(2,4,6-$Me_3C_6H_2$) was prepared by reaction of HO-(2,4,6-$Me_3C_6H_2$) with an excess of potassium metal in THF.

4.6.2. Synthetic Procedures

$KTp^{tBu,Me}$

A mixture of 3-tert-butyl-5-methylpyrazol (6.90 g, 50 mmol) and KBH_4 (455 mg, 8.4 mmol) was placed into the bottom of an elongated glass tube (30 cm length x 4.5 cm inner diameter) which had been predried and filled with N_2 (the upper end of the tube is attached to a stopcock). The mixture was gradually heated to 140 °C, producing a vigorous evolution of H_2. When hydrogen evolution subsided the temperature was slowly raised to 240 °C and heating continued until no more H_2 was given off. The stopcock was closed and the tube allowed to cool. When the temperature reached ca. 150 °C, the tube was evacuated for 3 days to sublime excess 3-tert-butyl-5-methylpyrazol to the upper part of the tube. After sublimation the tube was cut where there is a break between the crude product and sublimed 3-tert-butyl-5-methylpyrazol. The crude product was dissolved in THF and filtered.

Removal of THF from the filtrate gave a white powder which was placed into another glass tube with the same dimensions as above. The powder was heated at 120°C under dynamic vacuum for one day to remove occluded THF solvent and trace amounts of 3-tert-butyl-5-methylpyrazol. The treatment gave analytically pure potassium hydrotris(3-tert-butyl-5-methylpyrazolyl)borate (2.90g, 74%).

$(Tp^{Me2})YbI(THF)_2$ (11)

A solution of KTp^{Me2} (135 mg, 0.4 mmol) in 10 mL of THF was added dropwise to a solution of YbI_2 (0.4 mmol) in 10 mL of THF, resulting in immediate formation of a white precipitate of KI. The mixture was stirred for 4 hours at room temperature and filtered. The filtrate was concentrated to ca. 3 mL and placed in a fridge at -40°C, and yielded a crop of bright orange crystals of **11** (208 mg, 70%). IR (KBr): ν(B-H) 2548 cm^{-1}. ^1H NMR (C_6D_6, 25°C): δ 5.72 (s, 3H, pz-H), 3.62 (br. s, 8H, THF), 2.23 (s, 9H, pz-Me), 1.98 (s, 9H, pz-Me), 1.42 (br. s, 8H, THF). ^{11}B NMR (C_6D_6, 25°C): δ -2.22 (s). Anal. Calcd for $C_{23}H_{38}N_6BO_2IYb$: C, 37.26; H, 5.17; N, 11.34; I, 15.95. Found: C, 37.26; H, 5.04; N, 10.66.

$(Tp^{tBu,Me})SmI(THF)_2$ (12)

A solution of $KTp^{tBu,Me}$ (462 mg, 1.00 mmol) in 10 mL of THF was added dropwise to a solution of SmI_2 (1.00 mmole) in 10 mL of THF, and a white precipitate of KI formed immediately. The mixture was stirred for 4 hours at room temperature and filtered. The filtrate was concentrated to ca. 5 mL and placed in a fridge at -40°C, and yielded a crop of dark green crystals of **12** (440 mg). Further concentration of the filtrate afforded another batch of crystals (311 mg). Total yield is 89%. IR (KBr): ν(B-H) 2523 cm^{-1}. ^1H NMR (THF-d_8, 25°C): δ 4.50(s, 27H, pz-^{t}Bu, 14), 3.62(s, 9H, pz-Me, 4), 3.60(s, 8H, THF, 6), 2.35(s, 3H, pz-H, 3), 1.70(s, 8H, THF, 6).

^{11}B NMR (THF-d_8, 25°C): δ -13.9(s, 192). Anal. Calcd for $C_{32}H_{56}N_6BO_2ISm$: C, 45.49; H, 6.68; N, 9.95. Found: C, 44.90; H, 6.87; N, 10.58.

($Tp^{tBu,Me}$)YbI(THF) (13)

In a similar fashion, the reaction of 252 mg of $KTp^{tBu,Me}$ and 370 mg of $YbI_2(THF)_{3.5}$ in 10 mL of THF, produced **13** as a yellow crystalline solid in 80% yield. IR (KBr): ν(B-H) 2514 cm^{-1}. MS (EI, 70eV, 230°C): m/z 724 (M^+-THF). ^1H NMR (toluene-d_8, 25°C): δ 5.64 (s, 3H, pz-H), 3.23 (br. s, 4H, THF), 2.17 (s, 9H, pz-Me), 1.45 (s, 27H, pz-^{t}Bu), 1.13 (br. s, 4H, THF). ^{11}B NMR (toluene-d_8, 25°C): δ -8.01 (s). ^{171}Yb NMR (toluene-d_8, 25°C): δ 689 (s, 70Hz). Anal. Calcd for $C_{28}H_{48}N_6BOIYb$: C, 42.28; H, 6.08; N, 10.56; I, 15.95. Found: C, 42.46; H, 6.02; N, 10.37; I, 16.35.

Sm($Tp^{tBu,Me}$)I (14)

Complex **12** was dissolved in toluene (2 mL) and solvent was removed under vacuum. The process was repeated several times until a large amount of a dark green solid remained that did not redissolve in toluene and the toluene solution became light green. Complex **14** was obtained as a dark green solid in almost quantitative yield. IR (KBr): ν(B-H) 2528 cm^{-1}. MS (EI, 70ev, 200°C): m/z 571(M^+-I). ^1H NMR (toluene-d_8, 25°C): δ 1.78(s, 27H, pz-^{t}Bu, 13), 1.04(s, 3H, pz-H, 4), 0.81(s, 9H, pz-Me, 6) (The spectrum was recorded at 14 and 42 mM, but no concentration dependence of the chemical shifts was observed). ^{11}B NMR (C_6D_6, 25°C): δ -27.3(s, 480). Anal. Calcd for $C_{24}H_{40}N_6BSmI$: C, 41.14; H, 5.75; N, 11.99; I, 18.11. Found: C, 41.04; H, 5.61; N, 11.53; I, 18.04

[($Tp^{tBu,Me}$)SmI(THF)$_2$][BPh$_4$] (15)

Solid $AgBPh_4$ (169 mg, 0.396 mmol) was added in several portions to a solution of ($Tp^{tBu,Me}$)SmI(THF)$_2$ (320 mg, 0.380 mmol) in ca. 15 mL of THF. The

green color of the Sm(II) complex faded and black Ag metal precipitated. The mixture was stirred for 2 hours and filtered. The THF solvent was removed from the yellow filtrate under vacuum. The resultant sticky, yellow residue was triturated with 10 mL of hexane. After stirring for 2 hours, a white powder was obtained. The supernatant hexane was inverse filtered, THF (5 mL) was added to the white powder and the mixture was stirred for 6 hours. Since at this stage it appeared that almost no solid had dissolved, the THF solvent was filtered off again. To the remaining white powder 15 mL of THF were added and the mixture was stirred overnight; this caused most of the solid to dissolve in THF. The mixture was filtered and the solvent was stripped off from the filtrate under vacuum. The so obtained white powder was shown by ^{1}H NMR to be reasonably pure $[(Tp^{tBu,Me})SmI(THF)_2][BPh_4]$ (**15**) (240 mg, 55%). Recrystallization from THF, saturated solution and slow cooling, gave a crystalline solid. However, elemental analysis of the crystalline solid was still not satisfactory. IR (KBr): ν(B-H) 2571 cm^{-1}. MS (EI, 70eV, 220°C) m/z 571 $(M^+\text{-I-2THF-BPh}_4)^+$. ^{1}H NMR ($CD_2Cl_2$, 25°C): δ 7.30(m, 8H, Ph-H), 7.00(m, 8H, Ph-H), 6.85(m, 4H, Ph-H), 5.88(s, 3H, pz-H), 4.48(m, 8H, THF-H), 2.76(s, 9H, pz-Me), 2.09(m, 8H, THF-H), -0.72(s, 27H, pz-^{t}Bu). ^{11}B NMR (CD_2Cl_2, 25°C): δ -5.5 (s). Anal. Cacld for $C_{56}H_{76}N_6O_2IB_2Sm$: C, 57.78; H, 6.58; N, 7.22. Found: C, 58.41; H, 7.24; N, 6.46.

$(Tp^{tBu,Me})Sm[N(SiMe_3)_2]$ (16)

A solution of $NaN(SiMe_3)_2$ (92 mg, 0.50 mmol) in ca. 5 mL of toluene was added dropwise to a stirred solution of the samarium complex **12** (422 mg, 0.50 mmol) in 5 mL of toluene at -50°C. The mixture was stirred for 3 h at low temperature and for another 3 h at room temperature. The toluene solvent was removed under vacuum, the residue was extracted with 5 mL of diethyl ether and filtered. The dark

green filtrate was concentrated to ca. 2 mL and placed at -40°C overnight, yielding **16** as a dark green crystalline solid (204 mg, 56%). IR (KBr): ν(B-H) 2550 cm^{-1}. MS (EI, 70eV, 250°C) m/z 735 (M^+). ^1H NMR (C_6D_6, 25°C): δ 4.66 (s, 18H, $N(SiMe_3)_2$, 16), 2.74 (s, 9H, pz-Me, 4), 2.31 (s, 27H, pz-^{t}Bu, 16), 2.20 (s, 3H, pz-H, 3). ^{11}B NMR (C_6D_6, 25°C) δ -33.4 (br. s, 282). Anal. Calcd for $C_{30}H_{58}N_7BSi_2Sm$: C, 49.08; H, 7.96; N, 13.35. Found: C, 49.20; H, 7.32; N, 13.17.

($Tp^{tBu,Me}$)Yb[$N(SiMe_3)_2$] (17)

In a similar fashion, reaction of 170 mg of **13** and 39 mg of $NaN(SiMe_3)_2$ in 8 mL of toluene, yielded the ytterbium analogue **17** in 61% yield. IR (KBr): ν(B-H) 2562 cm^{-1}. MS (EI, 70eV, 220°C) m/z 757 (M^+). ^1H NMR (C_6D_6, 25°C): δ 5.64 (s, 3H, pz-H), 4.60 (br. s, 1H, B-H), 2.10 (s, 9H, pz-Me), 1.40 (s, 27H, pz-^{t}Bu), 0.36 (s, 18H, $N(SiMe_3)_2$). ^{11}B NMR (C_6D_6, 25°C): δ -6.82 (br. s). ^{171}Yb NMR (C_6D_6, 25°C): δ 711(s, 120). Anal. Calcd for $C_{30}H_{58}N_7BSi_2Yb$: C, 47.61; H, 7.72; N, 12.95. Found: C, 47.83; H, 7.83; N, 12.97.

($Tp^{tBu,Me}$)Sm[$CH(SiMe_3)_2$] (18)

A solution of $KCH(SiMe_3)_2$ (107 mg, 0.539 mmol) in 10 mL of diethyl ether was added dropwise to a stirred slurry of the samarium complex **14** (376 mg, 0.537 mmol) in ca. 10 mL of diethyl ether at -50°C. The mixture was stirred at -50°C for 6 hrs and at room temperature for 1 hr, and filtered. The filtrate was concentrated to ca. 5 mL and placed at -40°C overnight, giving a dark green crystalline solid (130 mg). Further concentration of the mother liquor gave another crop of crystalline solid (100 mg). Total yield of **18** is 58%. IR (KBr): ν(B-H) 2533 cm^{-1}. ^1H NMR (toluene-d_8, 25°C): δ 7.84 (s, 27H, pz-^{t}Bu, 12), 2.82 (s, 3H, pz-H, 2), -0.18 (s, 9H, pz-Me, 3), -2.46 (s, 18H, $CH(Si\mathit{Me}_3)_2$, 8), -5.5 (br. s., 1H, B-H, 200), -71.0(s, 1H, $C\mathit{H}(SiMe_3)_2$, 47). ^{11}B NMR (toluene-d_8, 25°C): δ -48.5 (s, 230). Anal. Calcd for

$C_{31}H_{59}N_6BSi_2Sm$: C, 50.78; H, 8.11; N, 11.48. Found: C, 50.32; H, 8.15; N, 10.44.

$(Tp^{tBu,Me})Yb[CH(SiMe_3)_2]$ (19)

In a similar fashion, reaction of 282 mg of **13** and 70 mg of $KCH(SiMe_3)_2$ in 10 mL of diethyl ether, yielded the ytterbium compound **19** as an orange crystalline solid in 41% yield. IR (KBr): ν(B-H) 2551 cm^{-1}. MS (EI, 70eV, 270°C) m/z 596 (M^+-$CH(SiMe_3)_2$). ^1H NMR (toluene-d_8, 25°C): δ 5.60 (s, 3H, pz-H), 4.70 (br. s, 1H, B-H), 2.04 (s, 9H, pz-Me), 1.30 (s, 27H, pz-^{t}Bu), 0.28 (s, 18H, $CH(Si\mathit{Me}_3)_2$), -1.24 (s, 1H, $C\mathit{H}(SiMe_3)_2$, with ^{171}Yb satellites, $^2J_{Yb-H}$ =24Hz). ^{11}B NMR (toluene-d_8, 25°C): δ -8.08 (s); ^{171}Yb NMR (toluene-d_8, 25°C): δ 865 (s, 40Hz). Anal. Calcd for $C_{31}H_{59}N_6BSi_2Yb$: C, 49.26; H, 7.87; N, 11.12. Found: C, 49.46; H,7.77; N, 10.65.

$(Tp^{tBu,Me})Yb[CH_2(SiMe_3)](THF)$ (20)

A solution of KCH_2SiMe_3 (118 mg, 0.934 mmol) in 7 mL of diethyl ether was slowly added to a stirred slurry of the ytterbium complex **13** (743 mg, 0.934 mmol) in 10 mL of diethyl ether at -50°C. The mixture was stirred for 12 hours and filtered. The ether solvent was removed from the filtrate under vacuum, the residue was extracted with 5 mL of hexane. The extractant was concentrated to 2 mL, stored at -40°C overnight and gave **20** as orange crystals (333 mg, 52%). IR (KBr): ν(B-H) 2553 cm^{-1}. MS (EI, 70eV, 270°C) m/z 596 (M^+-CH_2SiMe_3-THF). ^1H NMR (toluene-d_8, 25°C): δ 5.67 (s, 3H, pz-H), 4.60 (br. s, 1H, B-H), 3.10 (s, 4H, THF), 2.19 (s, 9H, pz-Me), 1.40 (s, 27H, pz-^{t}Bu), 1.18 (s, 4H, THF), 0.49 (s, 9H, $CH_2Si\mathit{Me}_3$), -0.95 (s, 2H, $C\mathit{H}_2SiMe_3$, with ^{171}Yb satellites, $^2J_{Yb-H}$ =18Hz); ^{11}B NMR (toluene-d_8, 25°C): δ -8.06 (s); ^{171}Yb NMR (toluene-d_8, 25°C): δ 985 (s, 42Hz). Anal. Calcd for

$C_{32}H_{61}N_6BOSiYb$: C, 50.72; H, 8.11; N, 11.09. Found: C, 50.29; H,7.51; N, 11.21.

Attempted Synthesis of $(Tp^{tBu,Me})Sm[CH_2(SiMe_3)](THF)_n$

A solution of KCH_2SiMe_3 (47 mg, 0.372 mmol) in 5 mL of diethyl ether was added dropwise to a stirred slurry of the samarium compound **14** (260 mg, 0.372 mmol) in ca. 10 mL of diethyl ether at -50°C. The mixture was stirred at -50°C for 16 hrs and filtered. A dark purple solid (100 mg, 54%) was obtained following removal of diethyl ether from the filtrate. This solid was identified as $Sm(Tp^{tBu,Me})_2$ (**21**) and has been fully characterized as described in chapter 5.

$(Tp^{tBu,Me})Yb\{O(2,4,6\text{-}Me_3C_6H_2)\}(THF)$ (22)

A solution of KO-(2,4,6-$Me_3C_6H_2$) (78 mg, 0.45 mmol) in THF was added dropwise to a THF solution of the ytterbium complex **13** (360 mg, 0.45 mmol). The mixture was stirred for 2 h at -50°C and for 30 minutes at room temperature. The color of solution changed from yellow to orange. The mixture was filtered and the THF was removed under vacuum. This gave **22** as an orange solid (225 mg, 78%). IR (KBr): ν(B-H) 2467 cm^{-1}. MS (EI, 70eV, 270°C) m/z 735 (M^+-THF). ^1H NMR (THF-d_8, 25°C): δ 6.55 (s, 2H, OAr-H), 5.93 (s, 3H, pz-H), 3.62 (s, 4H, THF), 2.40 (s, 9H, pz-Me), 2.19(s, 3H, OAr-Me), 1.78(s, 4H, THF), 1.38 (s, 27H, pz-^{t}Bu), 1.25 (s, 6H, OAr-Me); ^{11}B NMR (THF-d_8, 25°C): δ -6.84 (s). ^{171}Yb NMR (THF-d_8, 25°C): δ 600 (s, 42). Anal. Calcd for $C_{33}H_{51}N_6BOYb$: C, 55.29; H, 7.40; N, 10.46. Found: C, 54.05; H,6.86; N, 10.02.

Attempted Synthesis of $(Tp^{tBu,Me})Sm(OAr)(THF)_n$

A solution of KOAr (64 mg, 0.37 mmol) in ca. 5 mL of THF was added dropwise to a solution of the samarium complex (**12**) (310 mg, 0.37 mmol) in 10 mL

of THF at -50°C. The mixture was stirred for two hours at -50°C and for 30 minutes at room temperature. The color of the solution changed from dark green to violet. Filtration, followed by removal of toluene gave a dark purple solid identified as **21** (128 mg, 78%).

($Tp^{tBu,Me}$)Sm($HBEt_3$) (23)

A solution of $NaHBEt_3$ (0.40 mmol) in 2 mL of toluene was added dropwise to a stirred slurry of **14** (280 mg, 0.40 mmol) in 8 mL of toluene at -50°C. The mixture was stirred at room temperature for 1 h and the toluene solvent was removed under vacuum. The residue was extracted with 5 mL of hexane and filtered. The filtrate was concentrated to 3 mL and placed at -40°C, yielding **23** as a dark green crystalline solid (188 mg, 65%). IR (KBr): ν(B-H) 2548, 1936 cm^{-1}. MS (EI, 70eV, 230°C) m/z 576 (M^+-$HBEt_3$). ^1H NMR (toluene-d_8, 25°C): δ 6.50 (s, 27H, pz-^{t}Bu, 6), 3.59 (s, 3H, pz-H, 3), 1.38 (s, 9H, pz-Me, 2), -4.00 (s, 9H $HB(CH_2CH_3)_3$, 12), -37.0 (s, 6H, $HB(CH_2CH_3)_3$, 24). ^{11}B NMR (toluene-d_8, 25°C): δ -33.6 (s, $Tp^{tBu,Me}$, 180), -278 (s, $HBEt_3$, 128). Anal. Calcd for $C_{34}H_{64}N_6B_2Sm$: C, 53.56; H, 8.39, N, 12.49. Found: C, 53.51; H, 8.21, N, 12.33.

($Tp^{tBu,Me}$)Yb($HBEt_3$)(THF) (24)

In a similar fashion, reaction of 350 mg of **13** and 0.44 mmol of $NaHBEt_3$ in 8 mL of toluene, yielded the ytterbium complex **24** as as orange mono-solvated crystals in 65% yield. IR (KBr): ν(B-H) 2550, 1935 cm^{-1}. MS (EI, 70eV, 220°C) m/z 597 (M^+-$HBEt_3$-THF). ^1H NMR (C_6D_6, 25°C): δ 5.67 (s, 3H, pz-H), 4.80 (br. s, 1H, HB), 3.35 (br. s, 4H, THF), 2.60 (br. s, $HBEt_3$), 2.09 (s, 9H, pz-Me), 1.52 (t, 9H, $HB(CH_2CH_3)_3$), 1.33 (s, 27H, pz-^{t}Bu), 1.26 (br. s, 4H, THF), 1.00 (q, 6H, $HB(CH_2CH_3)_3$); ^{11}B NMR (C_6D_6, 25°C): δ -8.13 ($Tp^{tBu,Me}$), -9.95 ($HBEt_3$). ^{171}Yb NMR (C_6D_6, 25°C): δ 412 (d, $^1J_{Yb-H}$ = 200 Hz); $^{171}Yb\{^1H\}$ NMR (C_6D_6, 25°C): δ

413 (s, 70). Anal. Calcd for $C_{34}H_{64}N_6OB_2Yb$: C, 53.20; H, 8.40, N, 10.95. Found: C, 53.58; H, 7.98, N, 11.93.

($Tp^{tBu,Me}$)Sm[C≡CPh] (25)

A solution of HC≡CPh (52 mg, 0.50 mmol) in ca. 5 mL of toluene was added dropwise to a stirred solution of the samarium complex **16** (367 mg, 0.50 mmol) in 5 mL of toluene at -50°C. The mixture was stirred at -50°C for 5 hrs and toluene solvent was removed under vacuum. The residue was extracted with 7 mL of hexane and filtered. The filtrate was concentrated to ca. 3 mL and placed at -40°C, affording **25** as a brown crystalline solid (144 mg, 43%). IR (KBr): ν(B-H) 2541 cm^{-1}. ^1H NMR (toluene-d_8, 25°C): δ 9.80 (s, 27H, pz-^{t}Bu, 48), 7.58 (s, 2H, Ph, 16), 5.75 (s, 1H, Ph, 32), 5.35 (m, 2H, Ph, 16), 1.08 (s, 3H, pz-H, 12), -1.25 (s, 9H, pz-Me, 12), -5.8 (br. s. , 1H, B-H, 110). ^{11}B NMR (toluene-d_8, 25°C): δ -41.8 (br. s, 460). Anal. Calcd for $C_{32}H_{45}N_6BSm$: C, 56.95; H, 6.72; N, 12.45. Found: C, 57.15; H, 6.83; N, 12.30.

($Tp^{tBu,Me}$)Yb(C≡CPh) (26)

In a similar fashion, reaction of 197 mg of **13** and 27 mg of HC≡CPh in 6 mL of hexane, yielded the ytterbium analogue **26** as a dark reddish brown crystalline solid in 67% yield. IR(KBr): ν(B-H) 2554 cm^{-1}, ν(c≡c) 2051 cm^{-1}. MS (EI, 70eV, 220°C) m/z 595 (M^+-C_2Ph). ^1H NMR (toluene-d_8, 25°C): δ 6.81 (m, 3H, Ph), 6.61 (m, 2H, Ph), 5.69 (s, 3H, pz-H), 4.78 (br. s, 1H, B-H), 2.23 (s, 9H, pz-Me), 1.65 (s, 27H, pz-^{t}Bu); ^{11}B NMR (toluene-d_8, 25°C): δ -7.70 (br. s); ^{171}Yb NMR (toluene-d_8, 25°C): δ 673 (s, 32Hz). Anal. Calcd for $C_{32}H_{45}N_6BYb$: C, 55.10; H, 6.50; N, 12.05. Found: C, 55.31; H, 6.52; N, 10.85.

Hydrogenolysis of 19 and 20

A solution of **19** (or **20**) in hexane was placed under 1 atm of H_2. After overnight at room temperature, an orange crystalline solid was precipitated from the solution. The identity of the solid is under investigation.

Attempted Reactions of 23 and 24 with Phenylacetylene, Ethylene and Propylene

A solution of **23** (or **24**) in hexane was placed under 1 atm of ethylene and propylene. No reaction was observed, nor does it react with HC≡CPh at room temperature.

4.6.3. ^{171}Yb NMR Study

The ^{171}Yb chemical shifts are reported in ppm relative to $(C_5Me_5)_2Yb(THF)_2$ in THF. Pulse width for the ^{171}Yb NMR experiments were estimated by interpolation between ^{2}H and ^{77}Se with a 90° pulse of 13.0 ms. Typical direct acquisition experiments utilized a 20° pulse (3 ms) and acquisition time of 0.4 s.

4.6.4. X-ray Structure Determinations

The crystals were handled as described in previous Chapters. Complete X-ray structure determinations for compounds **11**, **13**, **17**, **19** and **24** were carried out by Dr. A. H. Bond and R. Roger at Department of Chemistry, Northern Illinois University. The X-ray data collection and structure refinement for complex **20** and **22** were carried out by Dr. R. McDonald at Structure Determination Laboratory, Department of Chemistry, University of Alberta. Complete X-ray structure determination for compound **15** was carried out by Dr. Charles F. Campana at Siemens company, Madison. Presently only preliminary data are available. The crystal and data collection parameters of the complexes are given in Table 4.5 and Table 4.6.

Table 4.5 Summary of Crystallographic Data for $(Tp^{Me2})YbI(THF)_2$ (**11**), $(Tp^{tBu,Me})YbI(THF)$ (**13**), $(Tp^{tBu,Me})Yb(CH_2SiMe_3)(THF)$ (**20**)

Compound	**11**	**13**	**20**
Empirical formula	$C_{23}H_{38}N_6BIO_2Yb$	$C_{28}H_{48}N_6BIOYb$	$C_{32}H_{59}N_6BOSiYb$
Crystal dimensions (mm)	0.15 x 0.20 x 0.75	0.15 x 0.18 x 0.50	0.48 x 0.33 x 0.26
formula weight	741.35	795.49	755.80
Cell dimensions			
a (Å)	14.229(7)	11.334(3)	10.934(1)
b (Å)	14.698(9)	16.276(5)	13.196(1)
c (Å)	16.264(4)	18.695(9)	14.031(1)
α (deg)			83.721(7)
β (deg)		99.87(3)	71.087(8)
γ (deg)			86.607(8)
Volume (Å^3)	3393	3398	1903.1
Z (formula units)	8	4	2
D(calcd), g cm^{-3}	2.90	1.55	1.319
μ(calcd), cm^{-1}	76.9	38.4	25.10
space group	Pnma	$P2_1/n$	$P\bar{1}$
radiation(l,Å)	Mo Ka	Mo Ka	Mo Ka
scan type	ω–2θ	ω-2θ	ω
2θ limits(deg)	50	50	50.0
temp, °C	20(1)	20	-50
Total no. reflection			6962
No. unique reflection	3373	6535	6614
No. with I>3σ(I)	1578	3963	5704
R	0.073	0.041	0.026
R_W	0.098	0.056	0.032
GOF	1.93	2.44	1.086

Table 4.6 Summary of crystallographic Data for $(Tp^{tBu,Me})Yb[N(SiMe_3)_2]$ (**17**), $(Tp^{tBu,Me})Yb[CH(SiMe_3)_2]$ (**19**), $(Tp^{tBu,Me})Yb[O\text{-}(2,4,6\text{-}Me_3C_6H_2)](THF)$ (**22**) and $(Tp^{tBu,Me})Yb(HBEt_3)(THF)$ (**24**)

Compound	**17**	**19**	**24**	**22**
Empirical formula	$C_{30}H_{58}N_7BSi_2Yb$	$C_{31}H_{59}N_6BSi_2Yb$	$C_{34}H_{64}N_6OB_2Yb$	$C_{40}H_{66}N_6BO_2Yb$
Crystal dimensions (mm)	0.12 x 0.20 x 0.40	0.30 x 0.20 x 0.20	0.28 x 0.40 x 0.55	0.80 x 0.50 x 0.30
formula weight	756.86	792.93	767.59	846.86
Cell dimensions				
a (Å)	15.071(3)	16.487(5)	12.172(6)	21.526(4)
b (Å)	12.304(3)	18.263(5)	17.228(7)	13.213(2)
c (Å)	20.746(6)	27.122(8)	18.727(3)	31.403(&)
α (deg)		90		
β (deg)	96.84(2)	92.320(6)		105.80(2)
γ (deg)		90		
Volume (Å^3)	3819.6	8160(4)	3927.0	8594(5)
Z (formula units)	4	8	4	8
D(calcd), g cm^{-3}	1.32	1.291	1.30	1.309
μ(calcd), cm^{-1}	26.6	23.80	25.4	22.06
space group	$P2_1/c$	C2/c	$P2_12_12_1$	C2/c
radiation(l,Å)	Mo Ka	Mo Ka	Mo Ka	Mo Ka
scan type	ω–2θ	ω-2θ	ω-2θ	ω
2θ limits(deg)	50	23.28	50	50.0
temp, °C	20(1)	-100	20(1)	-50
Total no. reflection		15486		8005
No. unique reflection	7336	5782	3899	7803
No. with I>3σ(I)	4885	4932	3241	4107
R	0.036	0.0393	0.038	0.040
R_W	0.036	0.0488	0.054	0.055
GOF	1.07	1.090	1.70	1.770

4.7. References

(1) Schaverien, C. J. *Adv. Organomet. Chem.* **1994**, *36*, 283.

(2) Evans, W. J.; Grate, J. W.; Choi, H. W.; Bloom, I.; Hunter, W. E.; Atwood, J. L. *J. Am. Chem. Soc.* **1985**, *107*, 941.

(3) Evans, W. J.; Drummond, D. K.; Zhang, H. M.; Atwood, J. L. *Inorg. Chem.* **1988**, *27*, 575.

(4) Swamy, S. J.; Schumann, H. J. *J. Organomet. Chem.* **1987**, *334*, 1.

(5) Cloke, F. G. N.; Dalby, C. I.; Hitchcock, P. B.; Karamallakis, H.; Lawless, G. A. *J. Chem. Soc., Chem. Commun.* **1991**, 779.

(6) Hasinoff, L.; Takats, J.; Zhang, X. W.; Bond, A. H.; Rogers, R. D. *J. Am. Chem. Soc.* **1994**, *116*, 8833.

(7) Trofimenko, S. *Chem. Rev.* **1993**, *93*, 943.

(8) Han, R.; Parkin, G. *Organometallics* **1991**, *10*, 1010.

(9) Gerrell, I. B.; Looney, A.; Parkin, G. *J. Chem. Soc., Chem. Commun.* **1990**, 220.

(10) Evans, W. J.; Hughes, L. A.; Hanusa, T. P. *Organometallics* **1986**, *5*, 1285.

(11) Evans, W. J. *Polyhedron* **1987**, *6*, 803.

(12) Deacon, G. B.; Feng, T.; MacKinnon, P.; Newnham, R. H.; Nickel, S.; Skelton, B. W.; White, A. H. *Aust. J. Chem.* **1993**, *46*, 387.

(13) Tilly, D. T.; Andersen, R. A.; Spencer, B.; Ruben, H.; Zalkin, A.; Templeton, D. H. *Inorg. Chem.* **1980**, *19*, 2999.

(14) Evans, W. J.; Rabe, G. W.; Ziller, J. W. *Inorg. Chem.* **1994**, *33*, 3072.

(15) Takats, J.; Zhang, X. W.; McDonald, B.; Day, V. W.; Eberspacher, T. A. manuscript in preparation

(16) Maunder, G. H.; Sella, A.; Tocher, D. A. *J. Chem. Soc., Chem. Commun.* **1994**, 885.

(17) Sella, A. *personal communication*

(18) Schaverien, C. J.; van Mechelen, J. B. *Organometallics* **1991**, *10*, 1704.

(19) Eaborn, C.; Hitchcock, P. B.; Izod, K.; Smith, J. D. *J. Am. Chem. Soc.* **1994**, *116*, 12071.

(20) Hitchcock, P. B.; Holmes, S. A.; Lappert, M. F.; Tian, S. *J. Chem. Soc., Chem. Commun.* **1994**, 2691.

(21) Sun, Y. M. *Ph.D. Thesis, University of Alberta, Edmonton* **1995**,

(22) Jeske, G.; Lauke, H.; Mauermann, H.; Swepston, P. N.; Schumann, H.; Marks, T. J. *J. Am. Chem. Soc.* **1985**, *107*, 8091.

(23) Gagne, M. R.; Nolan, S. P.; Marks, T. J. *Organometallics* **1990**, *9*, 1716.

(24) Gladysz, J. A. *Aldrichimica Acta* **1979**, *12*, 13.

(25) Berthet, J. C.; Le Marechal, J. F.; Ephritikhine, M. *J. Chem. Soc., Chem. Commun.* **1991**, 360.

(26) Evans, W. J.; Bloom, I.; Hunter, W. E.; Atwood, J. L. *J. Am. Chem. Soc.* **1981**, *103*, 6507.

(27) Green, M. L. H.; Hughes, A. K.; Michaelidou, D. M.; Mountford, P. J. *J. Chem. Soc., Chem. Commun.* **1993**, 591.

(28) Evans, W. J.; Ulibarri, T. A.; Chamberlain, L. R.; Ziller, J. W.; Alvarez, J., D. *Organometallics* **1990**, *9*, 2124.

(29) Boncella, J. M.; Tilly, T. D.; Andersen, R. A. *J. Chem. Soc., Chem. Commun* **1984**, 710.

(30) Evans, W. J.; Keyer, R. A.; Ziller, J. W. *Organometallics* **1993**, *12*, 2618.

(31) Tilley, T. D.; Andersen, R. A.; Zalkin, A. *J. Am. Chem. Soc.* **1982**, *104*, 3725.

(32) Tilly, T. D.; Andersen, R. A.; Zalkin, A. *Inorg. Chem.* **1984**, *23*, 2271.

(33) Boncella, J. M.; Andersen, R. A. *Organometallics* **1985**, *4*, 205.

(34) Atwood, J. L.; Hunter, W. E.; Rogers, R. D.; Holton, J.; McMeeking, J.; Pearce, R.; Lappert, M. F. *J. Chem. Soc., Chem. Commun.* **1978**, 140.

(35) Schumann, H.; Glanz, M.; Winterfeld, J.; Hemling, H.; Kuhn, N.; Kratz, T. *Angew. Chem. Int. Ed. Engl.* **1994**, *33*, 1733.

(36) Jeske, G.; Schock, L. E.; Swepston, P. N.; Schumann, H.; Mark, T. J. *J. Am. Chem. Soc.* **1985**, *107*, 8103.

(37) Schumann, H.; Genthe, W.; Bruncks, N.; Pickardt, J. *Organometallics* **1982**, *1*, 1194.

(38) van der Heijden, H.; Pasman, P.; de Boer, E. J. M.; Schaverien, C. J. *Organometallics* **1989**, *8*, 1459.

(39) Bruno, J. W.; Marks, T. J. *J. Organomet. Chem.* **1983**, *250*, 237.

(40) Evans, W. J.; Olofson, J. M.; Ziller, J. W. *Inorg. Chem.* **1989**, *28*, 4309.

(41) Shannon, R. D. *Acta Cryst.* **1976**, *A32*, 751.

(42) Marks, T. J. *Chem. Rev.* **1977**, *77*, 263.

(43) White III, J. P.; Deng, H. B.; Shore, S. G. *J. Am. Chem. Soc.* **1989**, *111*, 8946.

(44) Qiao, K.; Fischer, R. D.; Paolucci, G. *J. Organomet. Chem.* **1993**, *456*, 185.

(45) Koutsantonis, G. A.; Lee, F. C.; Raston, C. L. *J. Chem. Soc., Chem. Commun.* **1994**, 1975.

(46) Ghilardi, C. A.; Midollini, S.; Orlandini, A. *Inorg. Chem.* **1982**, *21*, 4096.

(47) Avent, A. G.; Edelman, M. A.; Lappert, M. F.; Lawless, G. A. *J. Am. Chem. Soc.* **1989**, *111*, 3423.

(48) Trofimenko, S.; Calabrese, J. C.; Kochi, J. K.; Korp, J. D.; Wolowiec, S.; Hulsbergen, F. G.; Reedijk, J. *Inorg. Chem.* **1992**, *19*, 3944.

(49) Jordan, R. F.; Echols, S. F. *Inorg. Chem.* **1987**, *26*, 383.

Chapter 5

Synthesis and Structure of the First Bis-hydrotris(3-^{t}Bu-5-Me pyrazolyl)borate Complexes, Ln(Tp$^{t\mathrm{Bu,Me}}$)$_2$ (Ln = Sm, Yb): Fluxionality, Bonding Mode Exchange and B-H-Ln Bridge Bonding.

5.1. Introduction

As described in Chapter 4, we have applied the bulky Tp$^{t\mathrm{Bu,Me}}$ ligand to divalent lanthanide metals and isolated and fully characterized the monomeric half-sandwich complexes (Tp$^{t\mathrm{Bu,Me}}$)LnI(THF)$_n$ (see Chapter 4) (Ln = Yb, n = 1; Sm, n = 2) and we have shown that the complexes are useful and versatile precursors to new types of (Tp$^{t\mathrm{Bu,Me}}$)LnER (ER = N(SiMe$_3$)$_2$, HBEt$_3$, and CH(SiMe$_3$)$_2$) complexes. Remarkably, the complexes proved to be stable toward ligand redistribution reactions, a feature which often complicates f-element chemistry and renders rational design of targeted complexes difficult. We attributed the inertness of the complexes to the bulky nature of the Tp$^{t\mathrm{Bu,Me}}$ ligand, and indeed this was the reason for using this ligand in the first place.

In this Chapter, we report that, contrary to expectation, the bis-Tp$^{t\mathrm{Bu,Me}}$ lanthanide complexes can be prepared and that they possess features that are unusual for lanthanide complexes normally held together by mostly ionic interactions. A version of this Chapter has been published.[1]

5.2. Synthesis of $Ln(Tp^{tBu,Me})_2$ (Sm, 21; Yb, 27)

The purple $Sm(Tp^{tBu,Me})_2$ complex (21) was first isolated unexpectedly from the reaction of $(Tp^{tBu,Me})SmI$ with one equivalent of KCH_2SiMe_3, eq 5.1. The reaction most probably involves the intermediacy of $[(Tp^{tBu,Me})Sm(CH_2SiMe_3)]$

$$(Tp^{tBu,Me})LnI(THF)_n + KCH_2SiMe_3 \xrightarrow[-50°C]{Et_2O} \begin{cases} \xrightarrow{Sm} Sm(Tp^{tBu,Me})_2 + \text{"}Sm(CH_2SiMe_3)_2\text{"} \quad \mathbf{21} \\ \xrightarrow{Yb} (Tp^{tBu,Me})Yb(CH_2SiMe_3)(THF) \end{cases} \qquad 5.1.$$

which then undergoes ligand redistribution to give **21**; the fate of the putative "$Sm(CH_2SiMe_3)_2$" complex is not known. It is interesting to note that the same reaction with the smaller Yb(II) center gives the desired complex with no evidence of ligand redistribution. Thus differences in metallic radii have profound influences on f-element chemistry, even with this sterically very demanding ligand system and serve notice of the care with which derivative chemistry of $(Tp^{tBu,Me})SmER$ complexes must be approached.

The unexpected isolation of **21** led us to deliberately prepare it and its Yb analogue by the rational metathesis route, namely the reaction of $(Tp^{tBu,Me})LnI$ with one equivalent of $KTp^{tBu,Me}$ or $LnI_2(THF)_n$ with two equivalents of the ligand. The reactions do proceed but only slowly and give the complexes in moderate yield after 2-7 days of reaction, eq 5.2. Similar observations were made by Thompson and

$$(Tp^{tBu,Me})LnI(THF)_n \xrightarrow{+KTp^{tBu,Me}} Ln(Tp^{tBu,Me})_2 \xleftarrow{+2KTp^{tBu,Me}} LnI_2(THF)_n \qquad 5.2$$

Sm (**21**) (47%)
Yb (**27**) (44%)

Trofimenko during their preparation of mixed $M(Tp^{iPr,4\text{-}Br})(Tp^{R,R'})$ (M = Co, Ni, Fe, Zn) complexes.[2] As the size of the $Tp^{R,R'}$ increased the reaction became slower. In a related phenomenon, the sterically congested $(C_5Me_5)_3Sm$ complex could not be prepared via simple metathesis between SmX_3 and NaC_5Me_5. However the desired complex was obtained by Evans *et al.* [3] from redox induced disproportionation between $(C_5Me_5)_2Sm$ and cyclooctatetraene.

Complexes **21** and **27** are highly air sensitive solids, soluble in aliphatic and aromatic hydrocarbons and ether type solvents. In solution they are thermally stable with no apparent decomposition up to 80°C as monitored by ^1H NMR spectroscopy in toluene-d_8. Attempted sublimations were not successful; the materials decomposed at 170°C and 1×10^{-3} torr.

The IR spectra show two well separated B-H stretches at 2530 and 2350 cm^{-1} for **21**, and at 2550 and 2300 cm^{-1} for complex **27**. The signals undergo the expected shifts in the corresponding isotopomers (1890 and 1705 cm^{-1}, **21**-d_2; 1900 and 1690 cm^{-1}, **27**-d_2). The higher frequency band is typical for terminal B-H stretches, while the lower frequency signal is in the region normally associated with an agostic B-H → M interaction[4,5] and gives the first hint that the two $Tp^{tBu,Me}$ ligands in the complexes are different.

The room temperature ^1H NMR spectra of complexes **21** and **27** are shown in Figure 5.1. The spectra are deceptively simple, comprising two equal intensity sets of resonances for the pyrazolyl rings and two B-H signals. As usual, the B-H signals are broad and the two distinct peaks of the diamagnetic ytterbium complex, at 5.9 and 4.7 ppm, respectively, are more readily apparent in the ^2H NMR spectrum of the isotopomer **27**-d_2. The appearance of two sets of signals is in accord with the IR data and implies two different $Tp^{tBu,Me}$ ligands in different chemical environments.

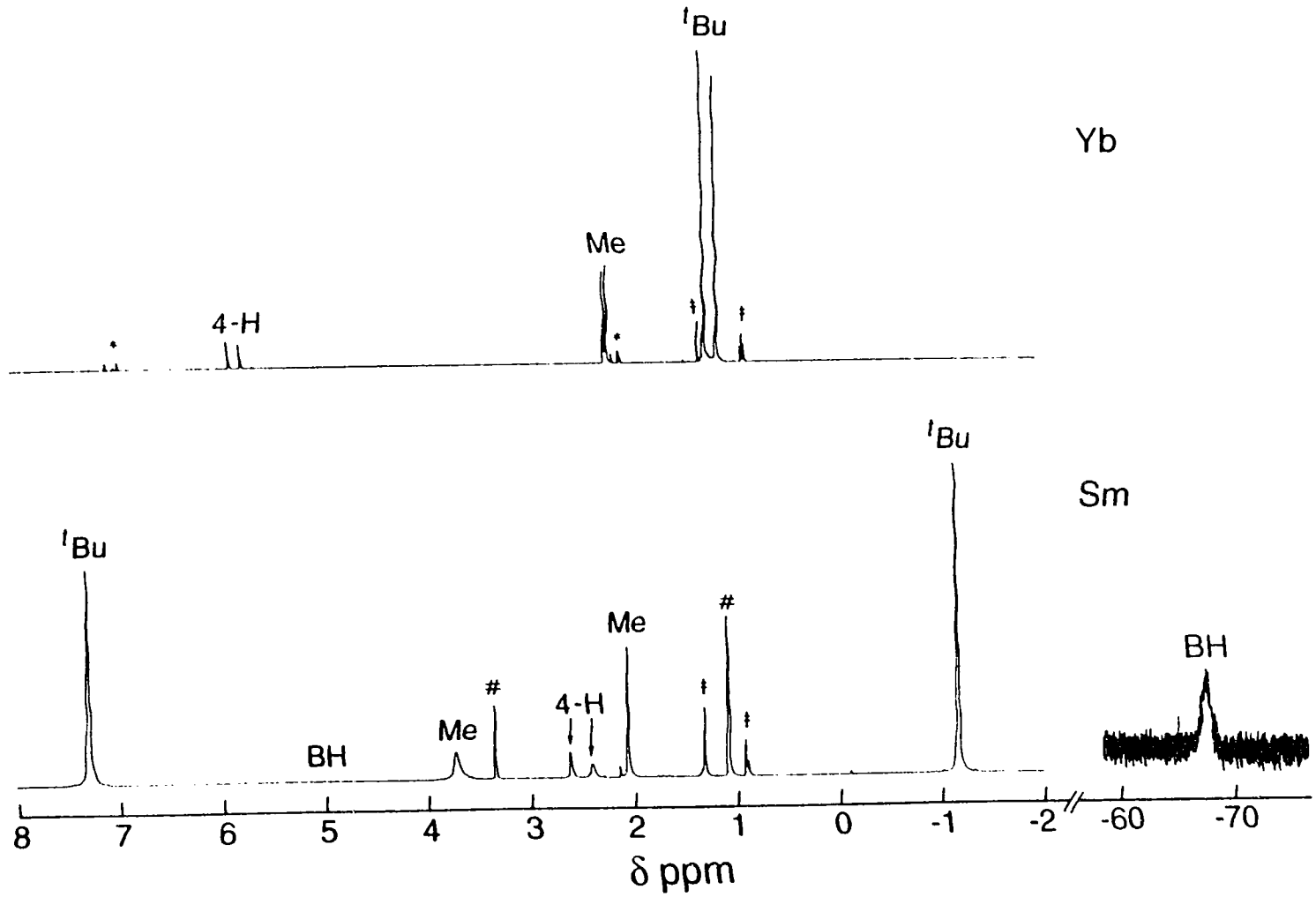

Figure 5.1 Room temperature ^1H NMR spectra (400 MHz) of $Sm(Tp^{tBu,Me})_2$ (**21**) and $Yb(Tp^{tBu,Me})_2$ (**27**) in toluene-d_8 (‡ small amount of pentane contamination in the sample).

The $^{11}B\{^1H\}$ NMR spectra of the complexes show two signals and corroborate the presence of two different $Tp^{tBu,Me}$ ligands. In the proton-coupled ^{11}B NMR spectrum of complex **27**, the signal at higher field (-6.3 ppm) remains a broad singlet with no resolvable B-H coupling, the lower field resonance (-0.9 ppm) is a doublet with B-H coupling of 85 Hz. This coupling is smaller than the typical terminal B-H value (*ca.* 120 Hz) and has been used as diagnostic of an agostic B-H $\rightharpoonup$ M interaction.[4,5] The presence of B-H $\rightharpoonup$ Yb interaction in complex **27** was confirmed by ^{171}Yb NMR. The proton coupled spectrum is a doublet, $J_{Yb\text{-}H}$ = 85 Hz, that collapses to a singlet when the B-H signal at 5.9 ppm is irradiated. As required by the bridging B-H $\rightharpoonup$ Yb unit, irradiation of this B-H signal also collapses the low field ^{11}B doublet to a singlet. Because of the broadness and the closeness of the two B-H signals, irradiation at 4.7 ppm also affects the ^{171}Yb signal, but it remains a distorted doublet. It is noteworthy that the magnitude of ^{171}Yb-H coupling in the present complex is substantially smaller than those observed in $(Tp^{tBu,Me})Yb(\mu\text{-}HBEt)_3$ (200 Hz) (see Chapter 4) and $[\{(C_5H_5)_2NbH_2\}_2Yb\bullet diglyme]$ (170 Hz).[6] More work is needed to put the magnitude of this coupling and the strength of the interaction on a firm footing. Although, for the samarium complex **21**, there is no coupling signature that can be used to unambiguously identify the agostic B-H $\rightharpoonup$ Sm interaction, indirect evidence comes from the presence of two drastically different B-H signals, at 5.1 ppm and -67.3 ppm. We assign the dramatically high-field shifted signal as belonging to the B-H $\rightharpoonup$ Sm unit as a result of it being under the direct influence of the paramagnetic Sm(II) center.

The NMR and IR features clearly signaled the presence of unusual Ln(II) complexes. Although intriguing possibilities could be envisioned, a single crystal X-ray analysis was the surest way to map out the full details of the structure of the complexes.

5.3. Molecular Structure of $Sm(Tp^{tBu,Me})_2$, 21

An ORTEP drawing of the molecule, with labeling scheme, is shown in Figure 5.2. Selected interatomic distances and angles are listed in Table 5.1.

The most remarkable feature of the X-ray analysis is that it shows *both* $Tp^{tBu,Me}$ ligands to be coordinated to the Sm(II) center. This is the *first* example of bis-chelate formation by this sterically very demanding Tp ligand system. Although both $Tp^{tBu,Me}$ ligands are bonded to samarium the large size of the ligand does not allow for symmetrical bis-chelate formation similar to other $Ln(Tp^{R,R'})_2$ complexes

Table 5.1 Selected Interatomic Distances (Å) and Angles (deg).[a]

			Distances				
Sm	N11		2.630(7)	Sm	N41		2.707(7)
Sm	N21		2.605(7)	Sm	N51		2.719(8)
Sm	N31		2.628(8)	Sm	H2		2.53[b]
Sm	B1		3.49(1)	Sm	B2		3.14(1)
			Angles				
N21	Sm	N21	83.4(2)	N21	Sm	N41	104.0(2)
N21	Sm	N31	86.9(2)	N21	Sm	N51	108.7(2)
N11	Sm	N31	65.2(2)	N41	Sm	N51	90.7(2)
N11	Sm	N51	104.4(2)	N31	Sm	N41	96.6(2)
N11	Sm	N41	160.3(2)	N31	Sm	N51	160.7(2)
N21	Sm	H2	152[b]				

[a]Numbers in parentheses are estimated standard deviations.

[b]Calculated by positioning H2 at its idealized position.

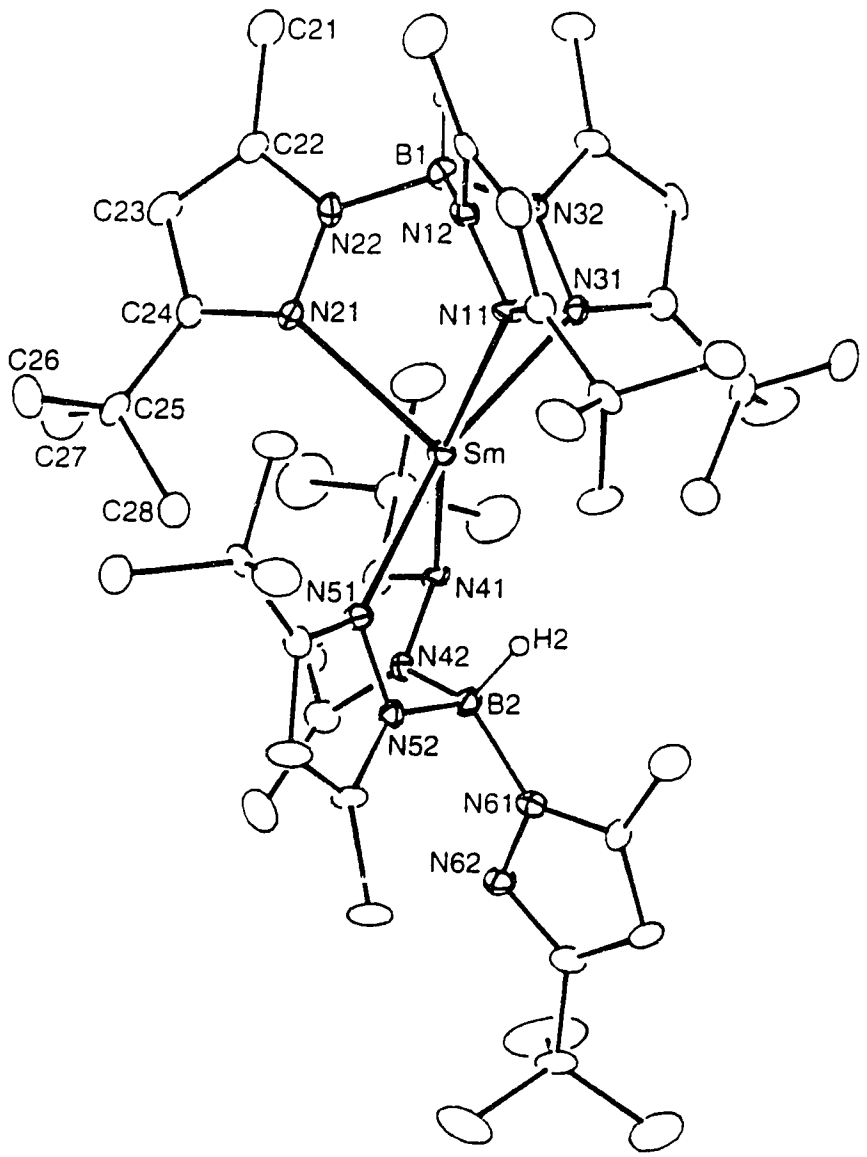

Figure 5.2 Perspective view of $Sm(Tp^{tBu,Me})_2$ (**21**) showing the atom labeling scheme. Non-hydrogen atoms are represented by Gaussian ellipsoids at the 20% probability level; hydrogens attached to boron atoms are shown artificially small, while other hydrogens are not shown.

(see Chapter 2).[7] This of course was already evident from the IR and NMR features discussed in the previous section. One of the ligands features the classical η^3-bonding mode (Sm-N11, N21, N31) commonly seen for $Tp^{R,R'}$ ligands. At first glance the other ligand appears bidentate *via* coordination through N41 and N51, with the third pyrazolyl ligand (N62) pointing away from the Sm center. However this is an oversimplification, the boron hydrogen (H2) points toward Sm and is poised to enter into additional agostic B-H $\rightarrow$ Sm interaction. Thus the X-ray study shows and corroborates the agostic B-H $\rightarrow$ Sm interaction postulated on the basis of solution IR and NMR data. Agostic interactions involving dihydrobis(pyrazolyl)borate ligands were first observed with molybdenum complexes[8,9] and more recently in a number of f-element complexes as well.[10-12] However, we are aware of only one other documented example of such interaction with a hydrotris(pyrazolyl)borate ligand, $(Tp^{iPr,4\text{-}Br})Co[(\mu\text{-}H)Tp^{Ph}]$.[2]

In order to more closely examine the coordination geometry of and the bonding interactions involving the Sm center we focus on Figure 5.3 where most of the carbon atoms have been removed for clarity. The coordination geometry, formed by the five pyrazolyl nitrogens and the boron hydrogen bonded to Sm, is distorted octahedral with N21 and H2 occupying the axial positions. The four equatorial nitrogens (N11, N31, N41, N51) are all within 0.1Å of the least-squares plane formed by these atoms while the Sm atom is displaced 0.32Å from the mean plane toward the axial nitrogen. Distortions from octahedral geometry are manifest in both interatomic angles *and* distances (Table 5.1). The angles from the axial N21 to the intra-ligand equatorial bonds are less than 90° (83.4(2)° and 86.9(2)° to N11 and N31, respectively) and greater than 90° to the inter-ligand nitrogens (104.0(2)° and 108.7(2)° to N41 and N51, respectively). In the equatorial plane the four angles range from 65.2(2)° to 104.4(2)°,

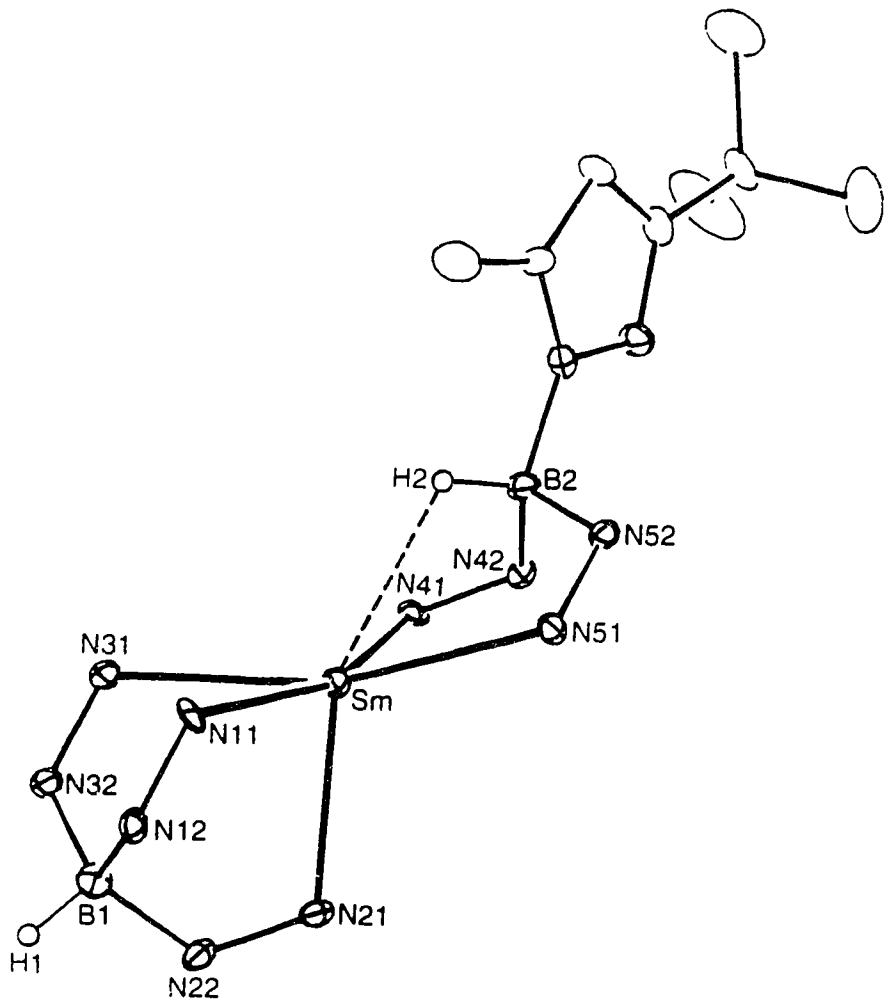

Figure 5.3 Alternative view of **21** emphasizing the coordination geometry of Sm and the twisted-boat conformation of the "η^2-Tp^{tBu,Me}" ligand; all carbon atoms are omitted except for those belonging to the non-coordinated pyrazolyl ring.

most noteworthy is the rather acute nature of the N11-Sm-N31 angle. The N21-Sm-H2 angle is 152°, comparable to the value seen in the above mentioned Co(II) complex, 150.7°. Although in the latter complex the other angles deviate less from the ideal octahedral values of 90° as a result of the shorter Co-N(pz) bond lengths. The distances to the η^3-Tp^{tBu,Me} and formally η^2-Tp^{tBu,Me} ligands are also different. The average Sm-N bond distance to the latter (2.713(8)Å) is almost 0.1Å *longer* than that to the η^3-Tp^{tBu,Me} ligand (2.621(8)Å). This, as we shall see later, has a profound effect on the solution behavior of the complex. Within the η^3-Tp^{tBu,Me} ligand, the bonding of the axial nitrogen appears to be marginally stronger (Sm-N21 2.605(7)Å) than the equatorial nitrogens (average Sm-N11/N31 2.629(8)Å). These Sm-N(pz) distances may be compared to those observed in Sm(Tp^{Me2})$_2$ (2.617(4)Å) (see Chapter 2).

The presence of the agostic interaction is clearly evidenced by the severely buckled "η^2-Tp^{tBu,Me}" chelate ring and the resulting short Sm-B2 separation (3.14Å). Typically in relaxed six-membered η^2-Tp chelate rings, with no agostic interaction, the M-B separation is *ca.* 3.4Å[13] and can reach 3.8Å.[14] In the present case, once the differences in the size of the metals are taken into consideration,[15] the Sm-B2 distance is *ca.* 0.2Å shorter than the similar distance in Y[H(μ-H)B(pz)$_2$]$_3$ (3.21Å)[11] and is about the same as that seen in (η^3-C$_7$H$_7$)(CO)$_2$Mo [H(μ-H)B(3,5-Me$_2$pz)$_2$] (2.80Å),[9] a molecule known to have rather strong agostic interaction. A Sm-H2 separation of 2.52Å is calculated by positioning H2 at its idealized position. This distance is only 0.25Å longer than the bridging Sm-H-Sm distances in (C$_5$Me$_5$)$_2$Sm(μ-H)(μ-η^1:η^5-CH$_2$C$_5$Me$_4$)Sm(C$_5$Me$_5$)[16] and compares favorably with the B-H → Co(II) separation of 2.26Å in (Tp$^{iPr,4-Br}$)Co[(μ-H)Tp^{Ph}],[2] again after correcting for the size differences of the metals.

As mentioned, the presence of the B-H→Sm interaction results in a highly distorted chelate ring. The classical conformation of the six-membered MN_4B ring, with or without B-H→M interaction, is that of a boat; shallow when there is no interaction and increasingly folded as the strength of the interaction increases. Such conformation is anticipated from the coplanarity of the M-N-N-B bonds, and indeed this is what is observed in the above Co(II) complex. In contrast, the conformation of the six-membered SmN_4B ring is best described as a twisted-boat. The four atoms, SmN41N42N51 are in one plane (each atom deviating less than 0.05Å from the mean plane) and the N42B2N52 plane makes an angle of 95° with it. It is this severe bending that brings B2 and H2 into close proximity with the samarium center. The distorted nature of the chelate ring is also manifested in the Sm-N-N-B torsional angles. One of these angles (Sm-N51-N52-B2) is close to 0°, 1.0(9)°. However the other (Sm-N41-N42-B2) is vastly different, 52.3(8)°. As a result the Sm-N41 bond vector is far from being coincident with the lone pair vector of this nitrogen atom. It is interesting to note that similar distortions (i.e., non coincidence of bond and nitrogen lone pair vectors), albeit much reduced, are also seen in the η^3-$Tp^{tBu,Me}$ part of the molecule. The torsional angles Sm-N11-N12-B1, Sm-N21-N22-B1 and Sm-N31-N32-B1 are 35.5(10)°, 14.5(12)° and 22.3(10)°, respectively. This then is another example of a "propeller like" distortion of an η^3-Tp ligand. Tollman[17] was first to call attention to such distortion in the structure of the $TlTp^{Mementh}$ complex and attributed it to "unfavorable intramolecular non-bonding interactions". The resultant "lack of directionality in bonding" was ascribed to a degree of ionic character in the thallium-Tp interactions. The same forces are operating in the present system also. The geometry of the complex is a compromise between the steric influences of the ^{t}Bu groups within the η^3-$Tp^{tBu,Me}$ ligand and between the two $Tp^{tBu,Me}$ ligands, N41 being the most affected, and the electronic demand of the Sm(II) center. Of

course, an ionic contribution to the bonding is a given for these electropositive lanthanide ions.

5.4. Variable Temperature NMR Studies: Solution Structure of $Ln(Tp^{tBu,Me})_2$ Complexes; Fluxionality and Bonding Mode Changes of the $Tp^{tBu,Me}$ Ligands.

The simple room temperature ^1H NMR spectra of complexes **21** and **27** do not agree with the asymmetric solid state structure just described for the Sm derivative. Since we have already established the presence of the agostic B-H $\rightarrow$ Ln interaction in solution, this opens the intriguing possibility that, at room temperature, the complexes are under the influence of some selective dynamic process which equilibrates the environment of each different $Tp^{tBu,Me}$ ligand but *without* changing their distinct bonding modes, or at the least the bonding mode change is slow on the NMR time scale. Such a situation has remained hitherto unobserved in complexes containing the $M(Tp)_2$ fragment and is rather unexpected for the normally labile f-element complexes. The related $(Tp^{Me2})_2UI$ complex features two differently bonded Tp^{Me2} ligands but the two exchange their bonding mode down to -110°C.[18] To establish the nature of the fluxional process(es) variable temperature NMR studies were carried out.

The ^1H NMR spectra of both complexes, **21** and **27**, are indeed temperature dependent. The low temperature limiting spectrum of $Sm(Tp^{tBu,Me})_2$ (**21**) is almost reached at -110°C and is in *complete* accord with the asymmetric solid state structure (Figure 5.4). The spectrum shows distinct sets of signals for the six different pyrazolyl rings and two B-H peaks at -8.7 ppm and -35.4 ppm, respectively. Of the expected 18 pyrazolyl ring resonances, 17 are seen as two Me signals at -5.8 ppm accidentally overlap. The assignment of the signals to ^{t}Bu, Me and H, respectively follows from integration. Although, on the basis of the fluxional behavior, it will be possible to determine which of the R groups (R = ^{t}Bu, H, Me) belong to the same $Tp^{tBu,Me}$ ligand (*vide infra*), assignment to individual pyrazolyl rings is not feasible.

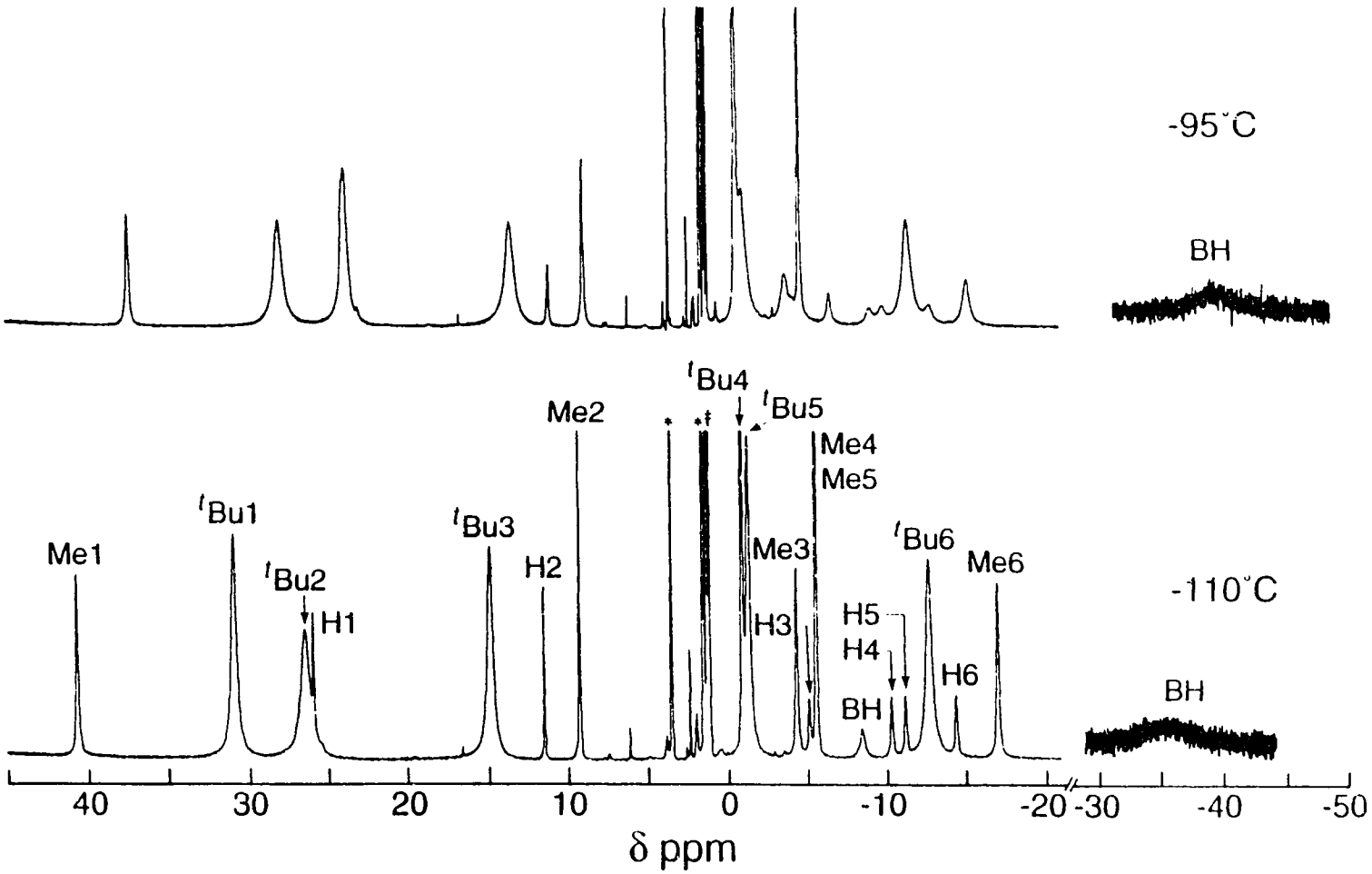

Figure 5.4 Low temperature ^{1}H NMR spectra (400 MHz) of $Sm(Tp^{tBu,Me})_2$ (**21**) in diethyl ether-d_{10}.

The variable temperature ^{1}H NMR spectra of **21** were not very revealing and therefore only two low temperature spectra were shown. As the temperature is raised the signals broaden and their chemical shift also changes with temperature. The temperature dependence of the chemical shifts is due to the presence of the paramagnetic Sm(II), which is also responsible for the observed large chemical shift range of the signals. The broadening of the signals is due to chemical exchange. Line shape changes of the resonances in this complex are further complicated by the temperature dependence of the chemical shifts and consequently it was not possible to decipher which signal was exchanging with which. To address this issue we carried out Spin Saturation Transfer (SST)[19,20] experiments at -90°C. This method is particularly suitable to identify exchanging sites at the onset of the exchange. Thus, irradiation of the ^{t}Bu2 signal at 22.60 ppm caused intensity decrease of the ^{t}Bu signals at 26.65 (^{t}Bu1) and 12.70 (^{t}Bu3) ppm, respectively and established that the three ^{t}Bu sites (^{t}Bu1, ^{t}Bu2, ^{t}Bu3) are coupled *via* exchange. Similarly, following a series of experiments where individual ^{t}Bu, Me and H signals were irradiated, it was shown that specific sets of three R groups, (^{t}Bu4, ^{t}Bu5, ^{t}Bu6; Me1, Me3, Me6; Me2, Me4, Me5; H1, H4, H6; H2, H3, H6) are exchange coupled. Thus the low temperature process exchanges pyrazolyl rings in sets of three and the only logical way for this to happen is that exchange occurs only within individual Tp^{tBu,Me} ligands. Unfortunately it does not appear to us that with the available information it is possible to assign exchange coupled set of signals/groups to a specific η^3-Tp^{tBu,Me} or "η^2-Tp^{tBu,Me}" ligand. At room temperature the fluxional process is fast enough that only averaged environments are seen for the two different Tp^{tBu,Me} ligands. Further increase in temperature causes renewed broadening of the signals and this can be interpreted as heralding the onset of the exchange between the bonding modes of the two ligands. Coalescence of the resonances was not seen up to +80°C.

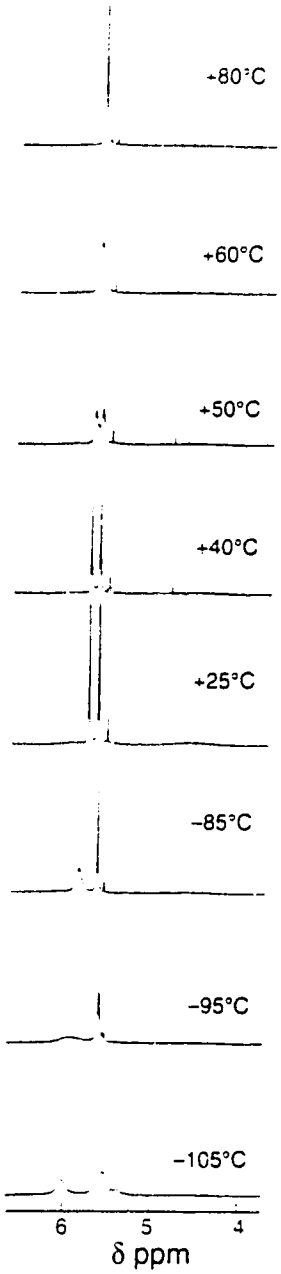

Figure 5.5 Variable temperature ^{1}H NMR spectra (400 MHz) of $Yb(Tp^{tBu,Me})_2$ (27) in toluene-d_8, only the pyrazolyl 4-H region is shown.

The variable temperature ^{1}H NMR spectra of Yb(Tp$^{t\mathrm{Bu,Me}}$)$_2$ (**27**) in the pyrazolyl 4-H region are shown in Figure 5.5. The ^{t}Bu and Me signals are also temperature dependent but, due to the small chemical shift differences at low temperatures, the signals are not well resolved and consequently are not informative. Focusing our attention to the behavior of the 4-H signals we see that at -105°C the room temperature singlets have split into three broad peaks, the middle peak with a shoulder at the low field side. The integrated intensity ratio is *ca.* 2:3:1. The implication of this spectrum is that the solution structure of complex **27** has a mirror plane at this temperature. The Yb complex is isostructural to its Sm analogue suggested by the identical IR spectra. Perhaps at lower temperature, the instantaneous structure would reveal the anticipated six 4-H signals. More likely, the much smaller chemical shift differences between different 4-H hydrogens in this diamagnetic complex are the reason for the accidental overlap of some of the signals and the appearance of the three line spectrum; contrast this situation to the beautifully resolved low temperature spectrum of complex **21** as a result of the chemical shift expansion provided by the paramagnetic Sm(II) center.

The small chemical shift differences between exchanging sites has a predictable effect on the coalescence temperature. Already at -95°C the three signals have emerged to two equal intensity averaged resonances; in the Sm complex the same feature is seen only at around -20°C. Although we could not carry out SST experiments the coalescence behavior of the signals is most consistent with the set of 2:1 ratio peaks giving one and the hardly resolved middle peak giving the other averaged signals. Exchange of pyrazolyl rings within individual Tp$^{t\mathrm{Bu,Me}}$ ligands is again the most rational way for the low temperature fluxional process to occur. As the temperature increases the two averaged signals continue to sharpen, the higher field signal faster. This is in accord with the smaller chemical shift difference between the

signals (5.51 and 5.45 ppm) responsible for this averaged feature compared to the low field peak (5.93 and 5.29 ppm). In this case, further increase in temperature brings about changes which clearly show equilibration between the two different $Tp^{tBu,Me}$ ligands. At +40°C the two Me resonances have coalesced already, however the 4-H and ^{t}Bu signals are still resolved. Warming to +60°C results in averaged 4-H and ^{t}Bu signals as well. Thus in the diamagnetic Yb complex the reduced chemical shift differences between exchanging sites allow an unequivocal demonstration of the high energy exchange process, conversely the chemical shift expansion by the paramagnetic Sm center was instrumental for the clear delineation of the low temperature process.

The variable temperature ^{171}Yb NMR of complex **27** revealed that ^{171}Yb chemical shift has very little temperature dependence in the temperature range of 25°C to -110°C. This is unexpected because normally ^{171}Yb chemical shifts are temperature dependent and we have observed such behaviour for $(Tp^{tBu,Me})YbN(SiMe_3)_2$ in Chapter 4. We have no explanation for this phenomenon.

To summarize the observations made so far. Complexes **21** and **27** undergo two distinct dynamic processes. The low temperature process involves exchange of pyrazolyl groups within individual $Tp^{tBu,Me}$ ligands, whereas at high temperature exchange between the bonding modes of the two different ligands is also set into motion.

The exchange of pyrazolyl groups could be initiated by breakage of the agostic B-H → Ln interaction or by one of the Ln-N(pz) bonds of the "η^2-$Tp^{tBu,Me}$" ligand. An unambiguous proof, which would definitely establish one of the mechanisms is not readily available. A variable temperature ^{171}Yb NMR study on compound **27** showed that the Yb-HB coupling of 85 Hz is maintained and remains invariant from room temperature to the low temperature limiting spectrum of -110°C. Although this observation is consistent with and hints at a process which keeps the B-H → Yb

interaction intact it does not conclusively rule out equilibration *via* rupture of the bond. The latter process would preserve the coupling as long as the H nucleus always returns to ytterbium with the same nuclear spin value. Nevertheless, we favor preferential Ln-N(pz) bond cleavage as the initiating step. Indeed as detailed in Scheme 5.1 this offers a remarkably simple and smooth pathway for pyrazolyl group exchange. On the

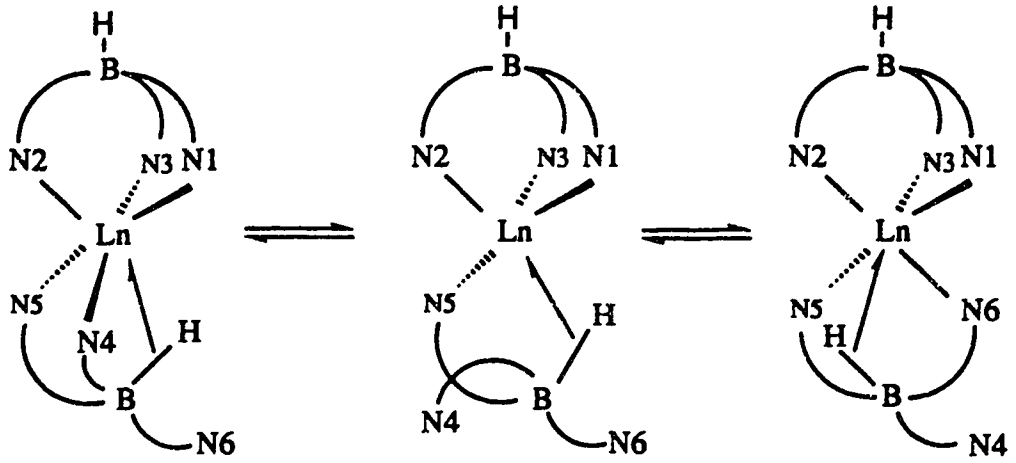

Scheme 5.1 Exchange of pyrazolyl groups within individual $Tp^{tBu,Me}$ ligand in **21** and **27**; low temperature process.

basis of the X-ray structure it is tempting to say that it is the Sm-N41 bond, the one where the N(pz) lone pair is not pointing at Sm, that is more prone to undergo bond cleavage. Conformational changes of the highly flexible five-membered $LnN_2B(\mu\text{-}H)$ ring would then simply bring the dangling pyrazolyl ring (N6) into bonding interaction and thereby restore the electron demand of the Ln(II) center. As shown in Scheme 5.1, the net effect is an exchange of the environments of the pyrazolyl rings of the η^3-$Tp^{tBu,Me}$ ligand as well, the two ligands moving together as two well oiled gears. This is in accord with the SST experiments which showed that the pyrazolyl rings are

exchanging in sets of three. Contrast this with the alternative mechanism which would involve, rupture of the agostic B-H → Ln bond, ring-flip of the six-member LnN_4B ring, displacement of one of the coordinated pyrazolyls by the dangling pyrazolyl group and finally re-establishment of the agostic B-H → Ln interaction. Clearly, this is a more complex and to us a less attractive scenario. The free energy of activation for the low temperature process is 8.5 kcal/mol, estimated at the coalescence temperature (-100°C) of the 4-H pyrazolyl hydrogens of the Yb complex. The rather different line widths of the signals of the paramagnetic Sm complex prevented a meaningful line shape analysis to be carried out for complex **21** at low temperature.

The high temperature dynamic process involves bonding mode change between the two $Tp^{tBu,Me}$ ligands. Intramolecular exchange is an attractive possibility, however in view of the known lability of lanthanide complexes and their tendency toward ligand redistribution reactions (cf. original preparation of complex **21**), an intermolecular process cannot be dismissed. To distinguish between the two possibilities the ^1H NMR spectra of a 1:1 mixture of **21** and **27** at high temperatures were recorded. If the process is intermolecular, in a mixture of **21** and **27** exchange of $Tp^{tBu,Me}$ ligands should also occur between Yb and Sm and hence all signals should broaden to eventually emerge as a single set of $Tp^{tBu,Me}$ resonances. Figure 5.6 shows the room temperature and 65°C spectra. It is clear from the figure that the above expectation is not met, instead the temperature behavior of the mixture is the same as that of the individual complexes. Indeed, at 65°C the signals of the two $Tp^{tBu,Me}$ ligands of the ytterbium complex have merged and furthermore the line widths of these averaged signals and those of the Sm complex are exactly the same as those of the individual complexes at this temperature. This then demonstrates that equilibration of the two different $Tp^{tBu,Me}$ ligands is intramolecular, or at the least that intermolecular ligand exchange is slow compared to the intramolecular process. We

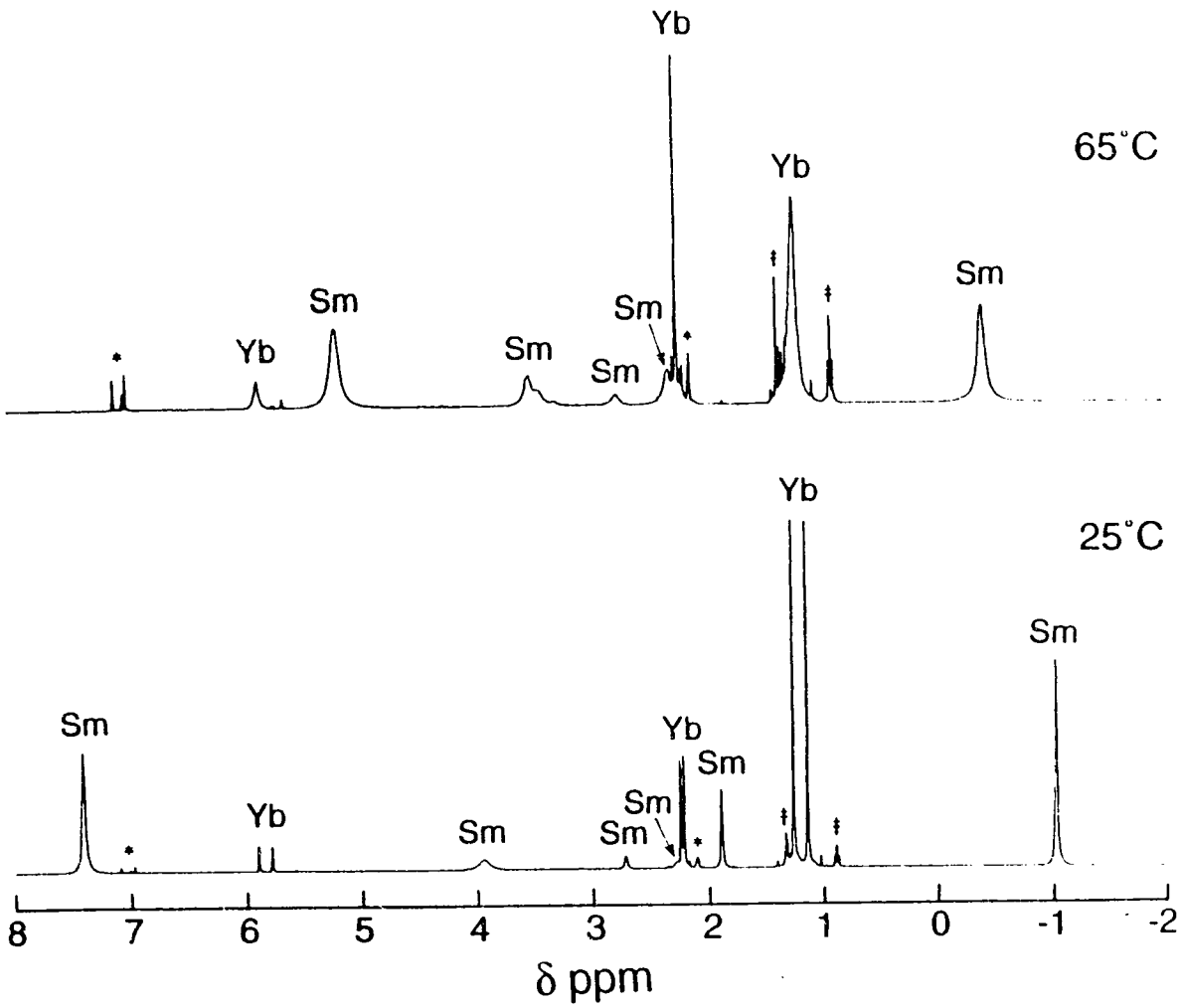

Figure 5.6 Variable temperature ^{1}H NMR spectra (400 MHz) of a 1:1 mixture of compounds **21** and **27** in toluene d_8.

have independent evidence which shows that the molecules also undergo intermolecular ligand exchange. Thus, when a mixture of $Yb(HTp^{tBu,Me})_2$ (**27**) and $Sm(DTp^{tBu,Me})_2$ (**21**-d_2) was warmed and the ^2H NMR spectrum recorded, **27**-d_2 was also observed. Work is underway to quantify the intermolecular exchange. The rapid intra- and slow intermolecular ligand exchange was also observed by Moss and Jones in $(Tp)_2Ln(\beta$-diketonate) complexes.[21]

The bonding mode change of the $Tp^{tBu,Me}$ ligands proceeds by a complex series of steps which at some stage must involve rupture of the agostic B-H $\rightharpoonup$ Ln interaction. We suggest that breakage of this bond is in fact the initiation step for the exchange, the subsequent steps have smaller activation energies. In an effort to obtain more evidence on this point, the variable temperature ^1H NMR spectra of **27** and its isotopomer **27**-d_2 were carefully run to detect isotope effects (if any) on the rearrangement energetics. Isotope effects were used by Reger[11] to support an agostic B-H $\rightharpoonup$ Y bond breaking process for the equilibration of pyrazolyl rings and BH_2 hydrogens in $[H(\mu\text{-}H)B(pz)_2]_3Y$. The following results were obtained. The line widths of the 4-H signals of **27** and **27**-d_2 were identical at low temperatures and this is consistent with the mechanism depicted in Scheme 5.1 for the low temperature process. The coalescence behaviour of these same signals was slightly different between 52-57°C, **27** coalescing marginally faster than **27**-d_2. Although an isotope effect is detectable, it is too small to offer reliable support for the postulated mechanism. The postulated sequence of events is shown in a schematic fashion in Scheme 5.2. Following breakage of the agostic interaction, the six-membered LnN_4B chelate ring is ready for relatively facile boat inversion.[22] The ring flip process puts the dangling pyrazolyl ring in a position favorable to displace one of the coordinated pyrazolyl moieties of the η^3-$Tp^{tBu,Me}$ ligand and to bond to the Ln center. Ring flip of the newly formed η^2-$Tp^{tBu,Me}$ ligand followed by attachment of its B-H unit

completes the exchange of the two different $Tp^{tBu,Me}$ ligands. The free energy of activation for the process estimated at the coalescence temperature of the Me groups (+40°C) and 4-H atoms (+60°C) of the pyrazolyl groups of the Yb complex **27** is

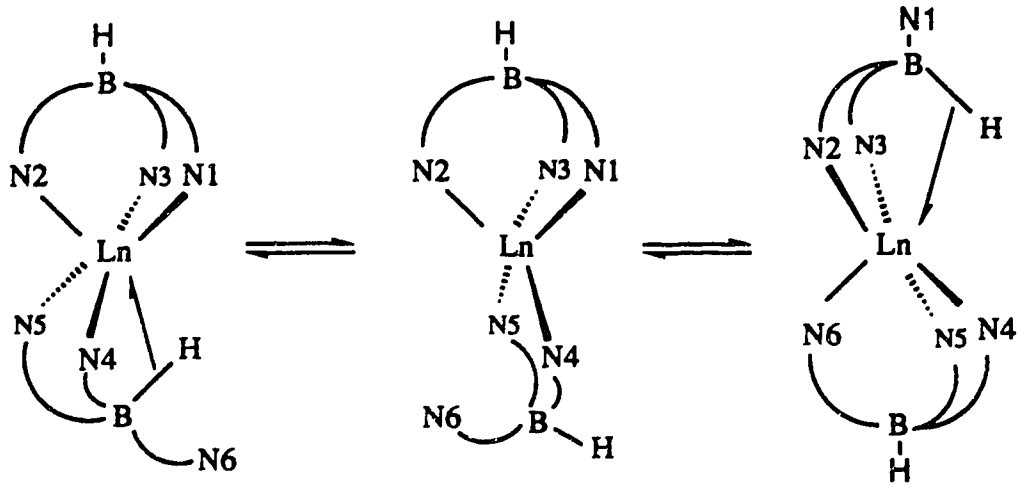

Scheme 5.2 Exchange of bonding mode between η^3- and η^2-$Tp^{tBu,Me}$ ligands in **21** and **27**; high temperature process.

16.0(3) kcal/mol, a similar value (17.2(1.1) kcal/mol) is obtained by simulating the line broadening features of the paramagnetic Sm complex **21**. These values are significantly higher than those observed for BH_2 exchange process in $Y[H(\mu\text{-}H)B(pz)_2]_3$[11] (11.5 kcal/mol) and $U[H(\mu\text{-}H)B(pz)_2]_3$[12] (12.2 kcal/mol), but comparable to the agostic C-H→Mo exchange in $[(\eta^3\text{-allyl})(CO)_2Mo[Et(CH_3CH(\mu\text{-}H))B(pz)_2]$ (17-19 kcal/mol).[23]

5.5. Conclusions

The use of the large Ln(II) ions has allowed the preparation of the first bis-hydrotris(3-^{t}Bu-5-Mepyrazolyl)borate complexes, $Ln(Tp^{tBu,Me})_2$ (Ln = Sm, **21**; Yb, **27**). The X-ray molecular structure of complex **21** revealed that both $Tp^{tBu,Me}$ ligands

are bonded to Sm, but the bonding mode of the two-ligands are vastly different. One $Tp^{tBu,Me}$ ligand is bonded *via* classical η^3-fashion. The other ligand is bonded *via* only two pyrazolyl nitrogens, however the B-H unit of this ligand is not innocent and participates in significant agostic interaction with the Sm center. The samarium is six-coordinate. The agostic B-H → Sm bonding manifests in a short Sm-B2 separation and a severely buckled six-membered SmN_4B chelate ring that exist in the unusual twisted-boat conformation. The instantaneous solution structures are the same as in the solid state. However the complexes are fluxional and exhibit two distinct dynamic processes. The low temperature process involves rapid exchange of the pyrazolyl rings within individual $Tp^{tBu,Me}$ ligands. During exchange the agostic B-H → Ln interaction appears to be preserved and this is supported by the temperature-independent ^{171}Yb-H coupling constant. At high temperature the two different $Tp^{tBu,Me}$ ligands undergo exchange, the high activation energy for the process lends further support for the strength of the agostic B-H → Ln bonding. The specificity of the exchange processes is remarkable for normally labile lanthanide complexes.

5.6. Experimental Section

5.6.1. Synthetic Procedures

Bis[hydrotris(3-^{t}Bu-5-Mepyrazolyl)borato]Samarium, [Sm($Tp^{tBu,Me}$)$_2$] (21)

A solution of $KTp^{tBu,Me}$ (924 mg, 2.0 mmol) in 10 mL of THF was added to 10 mL of a THF solution of $SmI_2(THF)_2$ (0.1M). The mixture was stirred for two days. The solvent was removed under vacuum and the residue extracted with 10 mL of pentane. Following filtration, the filtrate was concentrated to ca. 2 mL and cooled overnight at -40°C to yield purple crystals(472 mg, 47%). IR (KBr, cm^{-1}): 2530 (BH), 2351 (μ-BH); IR (Hexane, cm^{-1}): 2514 (BH), 2291 (μ-BH); MS (EI, 70 eV, 200°C) m/z 712 (M^+-HB(3-^{t}Bu-5-Mepz)$_2$); ^{1}H NMR (toluene-d$_8$, 25°C, ppm): 7.55(s,

^{t}Bu, 12), 5.1(s, br, BH, 255), 3.98(s, Me, 48), 2.69(s, 4-H, 12), 2.24(s, 4-H, 24), 1.86(s, Me, 7), -1.04(s, ^{t}Bu, 8), -67.3(s,br, BH, 306); ^{11}B NMR(toluene-d_8, 25°C, ppm): -21.8(s, br, 256), -53.0(s, br, 144); ^{1}H NMR (Et_2O-d_{10}, -110°C, ppm): 40.42(s, Me, 60), 30.59(s, ^{t}Bu, 160), 26.14(s, ^{t}Bu, 260), 25.64(s, 4-H, 40), 14.56(s, ^{t}Bu, 160), 11.23(s, 4-H, 24), 9.02(s, Me, 28), -1.17(s, ^{t}Bu, 40), -1.57(s, ^{t}Bu, 105), -4.58(s, Me, 60), -5.39(s, 4-H, 60), -5.79(s, 2Me, 40), -8.7(s, BH, 120), -10.54(s, 4-H, 60), -11.41(s, 4-H, 60), -12.90(s, ^{t}Bu, 160), -14.60(s, 4-H, 60), -17.21(s, Me, 60), -35.4(s, br, BH, 1290); ^{11}B NMR(Et_2O-d_{10}, -100°C, ppm): -44.0, -61.1. Anal. Calcd for $C_{48}H_{80}N_{12}B_2Sm$: C, 57.81; H, 8.09; N, 16.85. Found: C, 58.15; H, 8.62; N, 15.88.

Bis[hydrotris(3-^{t}Bu-5-Mepyrazolyl)borato]Ytterbium [Yb(Tp^{tBu,Me})$_2$] (27)

In the same fashion KTp^{tBu,Me} (861 mg, 1.863 mmol) and $YbI_2(THF)_{2.5}$ (566 mg, 0.933 mmol) after one week reaction time gave yellow crystals (419 mg, 44%). IR (KBr, cm^{-1}): 2550 (BH), 2300 (μ-BH); IR (hexane, cm^{-1}): 2550 (BH), 2290 (μ-BH); MS (EI, 70 eV, 230°C) m/z 734 (M^+-HB(3-^{t}Bu-5-Mepz)$_2$); ^{1}H NMR(toluene-d_8, 25°C, ppm): 5.9(s, br, HB, 236), 5.90(s, 4-H), 5.78(s, 4-H), 4.7(s, br, HB, 188), 2.24(s, Me), 2.20(s, Me), 1.25(s, ^{t}Bu), 1.13(s, ^{t}Bu). ^{11}B NMR(toluene-d_8, 25°C, ppm) : -0.9(d, J = 85 Hz, 180), -6.3(br, 390); ^{11}B {1H, 5.9} NMR(toluene-d_8, 25°C, ppm): -0.9(s, 100), -6.2(br, 400); ^{171}Yb NMR(toluene-d_8, 25°C, ppm): 329(d, J = 85 Hz); ^{171}Yb{1H, 5.9} NMR(toluene-d_8, 25°C, ppm): 329(s, 35); ^{171}Yb NMR(toluene-d_8, -100°C, ppm): 329(d, J = 85 Hz). Anal. Calcd for $C_{48}H_{80}N_{12}B_2Yb$: C, 56.53; H, 7.91; N, 16.48. Found: C, 56.13; H, 7.31; N, 15.55.

TlDB(3-^{t}Bu-5-Mepz)$_3$

Solid $NaBD_4$ (0.846g, 20.14 mmol) and (3-tert-butyl-5-methyl)pyrazole (16.94g, 122.75 mmol) were charged into an elongated tube. The mixture was heated gradually to 180°C and kept at this temperature for 2 hours. The temperature was then

gradually raised to ca. 290°C until no more hydrogen gas evolved. The mixture was cooled to room temperature under nitrogen, and was dissolved in THF (100 mL). To the THF solution was added a slurry of Tl_2SO_4 (10.20g, 20.21 mmol) in ca. 200 mL of water. After stirring overnight, the mixture was extracted with 100 mL of CH_2Cl_2. The CH_2CL_2 layer was separated and the aqueous layer was extracted with an additional 200 mL of CH_2Cl_2. Removal of CH_2Cl_2 with a rotary evaporator gave a white solid. The solid was placed into an elongated Schlenck tube (30 cm length X 4.5 cm inner diamet[illegible] [illegible]mation at 95°C under dynamic vacuum. After 3 days, excess (3-tert-butyl-[illegible]zole was deposited on the upper part of tube and the product TlDB(3-[illegible] [illegible]emained at the bottom of the tube(7.20g, 57%). IR (KBr, cm^{-1}): 1885(B[illegible]); [illegible] (hexane, [illegible]cm^{-1}): 1885(BD); ^1H NMR(toluene-d_8, 25°C, ppm): 5.80(d, 4-H), 2.25(s, Me), 1.35(d, ^tBu); ^{11}B NMR (toluene-d_8, 25°C, ppm): -6.4(s); ^2H NMR(toluene-d_8, 25°C, ppm): 4.9(s); MS (EI, 70 eV, 170°C) m/z 629 (M^+) Anal Calcd. for $C_{24}H_{40}N_6BTl$: C, 45.92; H, 6.42; N, 13.39. Found: C, 45.82; H, 6.49; N, 13.41. The reason for conversion of NaDB(3-^{t}Bu-5-Mepz)$_3$ to the Tl salt is that excess pyrazole can not be removed from the Na salt, both pyrazole and NaDB(3-^{t}Bu-5-Mepz)$_3$ cosublime.

Bis[deuteriotris(3-^{t}Bu-5-Mepyrazolyl)borato]Samarium, [Sm(d-Tp^{tBu,Me})$_2$] (21-d_2)

A solution of TlDB(3-^{t}Bu-5-Mepz)$_3$ (628 mg, 1.0 mmol) in 10 mL of THF was added to a THF solution of 0.1M SmI_2 (5 mL, 0.5 mmol). The mixture was stirred for 5 hours. The solvent was removed under vacuum and the residue extracted with 10 mL of pentane. Following filtration, the filtrate was concentrated to ca. 5 mL and cooled overnight at -40°C to yield a purple crystalline solid (198 mg). At this stage the product is a mixture of [(DB(3-^{t}Bu-5-Mepz)$_3$]$_2$Sm and TlDB(3-^{t}Bu-5-Mepz)$_3$ (molar ratio 2:1 by ^1H NMR). Pure 21-d_2 can be obtained by repeated crystallization

from pentane, but with much loss of **21**-d_2. IR (KBr, cm^{-1}) 1890(BH), 1705 (μ-BH); IR (hexane, cm^{-1}): 1880 (BH), 1695 (μ-BH); MS (EI, 70 eV, 200°C) m/z 713 (M^+-DB(3-^{t}Bu-5-Mepz)$_2$); ^{2}H NMR(toluene, 25°C, ppm): 4.8(s), -67.5(s); ^{11}B NMR(toluene-d_8, 25°C, ppm): -21.6(s), -52.8(s). Anal. Calcd for $C_{48}H_{78}D_2N_{12}B_2Sm$: C, 57.70; H, 7.87; N, 16.82. Found: C, 57.37; H, 7.82; N, 15.59.

Bis[deuteriotris(3-^{t}Bu-5-Mepyrazolyl)borato]Ytterbium, [Yb(d-Tp$^{t\mathrm{Bu,Me}}$)$_2$)] (27-d_2)

In the same fashion, TlDB(3-^{t}Bu-5-Mepz)$_3$ (578 mg, 0.92 mmol) and $YbI_2(THF)_{2.5}$ (279 mg, 0.460 mmol) after 5 hours gave a mixture of [(DB(3-^{t}Bu-5-Mepz)$_3$]$_2$Yb and TlDB(3-^{t}Bu-5-Mepz)$_3$ (molar ratio 1.2:1 by ^{1}H NMR). As the ligand and **27**-d_2 have similar solubility in common solvents, even repeated crystallization did not produce pure **27**-d_2. IR (KBr, cm^{-1}) 1900(BD), 1690 (μ-BD); MS (EI, 70 eV, 180°C) m/z 736 (M^+-DB(3-^{t}Bu-5-Mepz)$_2$); ^{11}B NMR(toluene-d_8, 25°C, ppm): -1.1(s), -6.5(s); ^{2}H NMR(toluene, 25°C, ppm): 5.6(s), 4.3(s); ^{171}YB NMR(toluene-d_8, -100°C, ppm): 328(s)

5.6.2. Variable Temperature NMR Studies

^{2}H NMR spectra were recorded at 61.42 MHz, on a Bruker AM-400 FT spectrometer. The temperature measurements were made with a Bruker B-VT 1000 temperature control unit. Temperatures are believed to be accurate to ±1K. Rate constants for the high temperature process of the samarium complex (**21**) were determined by visual comparison of computer-simulated and observed line shapes of the ^{t}Bu signals: k = 30±3 s^{-1}, 333K; 70±7 s^{-1}, 343K; 150±15 s^{-1}, 353K; 280±28, 363K. The activation parameters for the high temperature process were obtained by a least-squares linear regression fit to the Eyring equation ($\Delta H^{\neq}$ = 17.3±0.5 kcal/mol^{-1}, $\Delta S^{\neq}$ = -0.6±6.3 eu, $\Delta G^{\neq}$ = 17.2±1.1 kcal/mol). Computer simulation and calculation

of activation parameters were carried out with programs written by Professor R.E.D. McClung of this department.[24] Activation energies for the ytterbium complex (**27**) were calculated at the coalescence temperatures:[25] low temperature process, 4-H signals, T_c = -100±3°C (173K) and $\Delta\nu$ = 268 Hz; high temperature process, ^{t}Bu signals, T_c = 57±3°C (330K) and $\Delta\nu$ = 72 Hz. The free energies of activation based on the formula $\Delta G^{\neq} = 1.914 \times 10^{-2}\, T[9.972 + \log(T/\Delta\nu)]$ kcal/mol are 8.5(0.2) kcal/mol for the low temperature process and 16.0(0.3) kcal/mol for the high temperature process, respectively.

To study the effect of BH *versus* BD on the rearrangement, NMR samples of **27** and **27-d$_2$** were prepared by dissolving 12 mg of each complex in 0.6 mL of toluene-d$_8$. The ^{1}H NMR spectra were recorded at the following temperatures: -110, -105, -95, -85 and 45, 50, 55 and 60°C and at one degree intervals between 52 and 57°C. At each temperature the sample was allowed to equilibrate at least 20 minutes before starting acquisition. To maintain the same conditions the spectrum of **27** was always recorded before that of **27-d$_2$**.

To distinguish between intra *versus* intermolecular Tp$^{t\mathrm{Bu,Me}}$ ligand exchange, a mixture of 15 mg each of the samarium (**21**) and ytterbium (**27**) complexes was dissolved in 0.5 mL of toluene-d$_8$. The room temperature ^{1}H NMR spectrum was recorded immediately after sample preparation, subsequent spectra were acquired at the following temperatures: 35, 45, 55, and 65°C. At each temperature the sample was allowed to equilibrate for 10 minutes.

5.6.3. X-ray Structure Determination:

Purple black crystals of Sm(Tp$^{t\mathrm{Bu,Me}}$)$_2$ suitable for diffraction were grown from a hexane solution at -40°C. The crystal was handled as described in previous Chapters. The X-ray data collection and structure refinement for complex **21** was

carried out by Dr. R. McDonald at Structure Determination Laboratory, Department of Chemistry, University of Alberta. Important crystallographic data are presented in Table 5.2.

Table 5.2 Crystallographic Data for $Sm(Tp^{tBu,Me})_2 \cdot 1/2\ C_6H_{14}$.

A. Crystal Data	
formula	$C_{51}H_{87}B_2N_{12}Sm$
formula weight	1040.31
crystal dimensions (mm)	0.48 × 0.25 × 0.13
space group	$P2_1/n$ (a non-standard setting of $P2_1/c$ [No.14])
unit cell parameters	
a (Å)	12.177 (2)
b (Å)	26.140 (3)
c (Å)	17.826 (2)
β (deg)	93.13 (1)
V (Å^3)	5666 (3)
Z	4
ρ_{calcd} (g cm^{-3})	1.220
μ (cm^{-1})	10.80
B. Data Collection and Refinement Conditions	
diffractometer	Enraf-Nonius CAD4
radiation (λ [Å])	Mo K_α (0.71073)
monochromator	incident beam, graphite crystal
take-off angle (deg)	3.0
detector aperture (mm)	(3.00 + tanθ) horiz × 4.00 vert
crystal-to-detector distance (mm)	173
scan type	θ-2θ
scan rate (deg min^{-1})	6.7–1.6

(continued...)

Table 5.2 (continued)

scan width (deg)	$0.75 + 0.344\tan\theta$
data collection 2θ limit (deg)	50.0
total data collected	8821 ($\pm h +k +l$)
range of absorption correction factors	0.8032–1.2717
total unique data	8520
number of observations (NO)	4062 ($I \geq 3\sigma(I)$)
final no. parameters varied (NV)	575
R^a	0.050
$R_w{}^b$	0.058
GOF^c	1.455

$^a R = \Sigma | |F_o| - |F_c| | / \Sigma |F_o|$.

$^b R_w = [\Sigma w(|F_o| - |F_c|)^2 / \Sigma w F_o{}^2]^{1/2}$.

$^c \mathrm{GOF} = [\Sigma w(|F_o| - |F_c|)^2 / (NO - NV)]^{1/2}$.

5.7. References

(1) Zhang, X.W.; McDonald, R.; Takats, J. *New J. Chem.* **1995**, *19*, 573.

(2) Calabrese, J. C.; Donaille, P. J.; Thompson, J. S.; Trofimenko, S. *Inorg. Chem.* **1990**, *29*, 4429.

(3) Evans, W. J.; Gonzales, S. [illegible] iller, J. W. *J. Am. Chem. Soc.* **1991**, *113*, 7423.

(4) Reger, D. L.; Mahtab, R.; Baxter, J. C.; Lebioda, L. *Inorg. Chem.* **1986**, [illegible] 2045.

(5) Reger, D. L.; Swift, C. A.; Lebioda, L. *Inorg. Chem.* **1984**, *23*, 349.

(6) Green, M. L. H.; Hughes, A. K.; Michaelidou, D. M.; Mountford, P. J. *J. Chem. Soc., Chem. Commun.* **1993**, 591.

(7) Takats, J.; Zhang, X. W.; Day, V.; Eberspacher, T. A. *Organometallics* **1993**, *12*, 4286.

(8) Kosky, C. A.; Ganis, P.; Avitabile, G. *Acta Cryst.* **1971**, *b27*, 1859.

(9) Cotton, F. A.; Jeremic, M.; Shaver, A. *Inorg. Chim. Acta* **1972**, *6*, 543.

(10) Carvalho, A.; Domingos, A.; Gaspar, P.; Marques, N.; Pires de Matos, A.; Santos, Y. *Polyhedron* **1992**, *11*, 1481.

(11) Reger, D. L.; Lindeman, J. A.; Lebioda, L. *Inorg. Chem.* **1988**, *27*, 1890.

(12) Sun, Y.; Takats, J.; Eberspacher, T. A.; Day, V. W. *Inorg. Chim. Acta* **1995**, *229*, 315.

(13) Reger, D. L.; Knox, S. J.; Rheingold, A. L.; Haggerty, B. S. *Organometallics* **1990**, *9*, 2581.

(14) Cotton, F. A.; Frenz, B. A.; Murillo, C. A. *J. Am. Chem. Soc.* **1975**, *97*, 2118.

(15) Shannon, R. D. *Acta Cryst.* **1976**, *A32*, 751.

(16) Evans, W. J.; Ulibarri, T. A.; Ziller, J. W. *Organometallics* **1991**, *10*, 134.

(17) LeCloux, D. D.; Takar, C. J.; Osawa, M.; Hauser, R. P.; Keyes, M. C.; Tolman, W. B. *Organometallics* **1994**, *13*, 2855.

(18) Sun, Y.; McDonald, R.; Takats, J.; Day, V. W.; Eberspacher, T. A. *Inorg. Chem.* **1994**, *33*, 4433.

(19) Faller, J. W. *in Determination of Organic Structures by Physical Methods.* Zuckermann, J.J., Nachod, F.C., Eds., Academic, New York, **1973**, Vol. 5, p.75

(20) Forsen, S.; Hoffman, R. A. *J. Chem. Phys.* **1963**, *39*, 2892.

(21) Moss, M. A. J.; Jones, C. J. *Polyhedron* **1990**, *9*, 697.

(22) Calderon, J. L.; Cotton, F. A.; Shaver, A. *J. Organomet. Chem.* **1972**, *37*, 127, *38*; 105; *42*, 419.

(23) Cotton, F. A.; Stanislawski, A. G. *J. Am. Chem. Soc.* **1974**, *96*, 5074.

(24) McClung, R. E. D. *EXCHANGE: Program for the simulation of NMR Spectra of Weakly-Coupled Exchanging Systems, University of Alberta*

(25) Sandstrom, J. *Dynamic NMR Spectroscopy, Academic London* **1982**, p.96.

Chapter 6

Conclusions

The goal of this thesis was to examine the structure/reactivity characteristics of divalent lanthanide hydrotris(pyrazolyl)borate complexes as a function of the substituents R and R' on the pyrazolyl rings. The investigation was divided into two parts. The first stage dealt with the synthesis, characterization and reactions of bis-ligand complexes with a view to compare the chemistry with the C_5Me_5 analogues. The other project centered on the synthesis of half-sandwich complexes $(Tp^{R,R'})Ln(ER)$ (ER=iodide, amide, aryloxide, hydrocarbyl, hydride), since the number of half-sandwich lanthanide complexes is very limited because of their tendency to undergo ligand-redistribution to bis-ligand compounds.[1-4]

The hydrotris(pyrazolyl)borates $(Tp^{R,R'})$ proved very effective ligands for divalent lanthanides; the combination of hard nitrogen donors and large size satisfy the electrostatic and steric requirements of the large metal ions. The $Tp^{R,R'}$ ligands, like C_5Me_5, also generally provide stability and solubility to the complexes. The control of solubility and steric saturation is achieved by varying the substituents on the 3-position of the pyrazolyl ring.

A series of bis-ligand complexes, $(Tp^{R,R'})_2Ln$ (R=^{t}Bu, Me and R'=Me; R=Ph, Tn and R'=H) have been successfully synthesized. All these complexes except $(Tp^{tBu,Me})_2Ln$ are six-coordinate with Tp coordinated to Ln in an η^3-mode. They are sterically congested which is evidenced by the absence of solvent in the coordination sphere. The formation of $(Tp^{tBu,Me})_2Ln$ was unexpected due to the sterically very demanding nature of the ligand.[5] The first isolation of this complex was from the reaction of $(Tp^{tBu,Me})SmI$ and KCH_2SiMe_3. The two $Tp^{tBu,Me}$ ligands are different. One is coordinated in the classic η^3-fashion, the other is bonded via two pyrazolyl

nitrogens and an agostic B-H → Ln interaction. Remarkably, the complexes undergo selective dynamic processes in solution, a rarity in lanthanide chemistry.

Despite its insolubility, $(Tp^{Me2})_2Sm$ readily reacts with reducible substrates. The bulky Tp^{Me2} disfavors formation of $[(Tp^{Me2})_2Sm]_2$(substrate) and this is in contrast to the behaviour of $(C_5Me_5)_2Sm$ where $(C_5Me_5)_2Sm$(substrate) is often too reactive for isolation.[6] The cradle-like protective pocket provided by the two Tp^{Me2} ligands has allowed the isolation of the first superoxo and quinone lanthanide complexes. The O_2^- moiety is stabilized in the unique environment provided by two Tp^{Me2} ligands. Our study on $(Tp^{Me2})_2Sm$ shows that the reactivity of insoluble complexes can be underestimated.

The successful isolation of half-sandwich complexes is crucially dependent on the steric bulk of the ligands. With Tp^{Tn}, Tp^{Ph} and Tp^{Me2}, the half-sandwich compounds are not stable and tend to undergo ligand-redistribution to form $(Tp')_2Ln$. Yet, the preparation of $(Tp^{tBu,Me})LnI(THF)n$ is straightforward and, more importantly, the compounds are stable towards ligand-redistribution reactions. The stability of $(Tp^{tBu,Me})LnI(THF)_n$ has opened an exciting opportunity to explore and synthesize a variety of new complexes which are not accessible to other ligand systems (such as the C_5Me_5 moiety). The preparation of reactive divalent lanthanide hydrocarbyls, combined with the reducing power of Ln(II) marks the beginning of a new chapter in organolanthanide chemistry. It is not difficult to imagine that, with the bulky $Tp^{tBu,Me}$ ligand, other unknown species such as monomeric peroxides, oxides and imides $[(Tp^{tBu,Me})LnY$, $Y = O_2^{-2}, O^{-2}, NR^{-2}]$ may also be stabilized and isolated as long as a proper methodology can be developed.

6.1. References

(1) Evans, W. J.; Grate, J. W.; Choi, H. W.; Bloom, I.; Hunter, W. E.; Atwood, J. L. *J. Am. Chem. Soc.* **1985**, *107*, 941.

(2) Evans, W. J.; Drummond, D. K.; Zhang, H. M.; Atwood, J. L. *Inorg. Chem.* **1988**, *27*, 575.

(3) Swamy, S. J.; Schumann, H. J. *J. Organomet. Chem.* **1987**, *334*, 1.

(4) Cloke, F. G. N.; Dalby, C. I.; Hitchcock, P. B.; Karamallakis, H.; Lawless, G. A. *J. Chem. Soc., Chem. Commun.* **1991**, 779.

(5) Trofimenko, S. *Chem. Rev.* **1993**, *93*, 943.

(6) Evans, W. J.; Ulibarri, T. A.; Ziller, J. W. *J. Am. Chem. Soc.* **1990**, *112*, 2314.